Memorial University of Newfoundland

FACULTY OF SCIENCES
DEPARTMENT OF PHYSICS AND PHYSICAL OCEANOGRAPHY

Interaction of Antimicrobial Peptides with Bacterial Cell Envelopes

by

Nury Paula Santisteban Vela

A Thesis submitted to the School of Graduate Studies

in partial fulfilment of the requirements for the degree of

Doctor of Philosophy in Condensed Matter Physics

October 2019

St. John's Newfoundland

Abstract

Antimicrobial peptides (AMPs) are small chains of amino acids with the ability to cause bacterial death. AMPs are usually amphiphilic but diverse in charge and structure. The mechanism or mechanisms that AMPs implement to kill bacteria are still under discussion. Studies in model membranes have widely demonstrated the capacity of AMPs to interact with and disrupt the bacterial cell membrane. There are however, good reasons to suspect that AMP interactions with non-membrane components of bacteria are important. For instance, there is an enormous discrepancy between the peptide to lipid molar ratio (P:L) necessary to generate membrane disruption in model systems ($\sim$ 1:100), and the P:L necessary to stop bacterial growth, i.e. the minimal inhibitory concentration (MIC) ($\sim$ 10-100:1). One potential explanation for this discrepancy is that AMPs may interact with non-membrane components of the bacterial cell envelope. The peptidoglycan (PGN) layer is one of the primary non-membrane components of Gram-positive bacterial cell envelopes and is responsible for cell shape and stability. Currently, there is an open discussion about whether PGN can entrap AMPs and prevent them from reaching the cell membrane or, instead promote the accumulation of AMPs on the cell membrane. The primary experimental approach employed in this thesis was ^{2}H NMR spectroscopy of intact bacteria with ^{2}H-labeled membranes. Specifically, since the quadrupolar splittings obtained from the spectra are proportional to the order parameter of the lipid acyl chains, the spectra reflect the structure and dynamics of the membrane. In particular, ^{2}H NMR spectroscopy allows us to characterize the disruption of lipid bilayers caused by AMPs. In this study, different methods to grow ^{2}H-membrane-enriched bacteria were optimized to obtain ^{2}H NMR spectra of *E. coli* LA8, *E. coli* JM109 and *B. subtilis*. Additionally, ^{2}H NMR was used to observe the level of disruption of the cell membrane of *B. subtilis* caused by the presence of different AMPs, MSI-78 and BP100. Both MSI-78 and BP100 caused the same level of membrane disruption at similar concentrations. Separately, comparison of the ^{2}H NMR spectra of *B. subtilis* with intact and compromised PGN layers showed no differences. The lack of change in the spectra of PGN-compromised and PGN intact bacteria indicates that there is no change in the dynamics or structure of the lipid bilayer even with a weakened PGN layer. Finally, the disruption caused by MSI-78 and BP100 was measured in

B. subtilis with a compromised PGN layer. The results indicate that there is no change in the level of membrane disruption caused by MSI-78 and BP100 when the PGN layer is partially removed.

Acknowledgements

First and foremost, I would like to thank my parents for all the love and support. I am who I am because of you, I love you forever. To my sister for being the most annoying yet lovable sister. I thank my son, Mateo Moreno, for his unconditional support despite these two years apart during my Ph. D studies. Finally to my partner of live, Esteban Ricalde, whom came to our lives to stay, love and support us.

Primero que todo me gustaría agradecer a mis padres por todo su amor y apoyo. A ellos les debo todo, los amo infinitamente. A mi hermana por ser la hermana mas fastidiosa aunque adorable. Agradezco a mi hijo, Mateo Moreno, cuyo apoyo ha sido incondicional a pesar de que mis estudios de doctorado nos implico vivir dos años separados. Finalmente a mi compañero de vida, Esteban Ricalde, quien decidió entrar a mi vida para quedarse y a quien también agradezco su apoyo incondicional.

I would like to express my sincere gratitude to my supervisor Dr. Valerie Booth and my co supervisor Dr. Michael Morrow for the continuous support during my Ph. D journey. I was very fortunate to have their guidance and advice during the past five years. I specially thank Dr. Valerie Booth for give me the opportunity to work in her group, her enormous patience and constancy were the best mentorship that I could have asked for.

I specially thank my friends and lab members Gagandeep Sandhu, Suhad Sbeih, Tadiwos Getachew, Sarika Kumari and Yanitza Trozel, their support and collaboration was really important. But also my friends in distance specially Elizabeth Suesca, Luis Alejandro Barbosa and Alejandro Mahecha, for all the emotional support despite the distance help me get through good and rough moments.

I specially thank Donna Jackman, Marie Codner and Donna Hunt for their help, assistance and because they made me feel part of the biochemistry department despite me being a physicist in disguise.

Finally, I gratefully acknowledge the financial assistance of Memorial University, the Department of Physics and Physical Oceanography, the school of Graduate Students and the alliance Conciencias-Colfuturo.

Contents

List of Figures

List of Tables

Abbreviations

A_{600}	Absorbance at 600 nm
AU	Arbitrary units
AFM	Atomic force microscopy
AMP	Antimicrobial peptide
CAME	Cecropin A(1-8) - melittin(1-10)
C-D	Carbon - Deuterium
CL	Cardiolipin
Δ_2	Relative Mean Square Width of the Order Parameter Distribution
DLPC	Dilauroylphosphatidylcholine
DMPC	Dimyristoylphosphatidylcholine
DPC	Dodecylphosphocholine
DPPC	Dipalmitoylphosphatidylcholine
DSPC	Distearoylphosphatidylcholine
FID	Free induction decay
Gram +	Gram positive
Gram -	Gram negative
GMV	Giant multilamellar vesicles
LB Broth	Luria-Bertani broth
LPS	Lipopolysacharide
LTA	Lipoteichoic acid
MIC	Minimal inhibitory concentration
MIS	Magainin intervening sequence

MB Method	Mutated bacteria method
UB Method	Unmutated bacteria method
NAG	N-acetylglucosamine
NAM	N-acetylmuramic
NMR	Nuclear magnetic resonance
OA	Oleic acid
PA-d_{31}	Deuterated palmitic acid
PBS	Phosphate buffered saline
PC	Phosphatidylcholine
PE	Phosphatidylethanolamine
PG	Phosphatidylglycerol
PGN	Peptidoglycan
SMM	Sucrose, maleic acid and magnesium chloride
TA	Teichoic acid
wt/wt	AMP weight/Dry bacteria weight
WTA	Wall teichoic acid
2× YT	2× amount of yeast extract and 60% more tryptone than LB broth

Chapter 1

Overview

Antimicrobial peptides (AMPs) are chains of amino acids with the ability to kill pathogens, such as bacteria, fungi and viruses. They may also kill cancer cells. At the same time AMPs should cause little or no harm to host cells. The mechanism or mechanisms that AMPs implement to kill those pathogens is still under study. The main results regarding AMPs can be divided into results obtained from studies of model systems and results obtained in biological experiments. Model systems are phospholipid bilayers intended to mimic the bacterial membrane composition. From the study of model systems it is widely accepted that, in the case of bacteria, AMPs interact with and disrupt the bacterial cell membrane [2–4]. On the other hand, biological experiments have shown the ability of AMPs to inhibit bacterial growth over a wide spectrum of bacterial species. One way to establish a connection between the results from model system experiments and biological experiments is to extend the techniques used in model systems to whole cells. AMPs' disruption of lipid structures make ^{2}H nuclear magnetic resonance (NMR) an appealing technique to study their effects on fluidity of phospholipid acyl chains. The quadrupolar splitting in the deuterium magnetic resonance spectrum is related to the orientational order parameter of the lipid acyl chains. As a consequence, ^{2}H NMR spectra can be used to glean information about the molecular dynamics of the system and therefore the physical state of lipid assemblies can be determined [5]. In particular, ^{2}H NMR can be useful to identify changes to the lipid membrane state caused by AMPs. Because the natural abundance of

^{2}H atoms is 0.01%, ^{2}H NMR measurements in bacterial cells require the bacteria to be deuterium-labeled. Our group and others have developed methods that promote the uptake of deuterium-labeled acyl chains in bacterial cells to produce ^{2}H-membrane-enriched bacteria [1, 6–8]. In my thesis, changes in the ^{2}H NMR spectrum of different bacterial strains in the presence and absence of different AMPs are used to obtain information about how the peptides interact with and disturb bacterial membranes. This work is also intended address recent questions about whether the peptidoglycan (PGN) layer has a role on the AMP-lipid bilayer interaction [12, 108]. Such questions arise from the fact that bacterial cell envelopes also have non-lipid components located outside of the phospholipid membrane.

Chapter 2

Introduction

To achieve a better understanding of this project, some concepts need to be introduced. First, background on Gram + and Gram - bacterial cell envelopes and their primary differences will be described. Next will be a discussion of what AMPs are and why it is important to understand their ability to kill pathogens and, especially bacteria. Finally, essential information about ^{2}H NMR in lipid bilayers will be provided, followed by discussion of why this technique is implemented to study the dynamics of the AMP-lipid bilayer interaction and how to interpret ^{2}H NMR spectra obtained from whole bacterial cells.

2.1 Gram Positive (Gram +) and Gram Negative (Gram -) Bacterial Cell Envelopes

One of the most important bacterial organelles is the cell envelope. Some of the many bacterial cell envelope functions are: to separate the interior of the bacteria from the environment; to enable the transport of substances and information between the outside and the inside; to enable metabolism, growth and multiplication; and to provide structural stability to the cell [9].

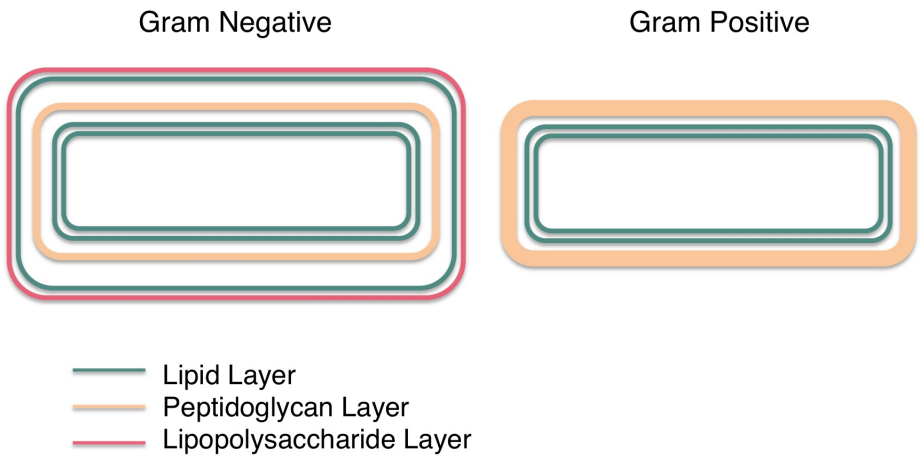

FIGURE 2.1: Gram - and Gram + cell envelope content

Although all structures in the bacterial cell envelope are adapted to enable the functions explained above, each species of bacteria accomplishes the same objectives in different ways. This makes the bacterial envelope a very complex organelle that varies with different bacteria types. Even so, there are structural components that are common to many or most of them. For example, structures such as a lipid bilayer and a peptidoglycan layer are essential components of the cell envelope of ALL bacteria, providing a barrier in the lipid bilayer case, and stability in the peptidoglycan case [9].

In 1884, Gram discovered a way to differentiate bacteria into two types using a staining method. Depending on the structure of the cell envelope, bacteria will retain a different amount of Gram's dye. Bacteria that stain with a dark blue to violet color are called Gram positive (Gram +) and bacteria that stain with a red color are called Gram negative (Gram -). The difference in color is due to the differences in the cell envelope composition between these two kinds of bacteria. Both of them have a peptidoglycan (PGN) layer but in Gram + bacteria this layer is much thicker than in Gram - bacteria. Also, Gram - bacteria have a second membrane with the inner leaflet composed of lipids and the outer leaflet containing Lipopolysaccharides (LPS) (See Figure 2.1)[9].

In order to clearly define the difference between Gram + bacteria and Gram - bacteria, the main components of the bacterial membrane will be explained first.

2.1.1 Phospholipids

The most common lipids in cells are the phospholipids. Phospholipids display a variety of charges, acyl chain lengths, and unsaturations. They are essential for the bacterial envelope, determining its structure and flexibility. In bacterial membranes, phospholipid composition depends on bacterial species and environmental conditions [10]. Typically, however, about 25% of the bacterial envelope consists of phospholipids and between 1-5% of the bilayer consists of cardiolipin, a glycerolphospholipid, whose role is also important for the bacterial bilayer [9].

The principal characteristic of phospholipids is their amphiphilic nature. They have two structural components, a hydrophobic hydrocarbon chain and a polar head group, which may be zwitterionic or may carry overall charge. Due to the dual interaction of phospholipids with water molecules, phospholipids tend to form bilayer or micellar structures consisting of a hydrocarbon nucleus and an external surface formed by polar heads [9]. Phospholipid bilayer structures have different phase states. The two more studied are the gel and the liquid-crystalline states. The gel phase is an ordered state in which lateral mobility is slow and the phospholipid acyl chains tend to be extended. In contrast, in the liquid-crystalline phase, lateral mobility is higher than in the gel state and the phospholipid acyl chains are less ordered than in the gel state. The liquid crystal-gel phase transition temperature depends on the phospholipid chemical structure. For instance, phospholipids with longer acyl chains typically have higher phase transition temperature. Unless otherwise, noted, the term "lipids" will refer to "phospholipids" throughout this thesis.

2.1.2 Lipopolysaccharides (LPS)

Like other components of the cell envelope, LPS are amphiphilic molecules with a positive charge. LPS molecules are combinations of lipids and polysaccharides,

which allows them to vary in size and structure, especially in the hydrophilic polysaccharide part. LPS is present in the outer leaflet of the outer membrane of Gram - bacteria along with lipid A, and it is essential for Gram - bacteria [9].

2.1.3 Peptidoglycan

The polymer responsible for the stability of the bacterial shape and for preventing expansion of the cell membrane under hypertonic conditions is called peptidoglycan (PGN). The PGN polymer is composed of alternating units of N-acetyl glucosamine (NAG) and N-acetyl muramic acid (NAM). PGN polymers are cross-linked by pentapeptide side chains (see Figure 2.2). The resulting structure is considered a highly rigid net. Depending on the kind of bacteria, the percentage of PGN composing the cell wall mass could vary from $\sim$ 10% for Gram - bacteria to 90 % for Gram + bacteria [9].

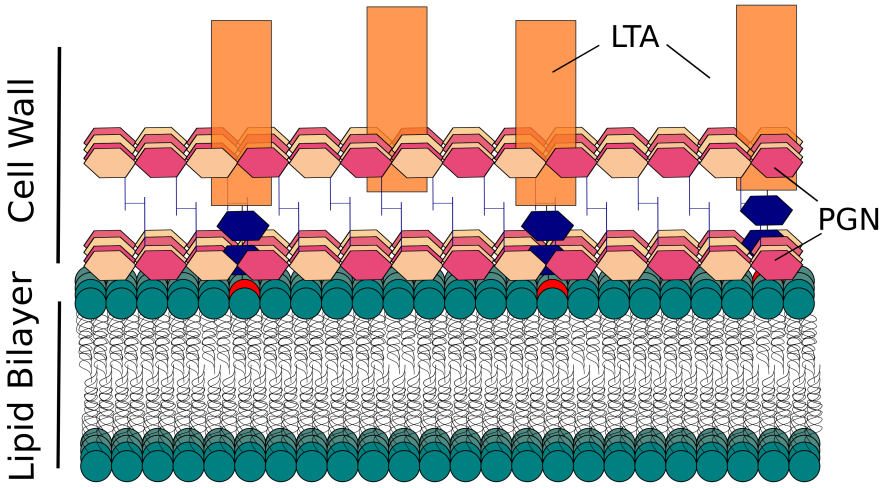

FIGURE 2.2: Schematic illustration of the Gram + cell wall and cell membrane. Lipid headgroups are represented by green circles, and hydrophobic acyl chains in black. The PGN structure is composed of alternating NAG-NAM (pink and beige) cross-linked by pentapeptide side chain in light blue. The LTA is represented as TA units, in orange, anchored to the cell membrane with two diglycosyl groups, in blue, and a glycolipid in red.

2.1.4 Teichoic Acid (TA)

Along with the PGN, teichoic acids (TAs) are an important part of the Gram + bacterial cell wall. Teichoic acids can be grouped into lipoteichoic acids (LTAs) and wall teichoic acids (WTAs). The main difference between LTA and WTA is that LTA is anchored to the cell membrane via a glycolipid while WTA is covalently anchored to the N-acetylmuramic acid (NAM) of the PGN [11, 12]. However, both LTA and WTA have positive and negatively charged groups, but, are overall negativelly charged [11]. LTAs and WTAs are usually both present at the same time and there is at least four different classes of teichoic acids. TAs consist of repeating units of water soluble polymers, which may vary in length between Gram + species [12]. In the case of *B. subtilis*, one of the bacterial strains used in my study, LTA is composed of 23 units of glycerol-phosphate, forming a polymer of approximately 4900 g/mol [13]. TAs are important for the bacterial shape and the regulation of cell division [12]. Unlike phospholipids, pure LTA in aqueous solution do not form stable monolayer structures but are able to form micellar structures [12].

In summary, Gram + and Gram - bacteria have a cytoplasmic membrane, which in both classes is the inner layer of the bacterial envelope. The cytoplasmic membrane is principally composed of lipids, mainly phospholipids, as well as sugars and proteins. Additionally, both classes of bacteria have a periplasmic space, which contains the PGN web. However, the outer envelope of Gram - bacteria is made of a single layer of PGN that makes the periplasmic space of Gram - bacteria smaller than the one in Gram +, which is made of many layers of PGN. Finally, the presence of an outer membrane in Gram - bacteria is another major difference between those bacterial types. The outer membrane is composed mainly of lipids in the internal leaflet and lipopolysaccharides in the outer leaflet.

2.2 Antimicrobial Peptides (AMPs)

All living creatures are in permanent contact with diverse types of microorganisms. Many of these microorganisms are pathogens, which means that these microorganisms can potentially cause infection and disease. Living organisms have developed different mechanisms to protect themselves from pathogenic microorganisms. One of those mechanisms is the production of AMPs.

AMPs are amino acid chains, i.e. polypeptides, of usually between 10 and 50 amino acids, with the ability to kill microbes. To date, over 3000 amino acid sequences have been identified or predicted to be AMPs [14]. Studies of AMPs have increased dramatically over the last 30 years. This is not surprising since there is a desperate interest to find novel antimicrobial agents in the face of the emergence of antibiotic resistant bacterial strains [15]. Research into AMPs includes discovery, characterization of their structure, design of new AMPs, and attempts to explain the mechanisms that AMPs use to kill bacteria.

As mentioned above, AMPs are one of the responses of the immune systems of different living organisms to pathogen threats. Some characteristics that most of the AMPs share are short amino acid chain length, positive overall charge, structures with both hydrophobic and hydrophilic sections and selectivity [16]. The amphiphatic characteristic of AMPs makes them prone to interact with the amphiphilic cytoplasmic membrane of bacteria. Selectivity in AMPs refers to their ability to inhibit the growth of pathogens at AMP concentrations that do not harm host cells [17]. Selectivity is commonly explained as a consequence of the positive charge of AMPs that allows them to bind to negatively charged bacterial membrane surfaces more strongly than to the host cells, which are usually neutral in charge [4].

Understanding the whole mechanism or mechanisms that AMPs employ to kill bacteria is imperative to full understanding of AMPs and, perhaps, to the use of AMPs as fully functional antibiotic replacements. Different aspects of AMPs have been studied in order to explore various hypotheses about AMP mechanisms. One approach has been to focus on the amino acid sequences (i.e. the primary structure) and secondary structures of AMPs, and on how specific AMP structures

are correlated with the effectiveness of such peptides. AMPs are diverse in amino acid sequence and secondary structure. AMPs with α-helix, β-sheet, random coil or disordered secondary structures can be commonly found, as well as peptides with cyclic sequences or even disulfide cross links [16, 18, 19]. The very diversity of AMP structures suggests that they may function via a range of mechanisms and that structure-function relationships might not be generalized across the vast number of AMPs [20–22].

Another aspect of AMPs that has been extensively studied is the permeabilizing effect that AMPs have on the lipid bilayer of the bacterial membrane [23]. The permeabilization is usually associated with the ability of AMPs to make pores and/or to cross the membrane lipid bilayer [24–27]. This permeabilizing effect on the lipid bilayer can rupture the bacterial membrane which can lead to cell disintegration, also known as lysis. There are a number of proposed models that may explain the permeabilizing effect of AMPs on the lipid bilayer [16, 23, 28, 29]. Those models can be separated into pore and non-pore models. Pore models state that once AMP monomers reach the lipid bilayer, they can generate membrane-spanning pores large enough to allow water and ions to exchange between the cell interior and exterior. Different shapes of pores have been proposed, such as toroidal or barrel stave pores. Non-pore models are more diverse. Most of them require high peptide concentrations over the membrane and propose various effects such as changes in the lipid packing, lipid clustering or even collapse of the lipid bilayer (See Figure 2.3). All of these models have been extensively studied in lipid bilayers composed of a small number of lipid types, that are highly simplified models of the cytoplasmic membrane of bacteria. Such studies generally support the conclusion that AMPs are able to compromise the lipid bilayer integrity, an activity that likely contributes to their abilities to kill bacteria .

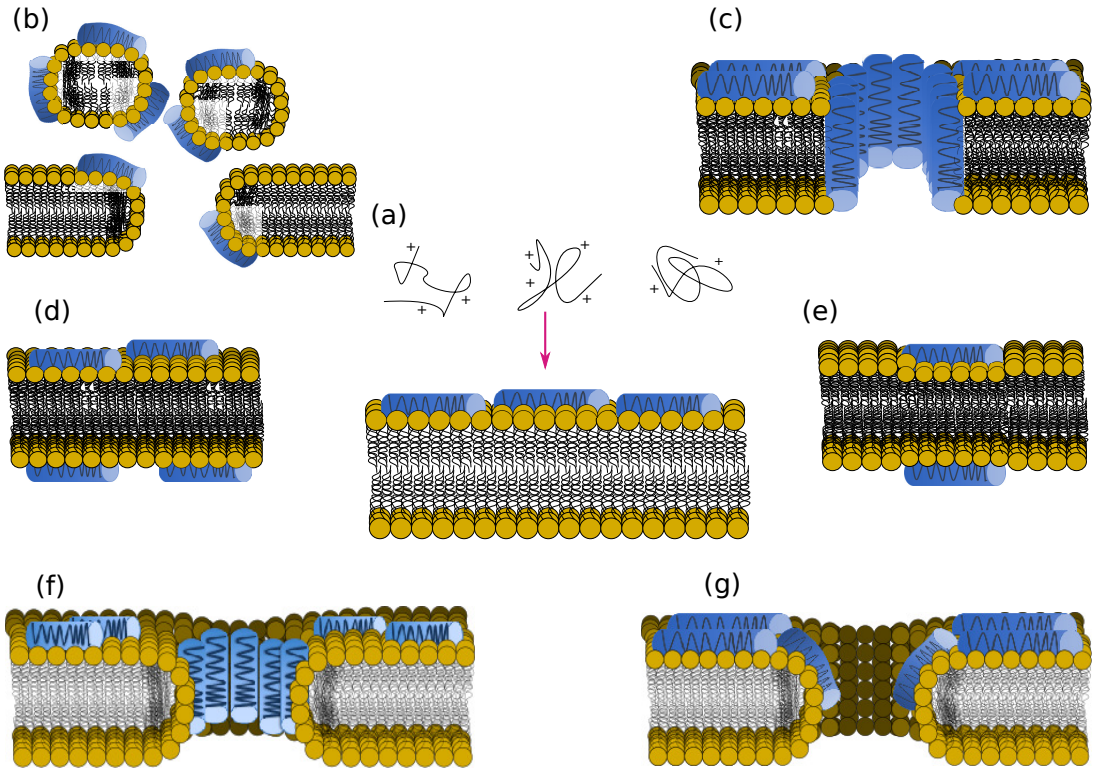

FIGURE 2.3: Collection of cartoons illustrating different models that could explain the permeabilizing effect of AMPs on lipid membranes. (a) Absorption of the AMP into the lipid membrane. (b) Carpet model. (c) Barrel stave model. (d) Translocation. (e) Membrane thinning. (f) Toroidal pore. (g) Disordered toroidal pore. Lipid headgroups are represented by yellow circles and hydrophobic acyl chains in black. In this picture, the same cationic AMPs are presented in two different ways: A disordered structure (just before absorption) represented as black curved lines, and α-helical structures (after absorption) represented by blue cylinders.

It is clear that the overall positive charge and the hydrophobic composition of AMPs underlie their ability to interact with negative lipid bilayers such as the cytoplasmic membrane of bacteria. However, recent studies have found evidence of AMPs translocating across the membrane and also interacting with other bacterial components that lie inside the cell, such as ribosomes, DNA, RNA, enzymes and chaperone proteins [29–32]. Such AMPs could be inhibiting cell wall synthesis, nucleic acid synthesis, protein synthesis and enzymatic activity, any of which could be lethal for bacteria [33]. Those findings make it necessary to re-evaluate whether the permeabilizing effect of the AMPs is the only mechanism that AMPs use to

kill bacteria or if the AMPs' permeabilizing effect is just one component of a multi-target mechanism for killing bacteria.

Some studies such as the one performed by He *et al.* in 2014 [34], have failed to detect a direct correlation between the lytic effect of AMP on lipid vesicles and AMP-induced cell death. Also, in 2006, William C. Wimley [16] pointed out the enormous difference between the peptide to lipid ratio in microbe sterilization experiments (as high as P:L=1000:1)[1], and in a typical vesicle leakage experiment (P:L=1:100). One possible explanation for this discrepancy could be that model systems, such as lipid vesicles, are an oversimplification of the bacterial cell envelope. Model systems lack important components of the bacterial membrane such as proteins embedded in the lipid bilayer, a peptidoglycan (PGN) layer and lipopolysaccharides (LPS). As a result, one new question arises: Are the non-lipid components of the bacterial cell envelope relevant for understanding AMPs' effects on the bacterial cell envelope's lipid bilayer?

It is thus necessary build a bridge that connects the historical work regarding AMPs interacting with model lipid bilayers to the relatively recent finding that at least some AMPs act on non-lipid targets. One approach is to extend the same techniques used to perform experiments in model systems to whole bacterial cells. That involves adapting those biophysical techniques for use in whole bacterial cells.

Biophysical techniques for studying membrane-peptide model systems are diverse and can be used to examine different characteristics of the AMP-lipid bilayer interactions. Neutron scattering, for example, is sensitive to changes in the scattering-length densities within the lipid bilayer, which means that it can be used to detect the presence of water molecules inside the lipid bilayer, especially if those molecules are passing through the bilayer due to the presence of a pore [35, 36]. X-ray crystallographic measurements can be used to determine the structure of the AMPs in different environments such as, for example, an oriented lipid bilayer [37]. Lamellar X-ray diffraction can be used to determine the distance between the

[1] Molar P:L were estimated from the literature. Calculations are explained in Appendix A

lipid headgroup phosphates located in different leaflets of the bilayer [26]. Small-angle X-ray scattering (SAXS) can be used to determinate lattice parameters and phase symmetry changes induced by the presence of AMPs [38].

Fluorescence microscopy and spectroscopy use different kind of probes, lasers, and forms of data acquisition. For example, fluorescent probes with high water solubility are often used to measure membrane leakage induced by AMPs [39]. Also, lipid mobility can be measured with techniques such as fluorescence recovery after photobleaching (FRAP) or single molecule tracking techniques [39]. Like FRAP, fluorescence correlation spectroscopy (FCS) can be used to measure the lateral diffusion of lipids. FCS measures the diffusion time of individual fluorescent molecules in a small volume [40]. The use of this technique in lipid bilayers in the presence of AMPs has helped to determine changes in the mobility of the lipids as a result of the presence of AMPs [25]. Circular dichroism (CD) is also a light spectroscopy technique and is commonly used to determine the secondary structure of peptides in general. In the case of AMPs, a change in the secondary structure is often observed when the peptide binds a lipid bilayer [41]. Atomic force microscopy (AFM) is a technique that can be used to get topological maps of supported lipid bilayers and to measure the force necessary to pierce the lipid bilayer with the cantilever tip [42]. In the presence of AMPs, the change in the integrity of the supported lipid bilayer can be observed [43].

For its part, Nuclear Magnetic Resonance (NMR) has found multiple applications in the study of AMPs and AMP-bilayer interactions. ^{1}H solution NMR, often in conjunction with ^{15}N NMR, can be used to determine the structure of AMPs [44]. ^{31}P NMR is sensitive to AMP-induced changes in the rate and symmetry of lipid motions in membranes and lipid structures [45]. ^{2}H NMR can be used to determine lipid membrane phases as well as changes in the lipid orientational order resulting from contact with AMPs [46].

As mentioned above, one of the ways to connect work on AMPs in model lipid systems with the real biological AMP/bacteria systems, is to translate these model system approaches to whole bacteria experiments. Translating these approaches, however, is usually not easy. Some of the techniques mentioned above can not be applied to whole bacteria systems because of the complexity of the cell itself, and

other techniques, like fluorescence microscopy and spectrometry, require the use of fluorescent probes, usually fluorescent molecules, that can disrupt the system under study. ^{2}H NMR is one of the techniques that can be performed in whole cells and just requires the replacement of the hydrogen atoms by deuterium atoms, which is a minimally perturbing probe. However, implementing ^{2}H NMR in whole cells is challenging.

Our lab and others have developed methods that promote the uptake of deuterated acyl chains into the bacterial membrane, resulting in a deuterium-rich lipid bilayer [1, 6–8]. These methods have been used so far with different mutated and unmutated bacterial strains. In this research, ^{2}H NMR experiments were performed to observe the changes in the lipid dynamics caused by the presence of two peptides: MSI-78 and BP100. More information about these peptides is presented next.

2.2.1 MSI-78

Magainin 1 and Magainin 2 belong to a family of peptides isolated from the skin of an African frog, *Xenopus laevis*, and reported in 1987 by Michael Zasloff [47]. MSI-78 (also called Pexiganan) is a synthetic analog of Magainin 2 with twenty-two (22) amino acids. The MSI-78 and Magainin 2 amino acid sequences are provided in Table 2.1. MSI-78 possesses more potent antimicrobial activities than Magainin 2 [48], but Magainin 2 and MSI-78 both have broad antimicrobial activity against Gram + and Gram - bacteria. ^{31}P-NMR experiments and differential scanning calorimetry (DSC) studies suggested changes on the curvature of lipid bilayers upon the addition of MSI-78. Those changes were consistent with the formation of toroidal pores similar to the pores formed by Magainin 2 [49]. MSI-78 reached phase III clinical trials as a treatment for infected foot ulcers affecting diabetic patients [50]. However, after approval for marketing, it was found that MSI-78 treatments did not prove to be more effective than treatments with regular antibiotics [51]. The MSI-78 story underlines the importance of better understanding how AMPs interact with pathogenic bacteria.

TABLE 2.1: Amino acid sequences and characteristics of AMPs used in this study, and selected related AMPs and toxin (Melittin). Blue color represents amino acids positively charged and red color represents amino acids negatively charged.

Peptide	Sequence	Net charge at pH 7	Non-polar amino acids	Polar, uncharged amino acids
Magainin 2	GIGKFLHSAKKFG KAFVGEIMNS-NH_2	+5	14	3
MSI-78	GIGKFLKKAKKF GKAFVKILKK-NH_2	+10	13	0
BP100	KKLFKKILKYL-NH_2	+6	5	1
CAME	KWKLFKKIGIGAVL KVLT -NH_2	+6	12	1
Cecropin A	KWKLFKKIEKVGQ NIRDGIIKAGPAVA VVGQATQIAK-NH_2	+7	22	5
Melittin	GIGAVLKVLTTGLP ALISWIKRKRQQ-NH_2	+6	16	5

2.2.2 CAME and BP100

Cecropins are a family of peptides that are part of the immune system of insects. In particular, cecropin A was isolated for the first time in 1981 when H. Steiner *et al.* found it in the immune system of the cecropia moth [52]. Cepropin A has thirty seven (37) amino acids that are separated into two domains. The N-terminal domain forms an amphipathic α-helix, while the C-terminus forms a hydrophobic helix [53].

Melittin is a bee venom toxin composed of twenty six amino acids. The initial studies about melittin were published in Germany in the 1960's [54–56]. In contrast to cecropins, melittin has a hydrophobic N-terminus and a basic C-terminus [53].

Although melittin's antimicrobial effect is well known, melittin has a toxic effect that arises from its ability to lyse, i.e break open, red blood cells.

Chimeric peptides of cecropin A and melittin were designed to increase the antimicrobial effect of cecropin A, while at the same time counteracting the toxic effect of melittin [53]. Hybrids of cecropin A and melittin are most commonly formed with the first half of cecropin A linked to the first half of melittin. The initial designed hybrids were approximately twenty six residues, while subsequent hybrids were considerably smaller ($\sim$ 11 residues) [57]. CAME and BP100 are both chimeric peptides from cecropin A and melittin. Due to its short amino acid sequence, low cytotoxicity, low susceptibility to protease degradation, and effectiveness against plant pathogenic bacteria such as *Erwinia amylovora* [58, 59], BP100 has potential to treat multiple plant diseases caused by pathogens at a moderate cost [60]. Biophysical studies revealed some details about the membrane permeabilizing effect caused by BP100 in model membranes. BP100 has a strong selectivity toward negatively charged lipids and it is able to translocate across lipid bilayers at both high and low peptide/lipid ratios [60]. The effect of BP100 on the membrane of *E. coli* was studied using AFM and zeta potential measurements. It was found that BP100 is able to cause major damage to the bacterial envelope [61].

2.3 Nuclear Magnetic Resonance

The lipid bilayer of the cell membrane is one of the meeting points between physical and biological sciences. Understanding its structure and dynamics is key to revealing the membrane's biological functions at a molecular level. One of the biophysical techniques that allows dynamical properties of lipid bilayers to be studied without employing labels that may perturb the membrane is ^{2}H NMR.

Nuclear magnetic resonance arises when magnetic nuclei are manipulated by application of a radio frequency magnetic field oscillating at a specific frequency appropriate to the nucleus and applied static field. For ^{2}H NMR of lipid bilayers, the hydrogen atoms of the lipid's acyl chains are replaced by deuterium atoms, which have spin 1 nuclei (See Figure 2.4). This replacement allows measurement of a particular spectral parameter, the quadrupolar splitting, for those deuterium

atoms attached to molecular segments undergoing anisotropic reorientations. As a result of the proportionality between the quadrupolar splitting and an acyl chain segment property known as the orientational order parameter, ^{2}H NMR is sensitive to the molecular order and motion of the lipid's acyl chains in a lipid bilayer or a cell membrane [5, 62]. In particular, ^{2}H NMR can be used to measure the AMP-induced changes in the distribution of quadrupolar splitting, and thus of orientational order, along the acyl chain. These changes, in turn, reflect changes in the physical state of the membrane lipid bilayer.

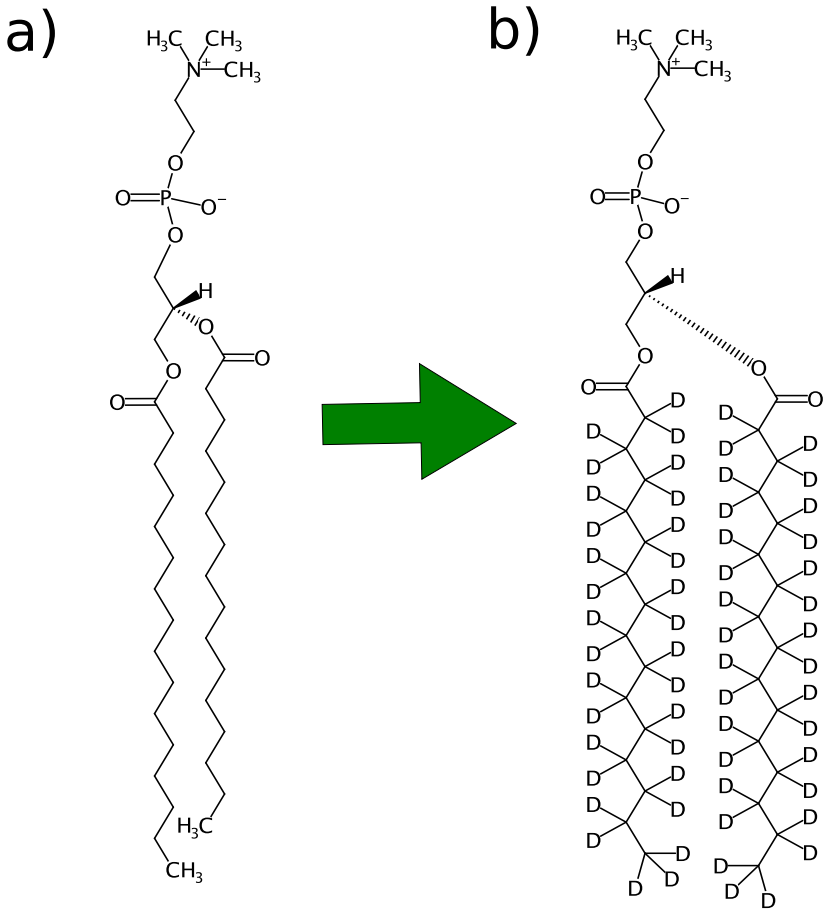

FIGURE 2.4: 1,2-dipalmitoyl-sn-glycero-3-phosphocholine (DPPC) or 16:0 PC, structure. a) DPPC is a saturated lipid whose fatty acyl chains are 16 carbons in length. b) DPPC-d_{62} is a saturated lipid whose fatty acyl chains are 16 carbons in length and whose acyl chain hydrogen atoms have been replaced with deuterons.

The theoretical background needed to understand quadrupolar splitting, as well as the powder pattern lineshapes and their interpretations, follows.

2.3.1 Deuterium Nuclear Magnetic Resonance

The NMR resonance frequencies satisfy the Planck equation

$$\Delta E = h\nu \tag{2.1}$$

where, in this system, ΔE is the difference between spin state energies of the target nucleus in the applied magnetic field, h is the Planck constant and ν is the resonance frequency. Getting the energies of the system involves solving the time independent *Schrödinger* equation.

The deuterium nucleus, known as a deuteron, consists of one proton and one neutron and thus is a spin 1 particle. As a result, it can exist in one of three states corresponding to $m = -1$, $m = 0$, or $m = +1$. Because of selection rules, the allowed transitions are only between adjacent levels so that $\Delta m = \pm 1$. For a deuterium nucleus in a C-D bond in the presence of an external magnetic field ($\vec{B}$), the Hamiltonian that describes its allowed energy levels can be written as the sum of Hamiltonians for the significant interactions as:

$$\hat{H} = \hat{H}_o + \hat{H}_Q + \hat{H}_{CS} + \hat{H}_D \tag{2.2}$$

where $\hat{H}_o$ is the Hamiltonian due to the Zeeman interaction, $\hat{H}_Q$ is the electric quadrupolar interaction Hamiltonian, $\hat{H}_{CS}$ is the Hamiltonian due to the anisotropic chemical shift interaction, and $\hat{H}_D$ is the Hamiltonian due to the dipolar interaction that arises from the interaction between two magnetic dipole moments.

The significance of each interaction is decided by its magnitude relative to the quadrupolar coupling. The maximum quadrupolar splitting value for a deuterium nucleus in a static C-D bond is 250 kHz, the chemical shift interaction for a deuterium nucleus is $\sim$ 1 kHz, and the frequency for the dipolar interaction between two deuterium nuclei is $\sim$ 4 kHz. As a result, the chemical shift interaction and the dipolar interactions can be neglected, [62], and the equation 2.2 can be written as:

$$\hat{H} = \hat{H}_o + \hat{H}_Q \tag{2.3}$$

[63]. The eigenvalues for the Zeeman Hamiltonian, $\hat{H}_o$, can be written as

$$E_m^Z = -gm\beta_N B \tag{2.4}$$

where B, is the magnitude of the external magnetic field $\vec{B}$, g is the gyromagnetic factor, β_N the nuclear magneton, and m is the magnetic quantum number.

As described by Davis in 1983 [62] and Seelig in 1977 [63], the eigenvalues for the electric quadrupole Hamiltonian, E_m^Q, can be written as

$$E_m^Q = \frac{e^2qQ}{4I(2I-1)}\left[3m^2 - I(I+1)\right]\left[\left(\frac{3\cos^2(\beta')-1}{2}\right) + \frac{\eta}{2}\sin^2(\beta')\cos(2\alpha)\right] \tag{2.5}$$

where eq is the magnitude of the C-D bond electric field gradient at the nucleus, eQ is the electric quadrupole moment of the deuteron, I is the spin quantum number and η is the asymmetry parameter. The orientation of the C-D bond, in the frame of reference of the electric field gradient tensor principal axis system, is defined by β' and α. β' is the angle between the C-D bond vector and the direction of the magnetic field $\vec{B}$ (along the z axis) and α is the angle between the projection of the C-D bond vector onto the x-y plane and the y axis (See Figure 2.5). So, the total energy E_m for the quadrupolar and the Zeeman interaction $(\hat{H}_o + \hat{H}_Q)$ is:

$$\begin{aligned} E_m &= -gm\beta_N B + \frac{e^2qQ}{4I(2I-1)} \times \\ &\quad \left[3m^2 - I(I+1)\right]\left[\left(\frac{3\cos^2(\beta')-1}{2}\right) + \frac{\eta}{2}\sin^2(\beta')\cos(2\alpha)\right] \end{aligned} \tag{2.6}$$

[62]. The selection rule for transitions between spin states only allows $\Delta m = \pm 1$ so the allowed transitions are

$$h\nu_+ = E_{-1} - E_0 \tag{2.7}$$

$$h\nu_- = E_0 - E_1. \tag{2.8}$$

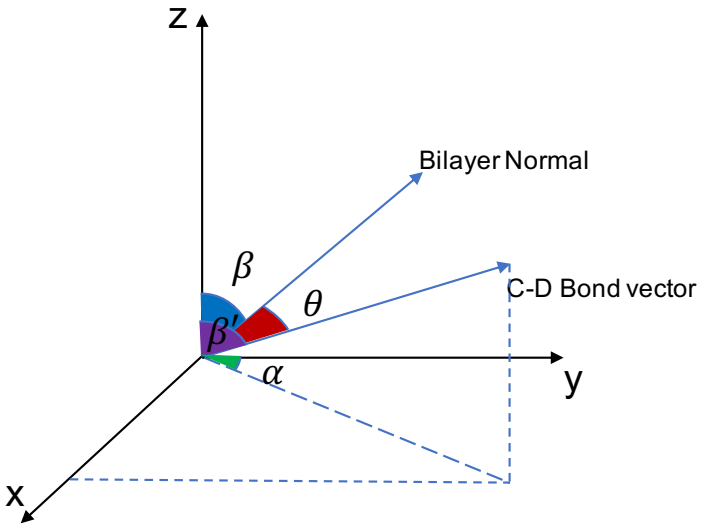

FIGURE 2.5: Schematic representation of the orientation of the bilayer normal and the C-D bond orientation in the x, y, and z plane. β defines the angle between the magnetic field (z axis) and the bilayer normal. θ defines the angle between the bilayer normal and the C-D bond vector. β' defines the angle between the magnet field and the C-D bond vector, and α defines the angle between the projection of the C-D bond vector onto the x-y plane and the y axis.

The corresponding transition frequencies are

$$\nu_{\pm} = \underbrace{\frac{g\beta_N B}{h}}_{\nu_o} \pm \underbrace{\frac{3e^2qQ}{4h}\left[\left(\frac{3\cos^2(\beta')-1}{2}\right)+\frac{\eta}{2}\sin^2(\beta')\cos(2\alpha)\right]}_{\frac{\Delta\nu_Q}{2}} \tag{2.9}$$

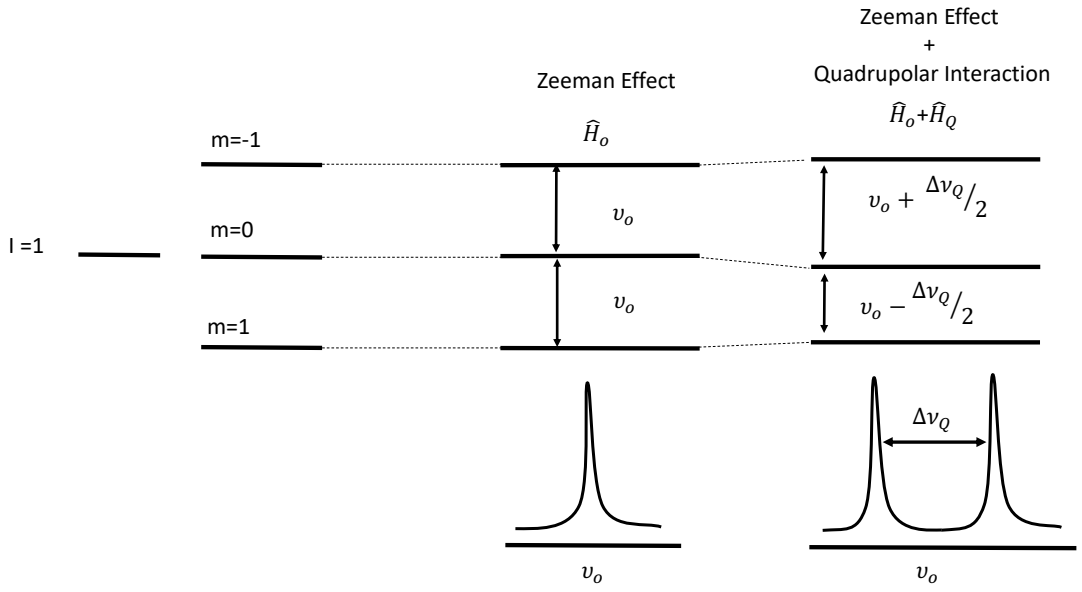

FIGURE 2.6: Schematic representation of the Zeeman effect and the Zeeman effect plus quadrupolar interaction on energy levels of the deuterium nucleus and on the resulting ^{2}H NMR spectra.

[63]. Both ν_+ and ν_- are composed of two terms. The first one arises from the Zeeman effect, ν_o, and the second one is from the quadrupolar interaction, $\Delta\nu_Q$. The Zeeman effect alone generates a single peak centred at ν_o, the Larmor frequency. The Zeeman effect plus the quadrupolar interaction however, generates two peaks centered at frequencies $\nu_o \pm (\Delta\nu_Q)/2$ (See Figure 2.6). The difference between ν_+ and ν_-, $\Delta\nu_Q$, is the quadrupolar splitting and is given by

$$\Delta\nu_Q = \frac{3e^2qQ}{2h}\left[\left(\frac{3\cos^2(\beta')-1}{2}\right)+\frac{\eta}{2}\sin^2(\beta')\cos(2\alpha)\right], \tag{2.10}$$

where e^2qQ/h is called the quadrupolar coupling constant and is 167 kHz for C-D bonds [64]. Because the electric field gradient for C-D bonds is nearly symmetric with respect to the bond direction, the asymmetry parameter, η, is approximately zero ($\eta \sim 0$) and equation 2.10 can be rewritten as

$$\Delta\nu_Q = \frac{3e^2qQ}{2h}\left(\frac{3\cos^2(\beta')-1}{2}\right). \tag{2.11}$$

For the case of a deuterium atom in a C-D bond, the primary contributions to the electric field gradient are due to the molecular electronic distribution. Because of that, the angles β' and α change as a result of molecular motion. For fluid phase bilayers, those motions occur on a timescale short in comparison with $1/\Delta\nu_Q$ so the observed quadrupolar splitting will be an average over molecular reorientations as follows

$$\langle \Delta\nu_Q \rangle = \frac{3e^2qQ}{2h} \left\langle \frac{3\cos^2(\beta') - 1}{2} \right\rangle . \tag{2.12}$$

Because the C-D bond is attached to the lipid's acyl chains in a lipid bilayer and the lipid bilayers are structures with a specific symmetry, a change in the frame of reference is helpful. The frame of reference so far is the electric field gradient tensor principal axis system, which describes the system in spherical coordinates with the angles defined above. The change in the frame of reference is accomplished with the Wigner rotation matrices and corresponds to the separation of β' into two angles: the angle between the bilayer normal with respect to the z axis, β, and the angle of the C-D bond vector with respect to the bilayer normal, θ. In terms of the angles β and θ, the quadrupolar splitting is expressed as

$$\Delta\nu_Q = \frac{3e^2qQ}{2h} \left(\frac{3\cos^2(\beta) - 1}{2} \right) \left\langle \frac{3\cos^2(\theta) - 1}{2} \right\rangle . \tag{2.13}$$

The averaged factor in equation 2.13 depends on the amplitude of motion for the C-D bond with respect to the bilayer normal. The distribution of β depends on sample geometry. In the case of unilamellar or multilamellar vesicles, the bilayer normals are randomly oriented and β will range between 0° and 90°, where 0° represents lipids in bilayers with normals oriented parallel or antiparallel to the magnetic field (i.e. toward the poles of a spherical distribution of directions) and 90° represents lipids in bilayers with normals oriented perpendicular to the magnetic field (i.e. toward the equator of a spherical distribution of directions). Because a random distribution of bilayer normal directions is more heavily weighted toward equatorial orientations, a largest intensity is expected for splittings corresponding to $\beta = 90°$. As a result, the ^{2}H NMR spectrum has a characteristic line shape known as Pake doublet that is shown in Figure 2.7. Notice that the Pake doublet in this figure, like all of the ^{2}H NMR spectra shown in this thesis, is plotted so that the center of the spectrum (ν_0) corresponds to zero frequency. Each branch

can be described by the function [62]

$$f(x) = \frac{1}{\sqrt{6}}\left[\frac{1}{(1/2+x)^{1/2}} + \frac{1}{(1/2-x)^{1/2}}\right] \qquad 0 \leq |x| < 1/2$$
$$= \frac{1}{\sqrt{6}}\frac{1}{(1/2+x)^{1/2}} \qquad 1/2 \leq |x| \leq 1 \tag{2.14}$$

with $x = 2\nu/\Delta\nu_Q$. The spectrum is symmetric about the origin when both branches are included.

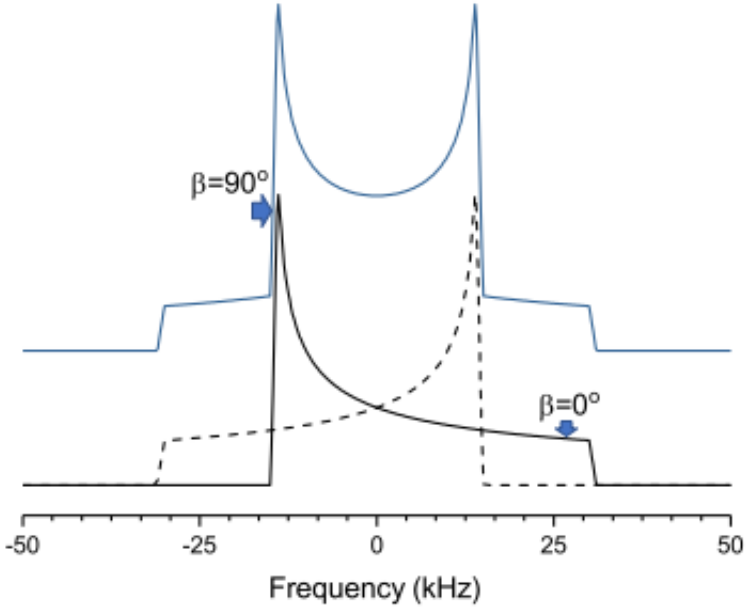

FIGURE 2.7: Schematic representation of the powder pattern spectrum of a vesicle with a unique C-D bond. The black lines represent the separation of the powder spectrum in two branches (one solid and one dashed) corresponding to the two deuteron transitions. The blue line is the sum of the two peaks which results in the powder pattern spectrum of a C-D bond.

Equation 2.13 can be written as

$$\Delta\nu_Q = \frac{3e^2qQ}{2h}\left(\frac{3\cos^2(\beta)-1}{2}\right)S_{CD} \tag{2.15}$$

where S_{CD}, the orientational order parameter for the C-D bond, is given by

$$S_{CD} = \left\langle \frac{3\cos^2(\theta) - 1}{2} \right\rangle . \tag{2.16}$$

The average in equation 2.16, is over reorientations of the C-D bonds with respect to the bilayer normal, i.e. axially symmetric motions, occurring during the timescale of the measurements (timescale shorter than $1/\Delta\nu_Q$). S_{CD} scales the splitting of the Pake doublet spectrum.

The amphiphilic nature of lipids determines their natural dynamics. In fluid or liquid crystalline phase bilayers, acyl chain carbons close to the polar head group tend to have a movement with smaller amplitude than the ones at the middle of the lipid bilayer. This behavior leads to larger orientational order parameters on C-D bonds close to the head group in comparison with C-D bonds close to the ends of the acyl chains. In vesicles with randomly oriented bilayers of chain-perdeuterated lipids, the ^{2}H NMR spectrum has the shape shown in black inside the red square of Figure 2.8. This is a superposition of Pake doublets with splittings for each acyl chain segment, ranging from larger values corresponding to chain segments near the lipid headgroup, to smaller values for segments near the chain ends. The purple spectrum inside the red square of Figure 2.8 is the result of transforming (dePaking) the "powder" spectrum to obtain the spectrum that would have been obtained if all of the bilayer normals had been aligned perpendicular to the magnetic field. Notice that the quadrupolar splittings, $\Delta\nu_Q$, of the first five C-D bonds are very similar.

The orientational order profile of a lipid assembly is the set of orientational order parameters corresponding to the different segments on the lipid acyl chains plotted as a function of the position along the chain. It can be obtained from the spectra of specifically deuterated phospholipids [65] or an approximation can be obtained from an oriented ^{2}H NMR spectrum or a dePaked spectrum [66]. Due to the proportionality between the orientational order parameter, S_{CD}, and the quadrupolar splitting, $\Delta\nu_Q$, the orientational order parameter for each carbon position, $S_{CD}(n)$, can be extracted from the quadrupolar splitting of each doublet. A sample order profile obtained from the dePaked spectrum of DPPC-d_{62} at 42° C from Figure 2.8 is shown in Figure 2.9. In the dePaked spectrum shown in

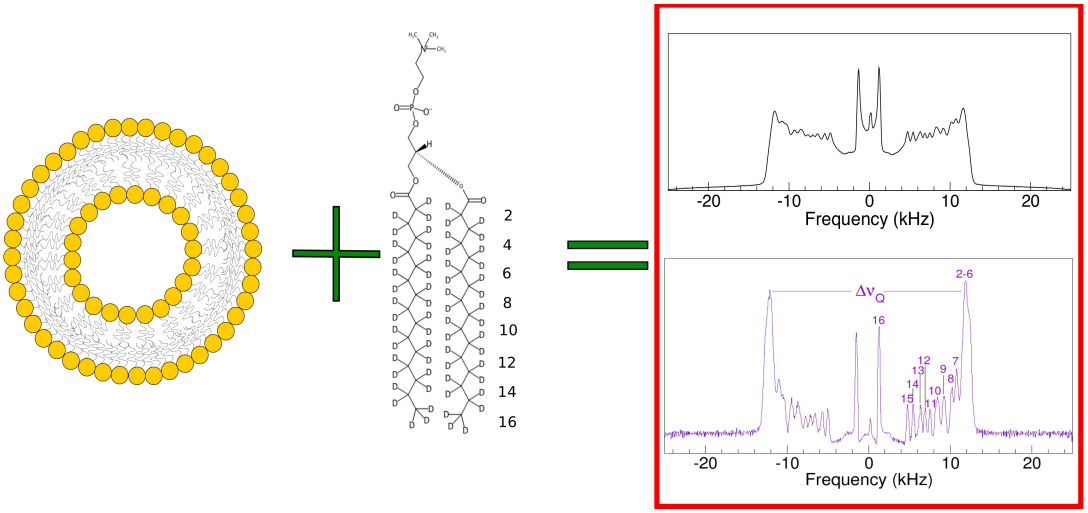

FIGURE 2.8: Schematic representation of the powder pattern spectrum (black) and the dePaked spectrum (purple) of a vesicle sample with multiple C-D bonds (miltilamellar vesicles of DPPC-d_{62} at 42° C prepared as explained in section 3.7). Larger splittings represents the C-D bonds closer to the lipid head groups. Numbers in the figure indicate the deuterated chain segment corresponding to each peak in the spectrum.

Figure 2.8, the doublets from segments 7-16 are resolved. Doublets from segments 2-6, on the other hand, have very similar splittings values. Thus, splittings for C-D bonds close to the headgroup are unresolved and form a constant line, in the order parameter profile, that is referred as the "plateau" region and is shown by the box in Figure 2.9. It should be noted that the orientational order parameter of chain segments in the plateau region are approximated as being constant due to the corresponding doublets being unresolved. In fact, specific labeling shows that the splittings for deuterons of carbon two can be smaller than for deuterons on other chain segments so that the actual profile is not flat in the plateau region [65].

2.3.2 Understanding ^{2}H NMR Spectra of Bacterial Membranes

As explained above, model system studies are typically intended to mimic the cytoplasmic membrane of bacteria, but the diversity of lipid headgroups and acyl chains in cell membranes makes this very difficult. In the case of ^{2}H NMR model

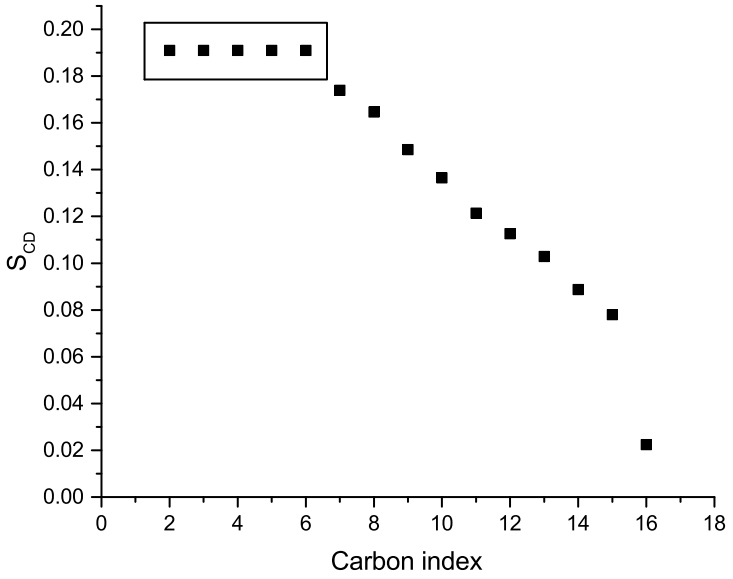

FIGURE 2.9: Order parameter profile of DPPC at 42° C (Obtained from multilamellar vesicles of DPPC-d_{62} prepared as explained in section 3.7). The box indicates the plateau region.

studies, perdeuterated phosphatidylcholines (PC) with zwitterionic head groups are often mixed with negatively charged phosphatidylglycerol (PG) in different proportions in order to mimic the intrinsic negative charge of the bacterial membrane. Additionally, different model membranes can be employed, for example, multilamellar vesicles, mechanically-oriented bilayers or magnetically-oriented bicelles.

Unlike single-component model membranes, where all lipid molecules undergo the same motions, bacterial membranes have a complex composition. Additionally, deuterium-labeling techniques can not guarantee the same lengths for all the deuterated acyl chains on the lipids. As a result, spectra of membrane deuterated bacteria do not display individual doublets that can be assigned to particular C-D bonds undergoing axially symmetric reorientations (See Figure 2.10) but rather, show a lineshape that is a function of the distribution of splittings. Nonetheless, the spectral lineshape does allow identification of quadrupolar splitting values for some of the C-D bonds close to the head group that give rise to the plateau in the orientational order parameter profile for bilayer lipids. This can be observed in

the ^{2}H NMR spectrum of bacterial samples as prominent edges (p in Figure 2.10). Additionally, the end of the acyl chain can be recognized by the methyl peak (m in Figure 2.10). Because of the natural amount of deuterium in water and the low signal available from deuterated bacterial membranes, it is normal to also see a narrow water peak at the centre of the spectrum (w in Figure 2.10).

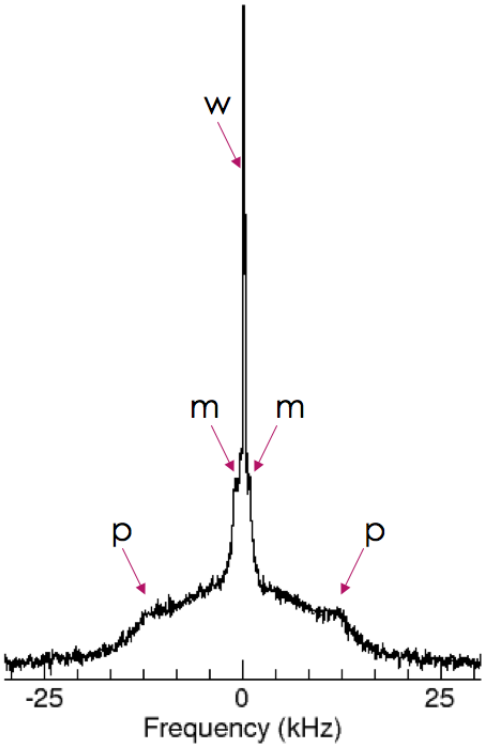

FIGURE 2.10: ^{2}H spectrum of *E. coli* enriched with deuterated acyl chains. Arrows to indicate: the prominent edges (p) that correspond to the quadrupole splitting of C-D bonds close to the lipid's head group, methyl deuteron doublet (m) that corresponds to quadrupole splitting of C-D bonds close to the center of the lipid bilayer, and the water peak (w).

Prominent edges help to define the plateau region in the orientational order parameter. From them, Stockton *et al.* [67] and Davis *et al.* [68] reported $(S_{CD})_{\text{plateau}}$ values of approximately 0.2 for *Acholeplasma laidlawii* at 42° C and 0.26 for *E. coli* L51 at 37° C respectively. $(S_{CD})_{\text{plateau}}$ values of ~ 0.2 were reported for 1,2-dilauroyl-d_{46}-sn-glycero-3-phosphocholine (DLPC-d_{46}) at 30° C, 1,2-dimyristoyl-d_{54}-sn-glycero-3-phosphocholine (DMPC-d_{54}) at 30° C, DPPC-d_{62} at 50° C and 1,2-distearoyl-d_{70}-sn-glycero-3-phosphocholine (DSPC-d_{70}) at 65° C by Petrache *et al.* in 2000 (See Figure 2.11), [69]. Thus, considering that the liquid crystal-gel phase transition temperature for pure DLPC is -2° C, pure DMPC is 24° C, pure

DPPC is 41° C and pure DSPC is 55° C, $(S_{CD})_{\text{plateau}}$ values of ~ 0.2 are typical of phospholipid liquid-crystalline phase.

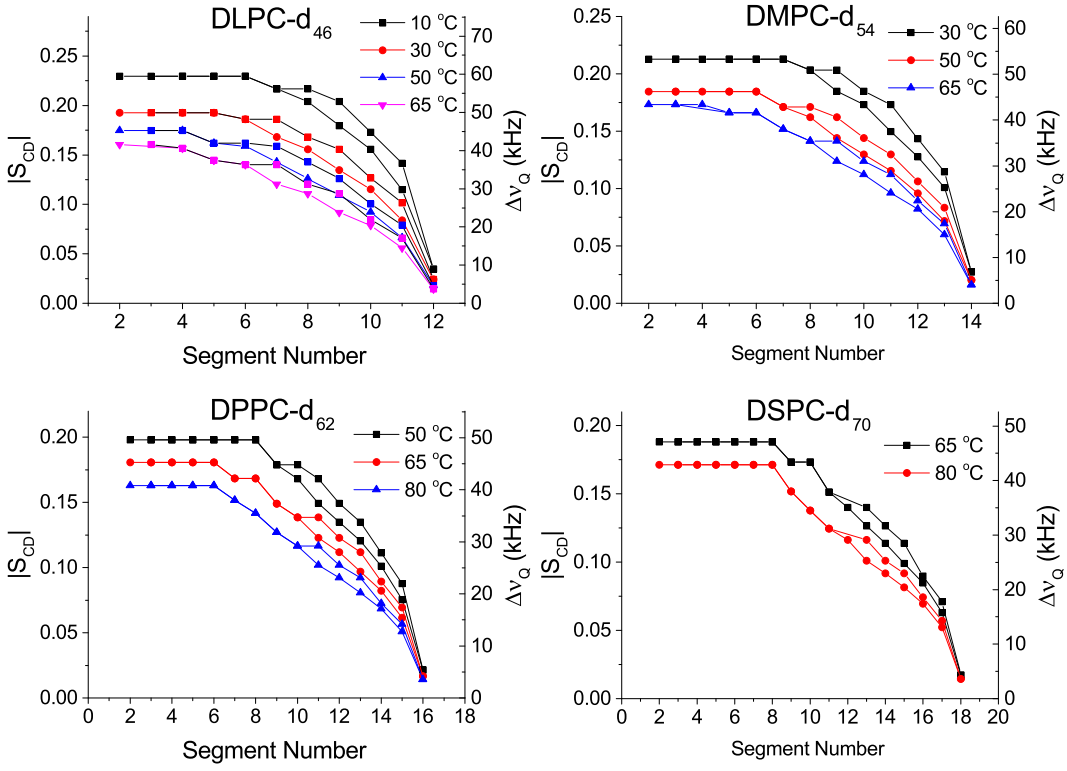

FIGURE 2.11: Order parameter profile obtained from the dePaked ^{2}H NMR spectra of DLPC-d_{46}, DMPC-d-$_{54}$, DPPC-d_{62} and DSPC-d_{70} at different temperatures. Data for sn-1 and sn-2 chains are shown separately. Order parameter profiles obtained from the $\Delta\nu_Q$ values reported in *Area per Lipid and Acyl Length Distributions in Fluid Phosphatidylcholines Determined by ^{2}H NMR Spectroscopy, Biophys. J. 79: 3172-3192.* by Petrache, H.I., S.W. Dodd, and M.F. Brown [69]. Used with permission.

A high signal-to-noise ratio in a spectrum indicates high levels of deuterated acyl chains being incorporated into the lipids of the bacterial membrane. It is thus useful to compare the intensity of the spectra. However, to compare the shape of the spectra it is often clearer to compare spectra that have been normalized by area. Hence, in this thesis, each ^{2}H NMR spectrum is presented in its normalized (spectra normalized by area) and unnormalized (absolute intensity spectra) form.

2.3.2.1 Moment Analysis

One way to quantify the spectral shape and the changes to spectral shape caused by AMPs is through moment calculation. In principle, the information contained in the moments is sufficient to fully characterize a distribution function. The nth moment of a distribution with lineshape function ($f(x)$) of a variable x is defined as

$$\langle x^n \rangle = \frac{\int_{-\infty}^{\infty} x^n f(x) dx}{\int_{-\infty}^{\infty} f(x) dx}. \tag{2.17}$$

where n are integer values. The first moment ($n = 1$) represents the mean of the distribution and the second moment ($n = 2$) represents the mean square of the distribution. Moments can also be calculated about some fixed point x_0 for example the mean of the distribution, in which case they are named central moments and are defined as

$$\langle (x - \bar{x})^n \rangle = \frac{\int_{-\infty}^{\infty} (x - \bar{x})^n f(x) dx}{\int_{-\infty}^{\infty} f(x) dx}. \tag{2.18}$$

The second central moment, is perhaps the most important central moment because it represents the variance of the distribution [70].

The nth moment of a spectrum with a lineshape function ($f(\omega)$) of the angular frequency (ω) with respect to the Larmor angular frequency (ω_0), $\omega - \omega_0$ (for simplicity called ω), is defined as [62, 68, 71]:

$$\widetilde{M_n} = \langle \widetilde{\omega^n} \rangle = \frac{\int_{-\infty}^{\infty} \omega^n f(\omega) d\omega}{\int_{-\infty}^{\infty} f(\omega) d\omega} \tag{2.19}$$

Due to the symmetry of the ^{2}H NMR spectrum, all odd moments will tend to zero. Redefining the limits of the moments calculation to avoid symmetry with respect to the Larmor angular frequency, ω_0, allows the use of the odd and even moments [62, 68]. Redefined moments are then

$$M_n = \langle \omega^n \rangle = \frac{\int_0^\infty \omega^n f(\omega) d\omega}{\int_0^\infty f(\omega) d\omega}. \tag{2.20}$$

The purpose of calculating the moments of the ^{2}H NMR spectra of bacteria is to characterize the distribution of splittings. In the liquid crystalline phase, where the C-D bonds are undergoing axial symmetrical movements, moments also characterize the distribution of order parameters [68].

Because the quadrupolar splittings are much larger than the linewidth of the spectrum, the moments M_n ($\langle \omega^n \rangle$) from $f(\omega)$ are proportional to $\langle \Delta\nu_Q^n \rangle$ and $\langle S_{CD}^n \rangle$, the moments of the distribution of quadrupolar splitings, $f(\Delta\nu_Q)$, and the moments of the order parameter distribution, $f(S_{CD})$, respectively

$$M_n = \langle \omega^n \rangle = A_n (2\pi)^n \langle \Delta\nu_Q^n \rangle = A_n \frac{3}{4} \left(\frac{2\pi e^2 qQ}{h} \right)^n \langle S_{CD}^n \rangle. \tag{2.21}$$

The coefficients A_n are a result of the axially symmetric lineshape function of the Pake doublet 2.14 [62] where, for example, $A_1 = (2/(3\sqrt{3}))$ and $A_2 = (1/5)$. The moments of the order parameter distribution ($\langle S_{CD}^n \rangle$) and the moments of the distribution of quadrupolar splittings ($\langle \Delta\nu_Q^n \rangle$) can be defined using equation 2.18.

There is thus a proportionality between the means of the angular frequency with respect to the Larmor frequency, quadrupolar splitting and order parameter distributions. The parameter Δ_2 is defined as the relative mean square width of the distribution of order parameters, or

$$\Delta_2 = \frac{\langle S_{CD}^2 \rangle - \langle S_{CD} \rangle^2}{\langle S_{CD} \rangle^2}. \tag{2.22}$$

Notice that Δ_2 is the second central moment or variance of the order parameter distribution divided by the squared mean order parameter. Δ_2 can also be defined in terms of $\langle \Delta\nu_Q \rangle$ and $\langle \Delta\nu_Q^2 \rangle$ or M_1 and M_2 as [68, 71].

$$\Delta_2 = \frac{\langle \Delta\nu_Q^2 \rangle - \langle \Delta\nu_Q \rangle^2}{\langle \Delta\nu_Q \rangle^2} = \frac{M_2}{1.35(M_1)^2} - 1 \tag{2.23}$$

Δ_2 gives the relative mean square width of the distribution of quadrupolar splittings. In particular, $\Delta_2 = 0$ for a powder pattern spectrum of a vesicle with a unique quadrupolar splitting value for each C-D bond, such as would be the case for the spectrum shown in Figure 2.8. Larger values of Δ_2 indicate wider ranges of $\Delta\nu_Q$ with respect to $\langle\Delta\nu_Q\rangle$. In other words, changes in Δ_2 values can be interpreted as changes in membrane heterogeneity [71].

Moment analysis provides a useful characterization of spectral shape and thus of the symmetry and amplitude of chain motions. Notice, however, that the strict proportionality of the moments of the angular frequency distribution to the moments of the order parameters distribution is restricted to lipid bilayers in the liquid crystalline phase when the ^{2}H NMR spectrum is the superposition of powder patterns with a zero asymmetry parameter η.

2.3.2.2 Kurtosis

The fourth central moment or kurtosis (Δ_4) is a measurement commonly used to compare the weight of the tails and the peakedness of the distribution with the normal distribution [72]. Since the changes induced in the ^{2}H NMR spectra of bacteria includes a change in the peakedness, it may be interesting to study the possible changes in kurtosis generated by the AMPs in future studies. However, it is possible that the noise of the spectra will interfere with the fourth moment calculation, meaning that some testing might be needed before trying to use such an approach.

2.4 Research Approach

The main goal of this project was to determine if the peptidoglycan layer, one of the non-lipid components of the bacterial cell envelope, is relevant for understanding AMPs' effects on the bacterial cell envelope. To do so, four objectives were defined. The first objective was to characterize the ^{2}H NMR spectrum of *B. subtilis*, since this was the first time Gram + bacteria were probed with this method, and to demonstrate reproducibility (Section 4.3). The second objective

was to study the changes in the *B. subtilis* ^{2}H NMR spectra in the presence of different concentrations of MSI-78 and BP100 (Chapter 5). The third objective was to explore possible changes in the *B. subtilis* ^{2}H NMR spectra caused by the partial or complete removal of the PGN layer (Section 6.1.1). Finally, the fourth objective was to study the ^{2}H NMR spectra of *B. subtilis* with a compromised PGN layer in the presence of BP100 and MSI-78 (Section 6.2).

Chapter 3

Materials and Methods

Because the natural amount of deuterium present in lipids is not enough to perform ^{2}H NMR experiments, our group and others have developed protocols to introduce deuterated acyl chains into the cell envelope lipid bilayer of intact bacteria [1, 6–8]. There are different strategies to maximize the proportion of lipids with deuteration in the membranes. The Pius *et al.*. [6, 7] protocol uses mutated bacteria unable to metabolize and/or synthesize fatty acids. As a result of the mutation, this bacteria needs fatty acids in the growth media to be viable and thus membrane deuteration can be achieved by providing deuterated fatty acids in the media. The Tardy-Laporte *et al.* protocol [1] employs non-mutated bacteria grown in media supplemented with deuterated fatty acids complexed with detergent micelles. Detergent micelles help to increase the uptake of acyl chains by the cells, allowing them to be incorporated in the cell envelope lipid bilayer. In this project both the Pius *et al.* protocol and a slightly modified version of Tardy-Laporte *et al.* protocol [8] were used. For simplicity henceforth, our modified version of the Tardy-Laporte *et al.* method will be referred to as "UB (Unmutated Bacteria) method" and the Pius *et al.* as "MB (Mutated Bacteria) method".

This chapter includes the protocols to achieve a deuterium-rich membrane in three bacterial strains, which require individualized growth conditions, as well as how to treat bacteria with AMPs, partially remove the PNG layer in *Bacillus subtilis*, perform Gram staining and extract lipids from bacteria. Additionally, the protocol to prepare multilamellar vesicles with perdeuterated lipids that were used

in Figures 2.9 and 2.8 is described. Finally, the procedure to perform ^{2}H NMR measurements is also detailed.

3.1 Media Preparation

The media preparation protocols below have been previously published as part of Santisteban *et al.* [8] .

3.1.1 Medium 63, LB broth and 2× YT

Medium 63, LB (Luria-Bertani) broth and 2× YT (2× amount of yeast extract and 60% more tryptone than LB broth) were each prepared by dissolving the appropriate components (See Table 3.1) into 800 mL of deionized water. Next, the pH was adjusted to 7.0 (if needed) using NaOH and the volume was brought up to 1 L with deionized water. 400 mL of the mixture (800 mL total) was placed in each of two 4L flasks (one for each of two cultures). Each flask was closed with a sponge plug and foil. The remaining volume of the mixture was placed in a 500 mL media storage bottle. Finally, media were autoclaved and stored at room temperature. The two-4L flasks were each used for one experiment and the remaining volume was used for overnight cultures and for washing cells.

3.1.2 1× SMM Buffer

200 mL of 1× SMM buffer (sucrose, maleic acid and magnesium chloride), was prepared dissolving all the components (See Table 3.1) into 200 mL of deionized water. Next, using a 20 mL syringe, 20 mL of the mixture was passed through a 0.2 μm filter unit into each of ten 50 mL falcon tubes. Each falcon tube was used for a lysozyme or AMP treatment. Ten 50 mL falcon tubes containing 20 mL of 1×SMM buffer each were stored at 4°C.

3.1.3 1× PBS Buffer

1 L of 1× phosphate buffered saline (PBS) buffer, was prepared by dissolving all the components (See Table 3.1) into 1000 mL of deionized water. All the mixture was placed in a 1 L media storage bottle. Finally, media was filtered using a 0.45 μm filter and stored at room temperature.

3.2 Labeling the Lipid Bilayer of the Bacterial Envelope with Deuterated Acyl Chains

Bacterial strains and the ^{2}H labeling methods used in this project are listed in Table 3.2. All bacterial strains were stored at -80°C in 1 mL aliquots. Each aliquot contains 500 μL of glycerol and 500 μL of cells in growth media. All growth media and buffer compositions are listed in Table 3.1. For NMR experiments with a final pellet of $\sim$ 400 μL, it was necessary to grow 400 mL cultures.

3.2.1 Mutated Bacteria Method (MB Method)

A small culture of bacteria was grown overnight at 30°C and used to inoculate a larger culture grown during the day at 37°C. Overnight cultures of *E. coli* LA8 were prepared in 50 mL falcon tubes by inoculating 9 mL of Medium 63-A (see Table 3.2 and Section 4.1) with 1 mL aliquots of frozen glycerol cell stocks[1]. Overnight cultures were placed in a 30°C incubator with shaking speed of 150 rpm with a loosely fitting cap. The large-scale cultures were started with 1 mL of overnight culture per 100 mL of fresh Medium 63-B (see Table 3.1) in a flask at least 4 times bigger than the culture total volume. Each culture was protected with a foam stopper and placed in an incubator at 37°C with shaking speed of 175 rpm. Cells were finally harvested in midlog phase at an absorption at 600 nm (A_{600}) of 0.6 - 1.0. The cells were centrifuged at 4100 g for 10 minutes at 4°C and then transferred to a NMR tube (see more tube details in Section 3.8). ^{2}H NMR

[1]Note that in this case, Media 63-A contains glycerol so, the final concentration of glycerol of the overnight culture is $\sim$ 67 g/L

TABLE 3.1: Media and buffers compositions.

Media/ Buffer	Composition	
Media 63	13.6 g/L KH_2PO_4[1]	0.5 mg/L $FeSO_4.7H_2O$[1]
	2 g/L $(NH_4)_2SO_4$[1]	4 g/L Glycerol[2]
	0.2 g/L $MgSO_4.7H_2O$[1]	
Media 63-A	13.6 g/L KH_2PO_4	4 g/L Glycerol
	2 g/L $(NH_4)_2SO_4$	1 mg/L Thiamine[2]
	0.2 g/L $MgSO_4.7H_2O$	3 g/L Casamino acids Difco^{TM}[1]
	0.5 mg/L $FeSO_4.7H_2O$	30 mg/L Kanamycin[2]
Media 63-B	13.6 g/L KH_2PO_4	3 g/L Casamino acids
	2 g/L $(NH_4)_2SO_4$	30 mg/L Kanamycin
	0.2 g/L $MgSO_4.7H_2O$	1 g/L Brij-58[2]
	0.5 mg/L $FeSO_4.7H_2O$	50 mg/L Deuterated palmitic acid (PA-d_{31})[3] (0.174 mM)
	4 g/L Glycerol	50 mg/L Oleic acid (OA)[4] (0.177 mM)
	1 mg/L Thiamine	
LB Broth	10 g/L Tryptone[1]	
	5 g/L Yeast extract[1]	
	5 g/L NaCl[1]	
2×YT Media	16 g/L Tryptone	
	10 g/L Yeast extract	
	5 g/L NaCl	
1×SMM Buffer	171.15 g/L Sucrose[1]	
	2.321 g/L Maleic acid[2]	
	1.904 g/L $MgCl_2$[2]	
1×PBS Buffer	8 g/L NaCl	1.44 g/L Na_2HPO_4[1]
	0.2 g/L KCl[1]	0.24 g/L KH_2PO_4[1]

[1] Fisher Scientific
[2] Sigma-Aldrich
[3] CDN Isotopes
[4] Avanti Polar Lipids

TABLE 3.2: Summary of bacteria and ^{2}H-labeling methods used.

Bacterial Strain	Type	^{2}H labeling Method
E. coli L8 (CGSC#5637)	Gram -	MB
E. coli JM109 (CGSC#8267)	Gram -	UB
Bacillus subtilis (ATCC#*E*6051)	Gram +	UB

experiments were started no more than two hours after cell harvesting. Bacteria with AMP treatment require additional steps that will be explained in Section 3.5.

3.2.2 Unmutated Bacteria Method (UB Method)

As explained above, UB method requires growing bacteria in media supplemented with deuterated acyl chains complexed with detergent micelles. However, in the case of *E. coli* JM109, the media were also supplemented with oleic acid (OA) complexed with detergent micelles. UB method was used with two strains of bacteria: *E. coli* JM109 and *B. subtilis*. Below is the protocol to form dodecylphosphocholine (DPC) micelles complexed with hexadecanoic-d_{31}, also known as palmitic acid-d_{31} (PA-d_{31}), or OA. Next, the particular protocol for each bacterial strain will be explained.

3.2.2.1 PA-d_{31} and OA complexed with DPC micelles

A 10 mL solution containing the desired amount (specified below) of PA-d_{31} and DPC sufficient to achieve the desired final concentration in the 400 mL culture was prepared in a 50 mL falcon tube at room temperature with distilled water. To ensure a correct concentration of PA-d_{31}, the stock needed to be at room temperature, i.e. the mixture should be clear with no precipitate. A second 10 mL mixture containing the desired amount (specified below) of OA and DPC sufficient to achieve the desired final concentration in the 400 mL culture was prepared in a 50 mL falcon tube at room temperature with distilled water. Next, using a 0.2 μm syringe filter unit, each solution was filtered and transferred to a second 50 mL falcon tube. Mixtures were subjected to at least 4 freeze-thaw cycles by heating in a boiling water bath for at least 4 minutes and then submerging in

liquid nitrogen until frozen solid. Finally, both tubes were warmed in a water bath at room temperature until the edges of the ice melted. The whole 10 mL of each mixture were added immediately to the growing media that was already in the incubator at 37°C and 175 rpm. Normally this is done within 30 minutes of inoculation.

3.2.2.2 UB method using *E. coli* JM109

Overnight cultures of *E. coli* JM109 were prepared in a 50 mL falcon tube by inoculating 9 mL of LB broth (see Table 3.1) with a 1 mL aliquot of frozen glycerol cell stock. Overnight cultures were placed in a 30°C incubator with a shaking speed of 150 rpm with a loosely fitting cap. Next day, LB broth (see Table 3.1) at 37°C in a flask at least 4 times bigger than the culture total volume was supplemented with 0.25 mM (final concentration) PA-d_{31} in 1 mM (final concentration) DPC, and 0.25 mM (final concentration) OA in 1 mM (final concentration) DPC. The large-scale cultures were started with 1 mL of overnight culture per 100 mL of fresh supplemented LB broth and grown at 37°C and 175 rpm. Each culture was protected with a foam stopper. Cells were grown to midlog phase at an absorption at 600 nm (A_{600}) of 0.6 - 1.0. The cells were harvested by centrifugation at 4100 g for 10 minutes at 4°C. Samples with AMP treatment require additional steps that will be explained in Section 3.5. For samples with no AMP treatment, the pellet resulting from the harvesting centrifugation was transferred into the NMR tube (see more tube details in Section 3.8). ^{2}H NMR experiments were started no more than two hours after cell harvesting.

3.2.2.3 UB method using *B. subtilis*

Overnight cultures of *B. subtilis* were prepared in a 50 mL falcon tube by inoculating 9 mL of 2×YT media (see Table 3.1) with a 1 mL aliquot of frozen glycerol cell stock. Overnight cultures were placed in a 30°C incubator with shaking speed of 150 rpm with a loosely fitting cap. 2×YT media (see Table 3.1) at 37°C in a flask at least 4 times bigger than the culture total volume, was supplemented with 0.083 mM (final concentration) PA-d_{31} with 0.33 mM (final concentration) DPC.

The large-scale cultures were started with 1 mL of overnight culture per 100 mL of fresh 2×YT media with PA-d_{31}/DPC and incubated at 37°C and 175 rpm. Each culture was protected with a foam stopper. Cells were harvested in midlog phase at an absorption at 600 nm (A_{600}) of 0.6 - 1.0. The cells were centrifuged at 5670 g for 20 minutes at 4°C. Samples with lysozyme and/or AMP treatment require additional steps that will be explained in Sections 3.3 and 3.5. For samples with no additional treatment, the pellet resulting from the harvesting centrifugation was placed in the NMR tube (see more tube details in Section 3.8). ^{2}H NMR experiments were started no more than two hours after cell harvesting.

3.3 Disrupting Peptidoglycan Layer with Lysozyme

Lysozyme from egg white was bought from Sigma-Aldrich. For a 400 mL culture, the desired amount of lysozyme in the sample was dissolved in 20 mL of 1×SMM. After the centrifugation to harvest the cells, the pellet was resuspended in 20 mL 1×SMM-lysozyme mixture and kept on ice for 10 minutes. Next, the cells were centrifuged at 5670 g for 20 minutes at 4°C. Samples with AMP treatment require additional steps that will be explained in Section 3.5. For samples with no additional treatment, the resulting pellet was transferred into the NMR tube (see more tube details in Section 3.8). ^{2}H NMR experiments were started no more than two hours after cell harvesting.

3.4 Gram Staining and Microscopy

Gram staining was used as the to method confirm the change in the peptidoglycan in the *B. subtilis* cell wall before and after the lysozyme treatment. The association of the positively charged crystal violet molecules with the negatively charged iodine molecules, forms large complexes that remain trapped in the peptidoglycan layer of the Gram + bacteria after the decolorization process with ethanol. Since the crystal violet is the reagent responsible for the purple color, Gram + bacteria remain purple during the rest of the Gram staining process. On the contrary, Gram - bacteria lose the crystal violet, along with the outer membrane. Thus, the

counterstain, in this case safranin, enters into the now exposed thin peptidoglycan layer giving a pink color to the bacteria. Gram's crystal violet and Gram's safranin solutions were acquired from Sigma-Aldrich and Gram's iodine solution was prepared by mixing 1 g of iodine, 2 g of potassium iodine in 300 ml of distilled water. A 1 mL aliquot of the bacterial sample was placed aside in a 1.5 mL micro centrifuge tube before the final centrifugation as described in Section 3.3 or 3.5. In a sterile environment, bacterial cells were placed and spread on a microscope slide using a sterile cooled loop. Bacterial cells were heat fixed onto the microscope slide by passing them several times through the flame of a burner until the medium was completely evaporated. The slide was allowed to cool for at least 10 seconds. Next, crystal violet was gently transferred on the slide, smearing to assure coverage, and let stand for 1 minute. Crystal violet was gently rinsed with distilled water. Next, iodine solution was gently transferred on the slide and allowed to stand for 1 minute. Iodine solution was gently rinsed with distilled water. The fixed smear was decolorized using 95% ethanol for about 5 to 10 seconds or until the ethanol ran almost clear. Ethanol was gently rinsed from the sample with distilled water. Safranin was gently transferred on the slide, smearing to assure coverage, and let stand for 45 seconds. Finally, safranin was gently rinsed with distilled water. The slide was placed over towel paper and allowed to air dry for about 5 minutes. Once the slide was completely dry, bacterial samples were observed under a conventional light microscope using a 100x immersion oil lens. To obtain an approximate scale bar, a 0.1 mm grid of a Motic microscope calibration slide was placed under a conventional light microscope using a 100x immersion oil lens. Pictures were taken using an iPhone SE and presented in section 6.1.

3.5 Treating Bacteria with AMPs

C-terminal amidated MSI-78 and BP100 peptides, were obtained from GenScript and HPLC-purified to purity $> 75\%$. All peptides were desalted via buffer exchange using Spectrum^{TM} Spectra/Por^{TM} dialysis membrane tubing (100-500 and 1000 Dalton MWCO). Samples were dialyzed against 95% purified water and 5% acetic-acid for 24 hours and 100% purified water for at least another 24 hours. The dialyzed sample was lyophilized and weighed. The amount of peptide for

each sample was determined as a percentage of the bacterial dry weight. The procedure to determine the bacteria dry weight using the absorption at 600 nm (A_{600}) will be explained first, followed by the protocol for treating bacteria with AMP.

3.5.1 Determining the Bacteria Dry Weight

The amount of AMP in each sample was calculated as a percentage of the final dry pellet mass. Because the amount of cells varies from sample to sample, a relationship between the absorption at 600 nm (A_{600}), just before the harvesting centrifugation, and the bacteria dry weight is needed. To obtain this relationship, a minimum of 5 cultures of bacteria enriched with palmitic acyl chains (Non-deuterated palmitic acyl chains were used instead of PA-d_{31} in samples for experiments that did not involve NMR measurements) were grown under the conditions explained in Section 3.2.1 for *E. coli* LA8, Section 3.2.2.2 for *E. coli* JM109 and Section 3.2.2.3 for *B. subtilis*. Cultures were harvested at different points of the log phase (an absorption at 600 nm $A_{600} = 0.6 - 1.0$) and pelleted using centrifugation under the conditions as in 3.2.1, 3.2.2.2 and 3.2.2.3. Next, each pellet was resuspended in 60 mL of growth media for 20 minutes with gentle shaking at room temperature. The final pellets were placed with a clean spatula in pre-weighed vessels and then placed in a vacuum chamber for 48 hours. After 48 hours each vessel was reweighed. The bacterial dry weight is obtained by subtracting the weight of the vessel from the weight of the vessel + dry bacteria.

As shown in Figure 3.1, an exponential relationship between the absorbance at 600 nm and the bacterial dry weight is expected. A linear fit of ln(dry weight) versus the absorption at 600 nm (A_{600}) gives the relationship equation that can be used to calculate the bacterial dry weight and thus the appropriate amount of AMP to add to the bacteria for NMR experiments. For example, if the absorbance of a *B. subtilis* culture is 0.75, the dry weight of the pellet is 200 ± 60 mg[2].

[2]Uncertainty calculations are displayed in Appendix A.2

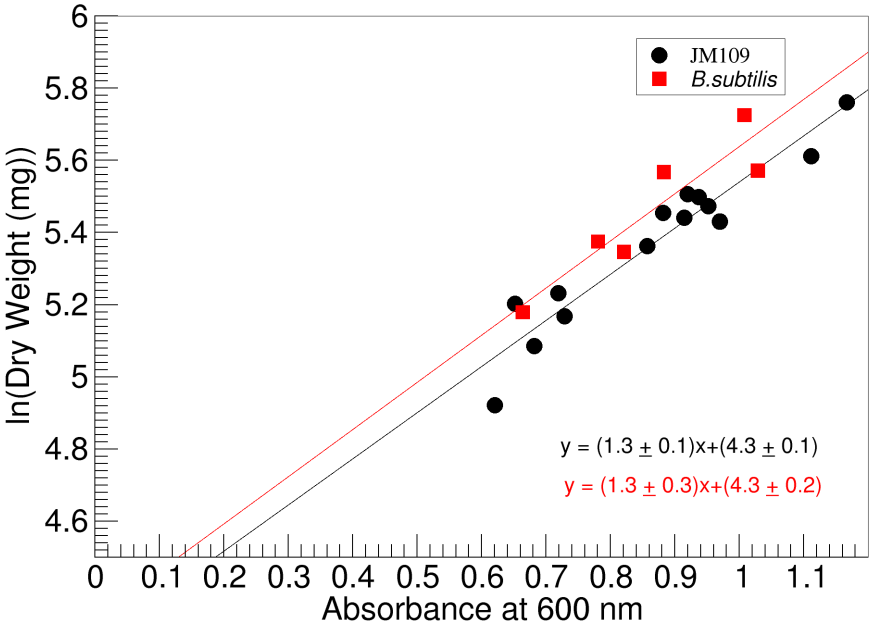

FIGURE 3.1: ln(Dry weight (mg)) cells vs absorbance at 600 nm (A_{600}) for *E. coli* (JM109) and *B. subtilis*. Linear regression were performed to obtain the relationships shown in the graph.

3.5.2 AMP Treatment

Using the absorption at 600 nm (A_{600}) just before harvesting, and the relationship obtained in Section 3.5.1, the proper amount of AMP needed in the sample was calculated. The peptide amount was weighed and dissolved in 60 mL of growth media (medium 63 for LA8, LB broth for JM109 and 2×YT media for *B. subtilis*) for the samples with no lysozyme treatment, or in 20 mL of 1×SMM buffer for the lysozyme treated samples. The media or buffer + AMP mixture was used to resuspend the pellet obtained after harvesting. The pellet was scraped from the bottom of the centrifuge tube and gently vortexed to achieve a homogeneous mixture. The centrifuge tube with the unattached pellet was then placed in an orbital shaker at 200 rpm for 10 minutes at room temperature. Next, cells were centrifuged at 4100 g (5670 g in the *B. subtilis* case), at 4°C for 10 minutes (20 minutes in the *B. subtilis* case). The final pellet was transferred into the NMR

tube (see more tube details in Section 3.8). ^{2}H NMR experiments were started no more than two hours after cell harvesting.

3.6 *B. subtilis* Lysate and Lipid Extraction

A 200 mL flask containing 69 mL of 2×YT media (see Table 3.1) was closed with a sponge plug and foil and autoclaved. Once the flask with media reached room temperature, overnight cultures of *B. subtilis* were prepared by inoculating the 69 mL of 2×YT media with 1 mL aliquots of frozen glycerol cell stocks. Overnight cultures were placed in a 30°C incubator with shaking speed of 150 rpm, protected with a foam stopper. Six 4L flasks containing 1 L of 2×YT media (see Table 3.1) each, were supplemented with 0.083 mM (final concentration) PA-d_{31} in 0.33 mM (final concentration) DPC and pre-warmed to 37°C. They were inoculated with 1 mL of overnight culture per 100 mL of fresh supplemented media and incubated at 37°C and 175 rpm. Each culture was protected with a foam stopper. Cells were harvested in log phase at an absorption at 600 nm (A_{600}) of 0.6 - 1.0. The cells were centrifuged at 5670 g for 20 minutes at 4°C. The resulting pellet was lysed by three cycles of french press at a pressure of 10000 psi (6.9×10^{7} Pa) and 4°C to generate cell lysate. The french press cycle consists of forcing the pellet through a small valve at high pressure. The cells then experience shear stress that generates cellular disruption resulting from the significant change in pressure. A cell lysate volume of $\sim$ 30 mL was typical. 5 mL of the cell lysate was stored in a 15 mL falcon tube at -20°C for cell lysate experiments, and the remaining cell lysate was used for lipid extraction.

A Bligh and Dyer method was implemented for lipid extraction [73] starting from cell lysate. The initial volume (V_i) was measured using a graduated cylinder. $3.75\times V_i$ of ice-cold chloroform/methanol (1:2) was mixed with the cell lysate to generate a single phase mixture. The mixture was vortexed for 2 minutes and left resting at room temperature for 5 minutes. $1.25\times V_i$ of PBS (see Table 3.1) and $1.25\times V_i$ of room temperature chloroform were added to the mixture to generate a two-phase solution. The solution was vortexed for 5 minutes and then transferred to a glass separation funnel. In order to obtain a clear lower phase, the solution

was left resting at room temperature for approximately 2 hours. The lower phase containing lipids suspended in chloroform/methanol was carefully recovered in a beaker and dried under a N_2 stream. The extracted lipids were placed under vacuum for 48 hours to ensure that any trace of chloroform/methanol was completely removed.

Multilamellar vesicles (MLV) were prepared by adding 5 mL of 2×YT media to the beaker containing the lipids and then vortexing the mixture until all the lipid material was completely suspended. The sample was left to settle out for at least one hour to allow MLV formation. The sample was kept at -20°C until needed. 400 μL of the mixture was transferred to an NMR tube for each experiment.

3.7 Preparation of DPPC Multilamellar Vesicles

Using a 1.5 mL eppendorf centrifuge tube, 30 mg of DPPC was added to 400 μL of PBS. The mixture was vortexed for 1 minute or until all the lipid material was completely suspended. The mixture was then transferred to an NMR tube. The sample was used immediately.

3.8 Performing NMR

^{2}H NMR experiments were performed with an in-house-assembled 9.4 T solid-state spectrometer. The NMR tube is a cylindrical tube with a round bottom with external diameter of $\sim$ 8.2 mm and length of $\sim$ 25 mm. The NMR sample was inserted in a 10 mm diameter transverse sample coil on the NMR probe. A Lakeshore Cryogenics Model 325 temperature controller was used to keep the sample temperature at 37°C. Probe tuning and matching were performed before each experiment. A quadrupole echo pulse sequence $((\pi/2) - \tau - (\pi/2) - acq)$ with a 30 μs pulse separation (τ), a 5 μs pulse duration and a 900 ms recycling delay, was used to acquire the time domain quadrupole echo signals. Each transient was acquired with a dwell time of 1 μs and 8192 points in each of the real and imaginary channels. The dwell time needed to achieve a spectral width of

250 kHz is 4 microseconds so this corresponds to oversampling by a factor of 4. This allowed separation of the time domain signal into 4 subsequences that were shifted and added to generate an echo with an effective dwell time of 4 μs and a resulting improvement in the signal-to-noise ratio [74]. In order to monitor for any change in spectral shape over time, transients were averaged in blocks of 8000 scans collected over 2 hours. Previous studies showed no major changes in spectral shape over 8 hours of acquisition [6] which allowed the 32,000 transients to be added together and processed. To minimize dispersive signal in the imaginary channel, baseline correction and phase shift were applied to the quadrupole echo. A Fourier transformation was applied to the free induction decay (FID), resulting in the ^{2}H NMR spectrum which was also baseline corrected and normalized by area.

3.8.1 Quadrupolar echo

A typical ^{2}H NMR spectrum of a lipid bilayer is acquired with a spectral width of at least 250 kHz. This means that important information is contained in the early part of the FID signal. At the same time, conventional spectrometers use the same coil to excite the deuterium nuclei and to detect the FID signal, which typically causes a dead time of about $\sim$ 20 μs and thus the potential loss of information in the early part of the FID. In their 1976 paper, Davis *et al.* proposed the quadrupole echo as an approach to avoid losing information in the early part of the FID due to the dead time of the spectrometers [5]. The quadrupole echo pulse sequence consists of two $\pi/2$ pulses separated by a time interval τ. The two pulses need to be 90° out of phase and τ should be longer than the "dead time". This quadrupole echo translates the $t = 0$ point of the FID beyond the "dead time" which prevents the loss of crucial information.

Chapter 4

Spectra of ^{2}H Labeled Bacteria

The first ^{2}H NMR study of bacterial cell membranes using a quadrupole echo pulse dates from 1975 when Stockton *et al.* studied the cell membrane extracted from *Acholeplasma Laidlawii*, a small bacterium that lacks a cell wall [75]. In 1979, Davis *et al.* published the first study of bacteria cell membranes of intact *E. coli* cells [68]. This study was done on a specific strain of *E. coli*, L51, that was forced to incorporate perdeuterated palmitic acid into the membrane bilayer due to its defective fatty acid oxidation pathway. More recently, Pius *et al.* studied the effect of the antimicrobial peptide MSI-78 in the cell membrane of LA8, a mutated strain of *E. coli* [6]. Also, Tardy-Laporte *et al.* [1] studied the effect of antimicrobial agents such as polymyxin, fullerenol and cetyltrimethylammonium chloride, in the cell membrane of pPD117, an ampicillin resistant strain of *E. coli*.

4.1 Obtaining ^{2}H NMR Spectra from *E. coli* (LA8)

One of the greatest challenges in this type of work is to demonstrate the reproducibility of the NMR data obtained from the intact cells. Thus, a necessary step was to perform multiple experiments with *E. coli* LA8 cells and compare the results to each other and to previous work in our group.

As explained in section 3.2.1, the MB method for preparing bacteria with deuterated membranes involves the use of bacteria with two specific mutations. One of

the mutations stops acyl chain synthesis so that bacteria are not able to produce acyl chains. The other mutation affects acyl chain metabolism. As a result, bacteria are not able to use acyl chains as fuel. To create this double mutation, James Pius started with L8 bacteria, a commercial strain of *E. coli* whose mutation affects total acid synthesis, and introduced a secondary mutation that modifies bacterial fatty acid metabolism [6]. The bacterial strain resulting from the two mutations was named *E. coli* LA8. The inability to metabolize or synthesize acyl chains restrains bacterial growth unless the growth media is supplemented with acyl chains. Therefore, cultivating LA8 cells in growth media supplemented with deuterated palmitic acid (PA-d_{31}) and oleic acid (OA) results in bacterial cells with deuterium-rich membranes.

Black spectra in Figure 4.1(a) show absolute intensity ^{2}H NMR spectra of *E. coli* LA8 and the red spectrum in Figure 4.1(a) shows absolute intensity ^{2}H NMR spectra of *E. coli* LA8 in the presence of 20% wt/wt MSI-78. The corresponding spectra in Figures 4.1(b) and 4.1(c) are normalized by area. Spectra in black correspond to six different preparations using the protocol in Section 3.2.1. Each preparation was labeled with a different number starting from NS01 to NS08. The five preparations giving the best signal-to-noise ratio are shown in Figure 4.1. Preparations NS01 and NS05 in Figure 4.1(b) represent the highest signal-to-noise ratio and preparations NS08 and NS09 the lowest. Preparations NS04, NS05 and NS08 in Figure 4.1 display prominent edges at $\sim \pm 12.5$ kHz. These prominent edges result from the plateau region of the order parameter profile and indicate multiple C-D bonds undergoing similarly constrained reorientations close to the hydrophilic/hydrophobic interface of the bilayer. The quadrupolar splitting of the prominent edges is $\sim$ 25 kHz. $(S_{CD})_{\text{plateau}}$ can be obtained using equation 2.15. Applying this equation, the resulting $(S_{CD})_{\text{plateau}}$ value is ~ 0.2 which, is consistent with a liquid-crystalline phase bilayer. In summary, the resulting spectra are characteristic of lipid bilayers in a liquid-crystalline state whose fatty acyl chains undergo fast axially symmetric chain reorientation. Additionally, the prominent edges correspond to the orientational order parameter plateau and the distribution of smaller splittings correspond to the less ordered chain segments toward the bilayer centre. Preparation NS05 was used as a reference to be compared with the AMP treated sample on Figure 4.1(c) because it exhibits the best signal-to-noise

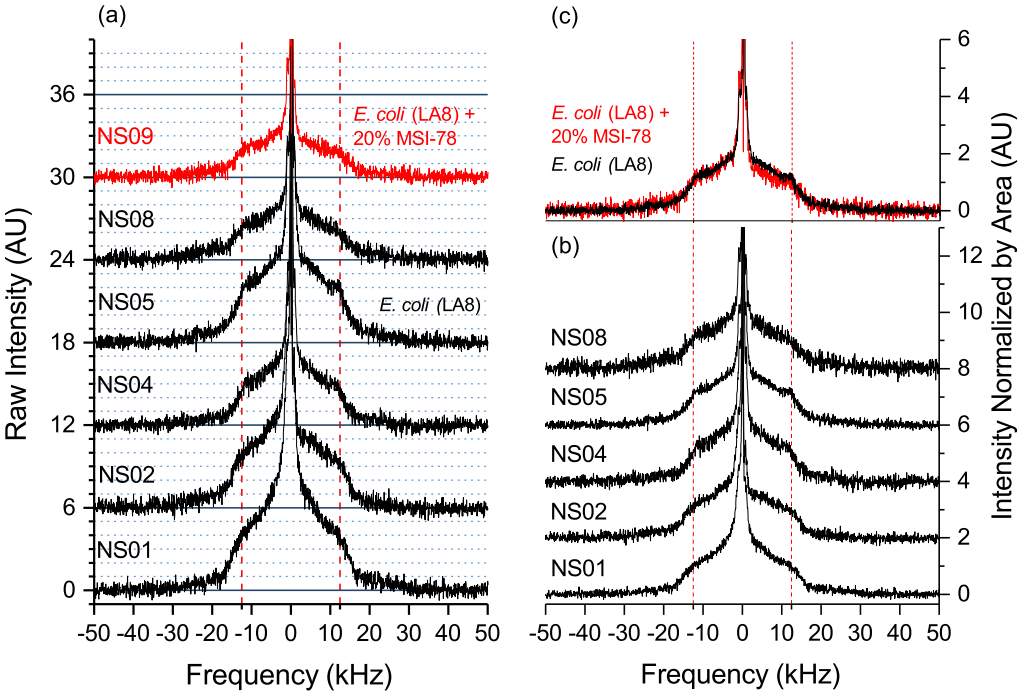

FIGURE 4.1: ^2H NMR spectra of *E. coli* (LA8) enriched with deuterated acyl chains from six different preparations using the protocol in Section 3.2.1 showing reproducibility of untreated cells in black and the effect of 20% MSI-78 (wt/wt) in the spectrum in red. (a): Absolute intensity spectra in the absence (black) and presence of AMP (red). (b): Spectra normalized by area in the absence of AMP. (c): Spectra normalized by area in the absence of AMP (Black) and in the presence of 20% MSI-78 (wt/wt) (red). Dashed lines at ± 12.5 kHz are provided to facilitate comparison of the spectra. All spectral intensities are represented in arbitrary units (AU). Each spectrum represents 32,000 scans recorded over eight hours at 37 $^\circ C$ in a 9.4 T NMR spectrometer.

ratio.

Figure 4.1(c) shows the comparison between the NS05 reference spectrum for *E. coli* LA8 and the spectrum of *E. coli* LA8 in presence of 20% (wt/wt) MSI-78. A slight reduction of the prominent edges at $\sim \pm 12.5$ kHz was observed in the AMP treated bacterial sample which may be due to the presence of the AMP, or just the normal variability between samples. As shown next, it is likely the latter.

Table 4.1 shows the values of the first and second moments, M_1 and M_2, and the relative mean square width of the order parameter distribution, Δ_2, for all the

TABLE 4.1: M_1, M_2 and Δ_2 values, as defined in section 2.3.2.1, for ^2H NMR spectrum of *E. coli* (LA8) showed in Figure 4.1.

Experiment	M_1 $\times 10^4 (s^{-1})$	M_2 $\times 10^9 (s^{-2})$	Δ_2	Details
NS01	4.34	3.46	0.36	untreated
NS02	4.43	3.45	0.31	untreated
NS04	3.98	2.85	0.33	untreated
NS05	4.52	3.79	0.37	untreated
NS08	4.58	3.77	0.33	untreated
Average over untreated samples	$\overline{M_1}$ $\times 10^4 (s^{-1})$	$\overline{M_2} \times 10^9 (s^{-2})$	$\overline{\Delta_2}$	
	4.4 ± 0.2	3.5 ± 0.3	0.34± 0.03	
NS09	4.31	3.40	0.35	20%(wt/wt) MSI-78

spectra shown in Figure 4.1. The values for five untreated samples were averaged and standard deviations calculated to help illustrate the variability between different samples using the same bacterial strain and protocol. It is fair to say that the AMP-treated samples would display a similar variability. The uncertainties in the averages reported in Table 4.1 are the standard deviations. The M_1, M_2, and Δ_2 values were similar, but not identical to those obtained by Pius *et al.* [6] and will be discussed below in section 4.5. Additionally, Table 4.1 shows that the addition of 20% MSI-78 did not induce significant changes to the moments or Δ_2 values with respect to the average over the untreated samples.

In summary, these results demonstrated that deuterated fatty acyl chains could be successfully introduced into the membrane of *E. coli* LA8 and reproducible spectra can be obtained. Cell viability is expected to be similar or better than that observed by Pius *at al.* [6] because there was no washing step before performing the NMR measurement. In this series of experiments, no AMP-induced change was observed to result from the addition of 20% MSI-78.

TABLE 4.2: Fatty acid composition of the membranes of unlabeled and labeled *E. coli* using the protocol explained in Tardy-Laporte paper in 2013. Data obtained from [1].

E. coli sample	% Fatty acid (w/w)				
	Palmitic acid (C16:0)	Deuterated Palmitic acid (C16:0D)	Palmitoleic acid (C16:1)	Heptadecenoic acid (C17:1)	Oleic acid (C18:1)
Labeled	7	76	9	1	7
Unlabeled	36	0	28	3	33

4.2 Obtaining ^{2}H NMR Spectra from *E. coli* JM109

In 2013 Tardy-Laporte *et al.* published an alternate method for growing deuterated-membrane-rich *E. coli* pPD117 [1]. This method offers the benefit of being applicable to non-mutated type bacteria instead of mutated strains. The next group of experiments was aimed at obtaining consistent ^{2}H NMR spectra of *E. coli* JM109. In this set of experiments, the main difference between our protocol and the protocol described by Tardy-Laporte *et al.* is the addition of oleic acid, complexed into DPC micelles, to the growth media in our protocol. The Tardy-Laporte protocol leads to a relatively high percentage of cell death compared with the Pius *et al.* protocol [6] which uses bacterial growth medium containing both palmitic acid and oleic acid. I hypothesized that the relatively high percentage of cell death is related to the absence of oleic acid in the growth medium when these bacteria typically have a significant amount of oleic acid (See Table 4.2) [1]. Thus, it was decided to incorporate oleic acid into the growth media to improve bacterial viability.

The black spectra in Figure 4.2(a) show the absolute intensity ^{2}H NMR spectra of *E. coli* JM109 and the red spectrum in Figure 4.2(a) shows absolute intensity ^{2}H NMR spectrum of *E. coli* JM109 in the presence of 17% (wt/wt) MSI-78. The corresponding spectra in Figure 4.2 (b) and (c) are normalized by area. Spectra in black correspond to two different preparations using the protocol detailed in Section 3.2.2.2. Both preparations (NS11 & NS12) exhibit similar values of raw intensity, i.e. similar values of signal-to-noise ratio. ^{2}H NMR spectra of untreated *E. coli* JM109 in Figure 4.2 display prominent edges at $\sim \pm$ 12.5 kHz with quadrupolar splittings of $\sim$ 25 kHz. As for *E. coli* LA8, these prominent

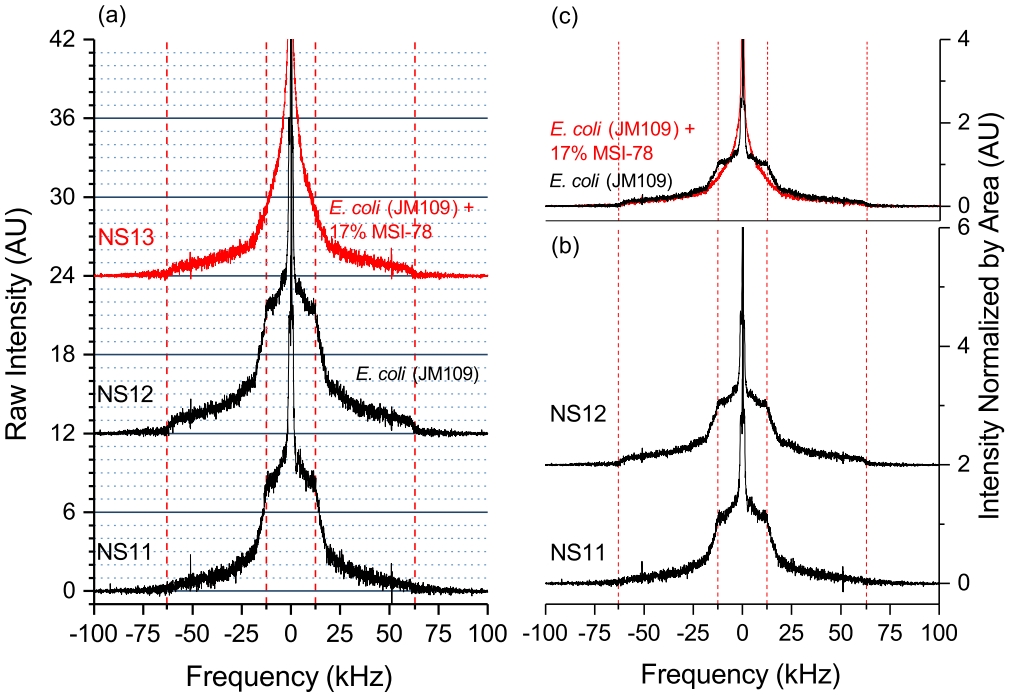

FIGURE 4.2: ^2H NMR spectra of *E. coli* JM109 enriched with deuterated acyl chains from two different preparations in black using the protocol in Section 3.2.1 (showing reproducibility) and the effect of 17% MSI-78 (wt/wt) in the spectrum, in red. (a): Absolute intensity spectra in the absence and presence of AMP. (b): Spectra normalized by area in the absence of AMP. (c): Spectra normalized by area in the absence of AMP (black) and in the presence of 17% MSI-78 (wt/wt) (red). Dashed lines at ±12.5 and ±62.5kHz are included to facilitate comparison of the spectra. All spectra intensities are represented in arbitrary units (AU). Each spectrum represents 32,000 scans recorded over eight hours at 37 $°C$ in a 9.4 T NMR spectrometer.

edges are a result of the plateau region of the order parameter profile and indicate multiple C-D bonds undergoing similarly constrained reorientations close to the hydrophilic/hydrophobic interface of the bilayer. Additionally, there is intensity out to frequencies of $\sim \pm$ 62.5 kHz. Such large splittings point to the presence of a highly ordered structure and indicate that the deuterated acyl chains are embedded in a structure where their movements are more restricted, i.e. not in the liquid-crystalline phase. The possible nature of this structure is discussed below. Preparation NS12 was used as a reference to be compared with the AMP treated sample in Figure 4.2(c) because it exhibits the best signal-to-noise ratio.

Figure 4.2(c) shows the comparison between a reference spectrum of *E. coli* JM109 and the spectrum of *E. coli* JM109 in the presence of 17% (wt/wt) MSI-78. A significant reduction of the prominent edges at $\sim \pm$ 12.5 kHz and an increase in the intensity at narrower splittings was observed for the AMP treated sample.

TABLE 4.3: M_1, M_2 and Δ_2 values, as defined in section 2.3.2.1, for ^2H NMR spectrum of *E. coli* JM109 showed in Figure 4.2.

Experiment	M_1 $\times 10^4 (s^{-1})$	M_2 $\times 10^9 (s^{-2})$	Δ_2	Details
NS11	8.5	14.9	0.517	untreated
NS12	10.1	19.5	0.414	untreated
Average over untreated samples	$\overline{M_1}$ $\times 10^4 (s^{-1})$	$\overline{M_2} \times 10^9 (s^{-2})$	$\overline{\Delta_2}$	
	9$\pm$ 1	17 $\pm$ 3	0.47$\pm$ 0.07	
NS13	8.2	15.4	0.680	17%(wt/wt) MSI-78

Table 4.3 shows the calculated values of the first and second moments, M_1 and M_2, from the spectra, along with the Δ_2 values, for all the spectra shown in Figure 4.2. The moment values (M_1 and M_2) and Δ_2 of two untreated samples were averaged and standard deviation calculated to help assess the variability between different samples using the same bacteria strain and protocol. The average of M_1, M_2 and Δ_2 were used to compare with previous reported values and the AMP treated sample presented here. The uncertainties in the averages reported in Table 4.3 are standard deviations. The M_1, M_2 values differ from the ones reported by Tardy-Laporte *et al.* [1] and will be discussed in section 4.5. Additionally, Table 4.3 shows that the addition of 17% MSI-78 does not change the M_1 and M_2 values within the uncertainty, however, there is an increase in the Δ_2 value. It appears that Δ_2 is more sensitive to the AMP-induced spectral changes.

4.3 Obtaining ^{2}H NMR Spectra from *B. subtilis*

Once the protocol using DPC complexes was successfully implemented in Gram - *E. coli*, a decision was made to translate the AMP studies to Gram + bacteria.

The change was performed because Gram + bacteria have a thicker peptidoglycan layer than Gram - bacteria and only a single membrane bilayer (See Section 2.1).

A first attempt to obtain membrane-deuterated *B. subtilis* using the same protocol as with *E. coli* JM109 failed because the bacterial growth time increased substantially. The increase in growth time was likely due to the bacteria struggling to thrive in the presence of acyl chains complexed with detergent micelles. The concentration of the DPC+PA-d_{31} complexes was optimized to decrease the growth time and to maximize the amount of deuterated acyl chains on the sample. Additionally, since the amount of oleic acid in the membrane lipids of *B. subtilis* is small, oleic acid + DPC complexes were removed from the *B. subtilis* growth media.

The black spectra in Figure 4.3(a) show absolute intensity ^{2}H NMR spectra of *B. subtilis* and the corresponding spectra in Figure 4.3(b) shows the spectra normalized by area. Spectra of six different preparations using the protocol detailed in Section 3.2.2.3 are shown. All preparations except for NS43 exhibit similar values of signal-to-noise ratio. ^{2}H NMR spectra of *B. subtilis* in Figure 4.3 display prominent edges at $\sim \pm$ 12.5 kHz. These prominent edges result from the plateau region of the order parameter profile. A low intensity spectral component between $\sim \pm$ 62.5 kHz is present in all the ^{2}H NMR spectra of *B. subtilis* and will be discussed below.

TABLE 4.4: M_1, M_2 and Δ_2 values, as defined in section 2.3.2.1, for ^2H NMR spectrum of *B. subtilis* showed in Figure 4.3.

Experiment	M_1 $\times 10^4 (s^{-1})$	M_2 $\times 10^9 (s^{-2})$	Δ_2	Details
NS39	5.9	7	0.52	untreated
NS40	5.3	6	0.46	untreated
NS43	5.3	6	0.69	untreated
NS44	6.5	9	0.62	untreated
NS53	7.9	13	0.60	untreated
NS60	6.3	9	0.62	untreated
Average over untreated samples	$\overline{M_1}$ $\times 10^4 (s^{-1})$	$\overline{M_2} \times 10^9 (s^{-2})$	$\overline{\Delta}_2$	
	6 ± 1	8 ± 3	0.59 ± 0.08	

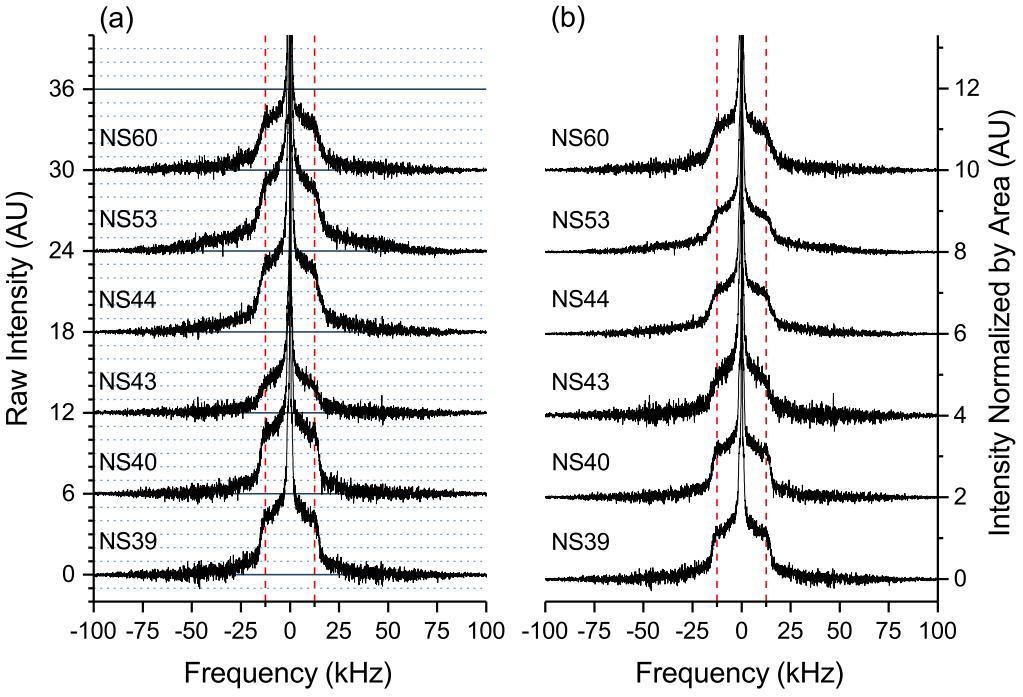

FIGURE 4.3: ^2H NMR spectra of *B. subtilis* enriched with deuterated acyl chains from six different preparations using the protocol in Section 3.2.2.3 showing reproducibility of spectra obtained from untreated cells. (a): Absolute intensity spectra. (b): Spectra normalized by area. Dashed lines at ± 12.5 kHz are included to facilitate comparison of the spectra. Each spectrum represents 32,000 scans recorded over eight hours at 37 $°C$ in a 9.4 T NMR spectrometer.

Table 4.4 shows the calculated values of the first and second moments, M_1 and M_2, along with the Δ_2 values for all the spectra shown in Figure 4.3. The moment values (M_1 and M_2) and Δ_2 of six untreated samples were averaged and the standard deviation was reported to indicate the variability between different samples. A substantial variation in the M_2 value between the samples is observed. This variation likely reflects differences in the intensity of the high order spectral feature. Preparation NS53 was used as a reference spectrum for assessing AMP effects because it exhibits the best signal-to-noise ratio. However, because M_1 and M_2 values of NS53 are larger than those obtained from similarly prepared samples, the averaged values of M_1, M_2 and Δ_2 were used as a reference for comparison to data discussed in Section 4.5.1, Chapter 5 and 6.

4.4 Highly Ordered Structure in the ^{2}H NMR Spectra of *E. coli* JM109 and *B. subtilis*

Despite the fact that the MSI-78 did not show any effect on the higher order component in the ^{2}H NMR spectra of *E. coli* JM109 and *B subtilis* (presented below), I was curious to explore the nature of this highly ordered structure. The appearance of spectral intensity between $\sim \pm$ 62.5 kHz in the ^{2}H NMR spectra of *E. coli* JM109 and *B. subtilis* suggests the presence of a fatty acid structure or membrane structure in a gel-like phase. Quadrupolar splittings near 125 kHz indicate that most of the chain is exclusively undergoing reorientations about its long axis. It is clear that spectral intensity corresponding to this highly ordered structure appeared only in the ^{2}H NMR spectra of unmutated bacteria prepared using the protocol described in Section 3.2.2 that employs PA-d_{31} + DPC mixtures in the growth media. So, the first possible explanation was that the sample contained some PA-d_{31} + DPC that was not taken up by the cells and that possibly was forming a gel phase-like fatty-acid-structure. In order to test this possible explanation, the ^{2}H NMR spectra of 2 mM DPC + 0.5 mM PA (the concentration of the DPC+PA mixture was doubled to ensure there was enough deuterium in the sample) at 37°C was obtained (see Figure 4.4). The ^{2}H NMR spectrum of PA-d_{31} + DPC mixture (black in Figure 4.4) shows a spectral doublet, characteristic of axially symmetric reorientation, with sharp edges at $\sim \pm$ 16 kHz and a narrow central peak characteristic of isotropic reorientation. There is, however, little intensity at higher splittings. This implies that the PA-d_{31} + DPC mixture does not form a highly ordered structure in the absence of cells. Hence, residual PA-d_{31} + DPC in the sample is not responsible for observation of the highly ordered structure in the ^{2}H NMR spectra of *E. coli* JM109 or *B. subtilis*.

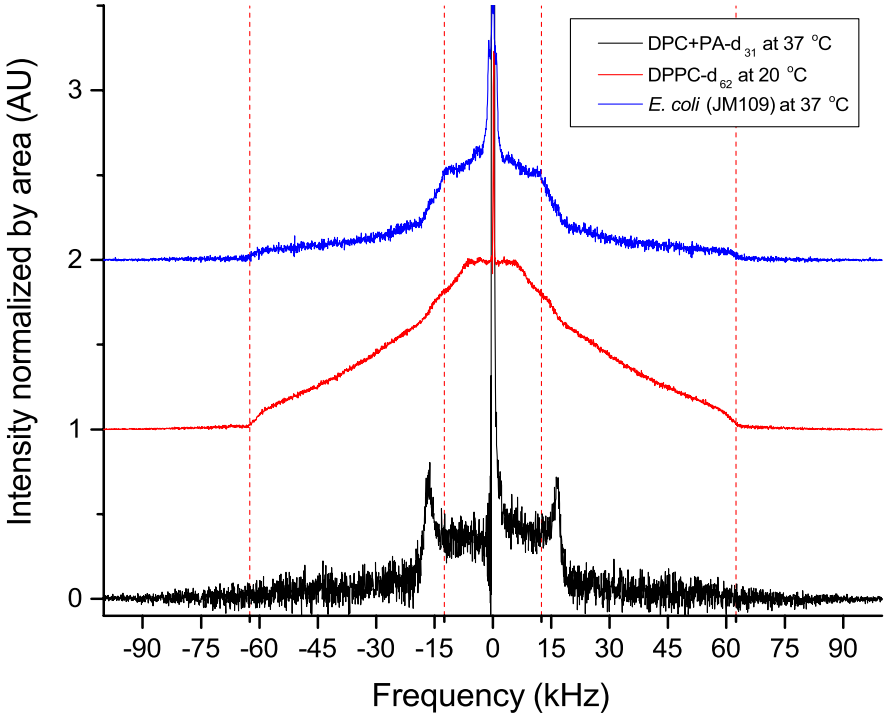

FIGURE 4.4: Comparison of the ^{2}H NMR spectra of the mixture 2 mM DPC + 0.5 mM PA-d_{31} at 37°C (black), DPPC-d_{62} at 20°C (red) and *E. coli* JM109 (NS12) enriched with deuterated acyl chains at 37°C (blue). Dashed lines at ± 16 and ± 62.5 kHz are included to facilitate comparison of the spectra. Each spectrum represents 32,000 scans recorded over eight hours in a 9.4 T NMR spectrometer.

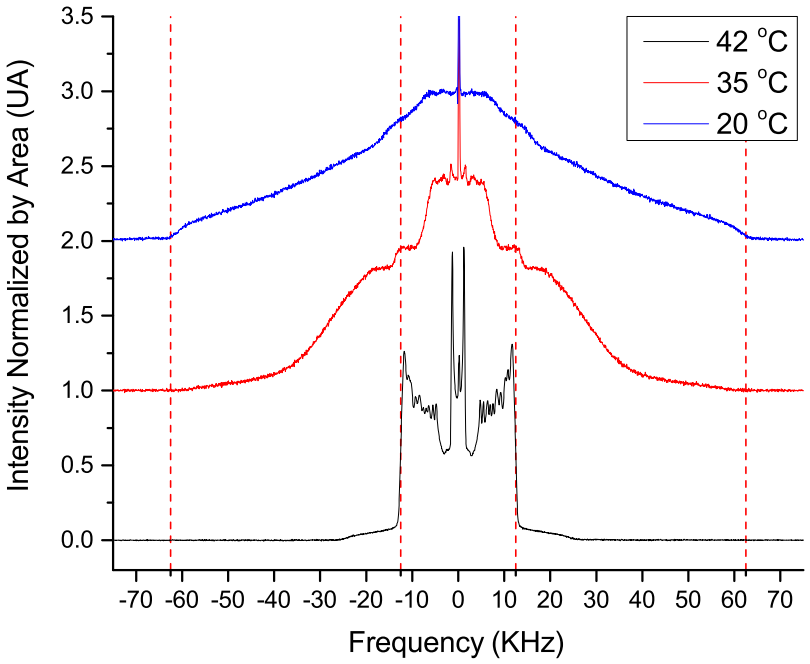

FIGURE 4.5: ^{2}H NMR spectra of 30 mg of DPPC-d_{62} dissolved in 2×YT media at 42°C (black), 35°C (red) and 20 °C (blue). Dashed lines at ±16 and ±62.5kHz are included to facilitate comparison of the spectra. Each spectrum represents 32,000 scans recorded over eight hours in a 9.4 T NMR spectrometer.

Whatever the intensity between ∼ ± 62.5 kHz is, it must derive from highly ordered lipid or fatty acid. For example, it would be expected for DPPC-d_{62} in gel state (below 37°C[1]) or for mixtures of perdeuterated palmitate and water in the gel phase at 38°C [71]. Figure 4.5 shows how the spectrum of DPPC-d_{62} changes from the liquid crystalline phase at 42°C to the gel phase at lower temperatures. In the gel phase, the acyl chains are ordered and reorientation about the chain axis is too slow to be axially symmetric on the NMR timescale. For splittings close to ± 62.5 kHz, the shape of the DPPC-d_{62} gel phase spectrum (20°C) is similar to the spectral component seen at similar splittings in the spectra of *E. coli* JM109 and *B. subtilis* at 37°C. This suggests that the broad spectral component seen for these samples arises from slow reorientation of highly ordered acyl chains. It thus

[1]Note that the transition temperature of DPPC-d_{62} is around 5°C below the transition temperature of DPPC.

seems plausible that the bacteria are retaining and storing lipids in a non cell-membrane site in a gel-like phase state or that gel-like domains are being formed in the bacterial membrane.

Bacteria are known for being able to store nutrients and even proteins [76, 77]. Also, the formation of lipid domains has been suggested in *B. subtilis* and *E. coli* membranes [78, 79]. So, given the excess of acyl chains in the growing media, unmutated bacteria could be producing lipids with high bilayer transition temperatures and either storing them or placing them into the bacterial membrane. Determining the phospholipids that each bacteria might be producing would require a complete study of the bacterial phospholipid composition of *E. coli* JM109 and *B. subtilis* grown using the UB method described in Section 3.2.2. Nonetheless, some clues can be obtained from an analysis of previous studies.

In 2013, Tardy Laporte *et al.* reported the change of the fatty acid composition of *E. coli* pPD117 induced by the presence of DPC+PA-d_{31} in the growth media [1]. Their findings were summarized in Table 4.2. It is clear that *E. coli* pPD117 considerably modified its fatty acid composition in response to the acyl chains available in the growth media. Thus, it is reasonable to suppose that the presence of DPC+PA-d_{31} (and DPC+OA for *E. coli* JM109) in the growth media could lead to the presence of phospholipids whose acyl chain components are deuterated palmitic acid, 16-carbon chains, (and oleic acid, 18-carbon chains, with a cis unsaturation on the ninth carbon) in the case of *E. coli* JM109). Phospholipids with one saturated acyl chains, such as palmitic acid, have higher transition temperatures than the ones with acyl chains with one unsaturation, regardless of the phospholipid head group [80]. However, the phase state of phospholipids also depends on the phospholipid headgroup. As mentioned in section 2.1.1, phospholipid composition changes depending on the environmental conditions, growth phases and bacterial strains [10] however, previous lipidomics studies performed in *E. coli* reported the presence of primary phosphatidylethanolamine (PE), phosphatidylglycerol (PG) [81**?**] and, cardiolipin (CL) [82]. With this in mind, it may be that unmutated *E. coli* and *B. subtilis* grown using the UB method (described in Section 3.2.2) produce significant amounts of DPPE as well as cardiolipin with more than one deuterated palmitic acid chain. The transition temperature between the

liquid crystalline and gel phase of DPPE is 63°C. For cardiolipin with four palmitic acids, the transition temperature is 62.2°C. So, if *E. coli* JM109 and *B. subtilis* are producing DPPE or cardiolipin with more than one 16-carbon acyl chain, those lipid aggregates (lipid domains or lipid aggregates inside the cell) would be in the gel-phase state, at 37°C (25°C below their transition temperatures). This is consistent with the observation that the ordered phase in the ^{2}H NMR spectra from *E. coli* JM109 is similar to that observed in the spectrum of DPPC-d_{62} at 20°C (17°C below its transition temperature) shown in Figure 4.5. The lack of this highly order structure in the spectra of the mutated *E. coli* LA8 suggests that the PA-d_{31} is possibly not incorporated in as large a range of lipids as in *E. coli* JM109 and *B. subtilis*.

4.5 Discussion

This chapter describes the ^{2}H NMR spectra of deuterated lipids in *E. coli* LA8, *E. coli* JM109 and *B. subtilis*. All the spectra exhibit characteristics that indicate the presence of a lipid liquid-crystalline phase, despite the differences in lipid composition and bacterial envelope composition between the organisms. All the bacteria preparation protocols resulted in reproducible spectra (Figures 4.1, 4.2 and 4.3).

In order to compare the results obtained here for *E. coli* LA8 with previous studies, the values of M_1, M_2 and Δ_2 for untreated samples from Table 4.1 were compared with the values reported by Pius *et al.* in 2012 [6]. The values reported by Pius *et al.* ranged from 4.5 $\times 10^4$ s^{-1} to 4.9 $\times 10^4$ s^{-1} for M_1, from 3.4 $\times 10^9$ s^{-2} to 4.1 $\times 10^9$ s^{-2} for M_2, and from 0.27 to 0.28 for Δ_2. Thus, the M_1 and M_2 values obtained here are between the Pius *et al.* M_1 and M_2 values. Δ_2 is a measure of the overall shape in the spectrum, i.e. the distribution of splittings (see Section 2.3.2.1) and is also inversely proportional to M_1. As a consequence, the slightly lower M_1 values observed in the spectra reported here are expected to lead to the slightly higher values of Δ_2. While there may be some minor differences in bacterial preparation protocols that lead to slightly different Δ_2 values, the most important result is

that within the dataset reported here, the spectra and moments calculated from the spectra are consistent.

The results obtained for *E. coli* JM109 were also compared with previous results in ampicilin resistant *E. coli* pPD117. The values of M_1, M_2 and Δ_2 from Table 4.3 were compared with the values of M_1, M_2 and Δ_2 reported by Tardy-Laporte *et al.* in 2013 [1]. The values reported by Tardy-Laporte *et al.* are 6.3 $\times 10^4$ s^{-1} for M_1, 9.0 $\times 10^9$ s^{-2} for M_2 and 0.68 for Δ_2. The average M_1 and M_2 values in this study are 48% and 98 % larger (respectively) than those in Tardy-Laporte *et al.* while the Δ_2 value reported value here is 30% smaller. The main difference between the spectra reported in Figure 4.2 and the one reported by Tardy-Laporte *et al.* is the presence of intensity out to frequencies of $\sim \pm$ 62.5 kHz, also referred to in this thesis as the "highly ordered structure". This feature is responsible for the larger M_1 and M_2 values reported here. Overall, the M_1 and M_2 values reported here indicate that the proportion of lipids in a gel-like phase is greater for the deuterated bacteria relative to those reported by Tardy-Laporte *et al.*

4.5.1 Comparison of the *E. coli* (LA8), *E. coli* JM109 and *Bacillus subtilis* ^{2}H NMR Specta

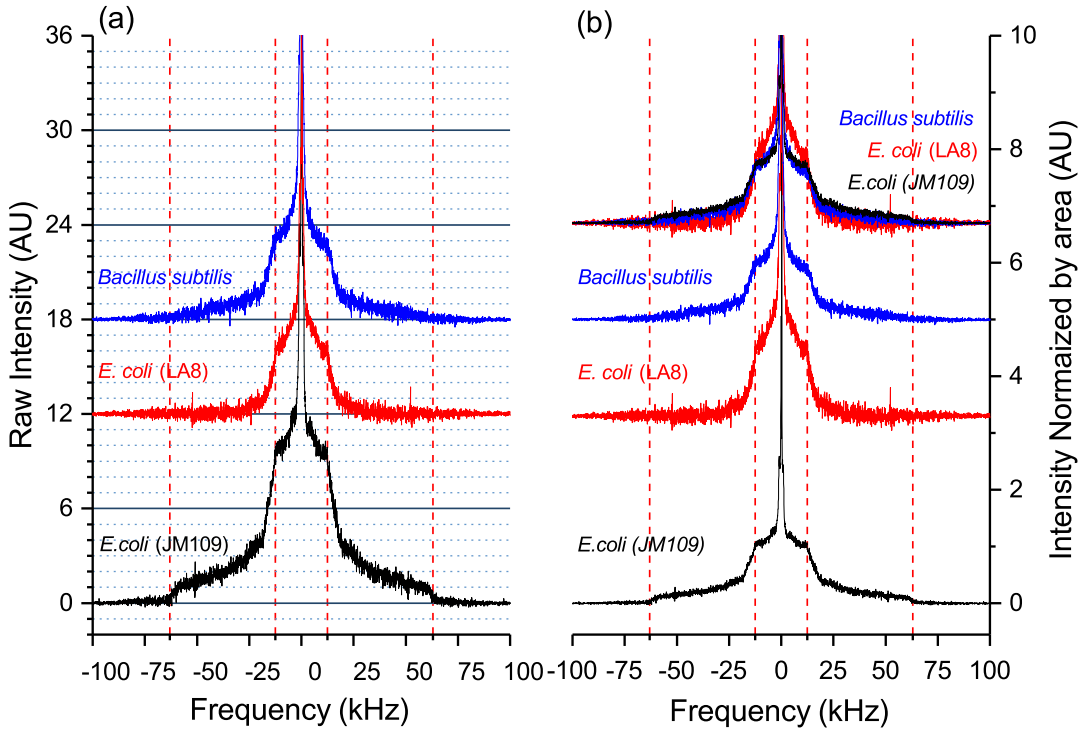

FIGURE 4.6: Comparison of the ^{2}H NMR spectum of *E. coli* JM109, *E. coli* (LA8) and *B. subtilis* enriched with deuterated acyl chains. (a): Absolute intensity spectra. (b): Spectra normalized by area. Dashed lines at ± 12.5 and ± 62.5 kHz are included to facilitate comparison of the spectra. Each spectrum represents 32,000 scans recorded over eight hours at 37 $^\circ C$ in a 9.4 T NMR spectrometer.

As mentioned above, the bacterial cell envelope has several functions but each species of bacteria accomplishes the same objectives in different ways. In particular, even though the lipid bilayer of the bacterial cell envelope is an essential component for all bacteria, each bacteria species has a distinctive lipid composition [10]. Due to the differences in bacterial cell envelope and lipid composition between *E. coli* LA8, *E. coli* JM109 and *B. subtilis* they might not necessarily be expected to give the same ^{2}H NMR spectra.

TABLE 4.5: Comparison of the deuterated acyl chains provided in the media for growing *E. coli* (LA8), *E. coli* (JM109) and *Bacillus subtilis*.

Bacterial species	PA-d_{31} concentration ([PA-d_{31}]) (mM)	Raw intensity at + 12.5 kHz (AU)	Raw intensity ratio to [PA-d_{31}]
E. coli LA8	0.174	3.5 ± 0.7	20 ± 4
E. coli JM109	0.25	10 ± 2	39 ± 7
B. subtilis	0.083	4.2 ± 0.9	51 ± 10

The ^2H NMR spectra of *E. coli* (LA8), *E. coli* JM109 and *B. subtilis* are shown together in Figure 4.6. Figure 4.6(a) shows absolute intensity ^2H NMR spectra and Figure 4.6(b) shows the corresponding ^2H NMR spectra normalized by area. One of the more evident differences between the three ^2H NMR spectra shown in Figure 4.6 is the difference in the raw intensity (Figure 4.6(a)). Considering that the mass of cells loaded into the NMR tube is very similar (See the relation between the ln(Dry weight) and A_{600} for *E. coli* JM109 and *B. subtilis* in Figure 3.1), the differences in the raw spectral intensity are likely due to the amount of deuterated acyl chains incorporated into the bacterial cell envelopes.

Another comparison of interest is the relative amount of uptake of deuterated acyl chains by the three types of bacteria. Henceforth, the concentrations of deuterated palmitic acid ([PA-d_{31}]) in the growing media will be referred as PA-d_{31} concentration. Thus, the raw intensity to PA-d_{31} concentration ratio can be considered as an indicator of the acyl chain uptake of each strain. As explained above, the concentration of deuterated acyl chains in the growth media is different for each species of bacteria depending on the membrane-deuteration strategy and on the lipid membrane composition of each species (See Section 3.2). The raw intensity to PA-d_{31} concentration ratio was calculated for each spectrum shown in Figures 4.1, 4.2, 4.3 and tabulated in Table 4.5, along with the PA-d_{31} concentration and the average over all raw intensity samples at + 12.5 kHz and the standard deviation was reported as the uncertainty. Notice that *E. coli* LA8 has the lowest raw intensity to PA-d_{31} concentration ratio and *B. subtilis* the largest. It appears that *B. subtilis* achieves a more efficient PA-d_{31} uptake and that *E. coli* LA8 shows the lowest uptake. Comparison of the ratio of *E. coli* LA8 and JM109 strains indicates that using DPC + fatty acids in growth media results in more ^2H incorporation into the membrane than using the mutated *E. coli*.

Figure 4.6(b) shows that all bacterial spectra share sharp edges at $\sim \pm$ 12.5 kHz. This is an indicator that the bacterial membranes of the three bacteria are in the liquid-crystalline state.

4.5.2 ^{2}H NMR spectra of whole bacteria in the presence of AMPs

The small changes observed in the spectral shape of *E. coli* LA8 (Figure 4.1) and in the M_1, M_2 and Δ_2 values of the AMP-treated bacterial sample (Table 4.1) are likely within the normal variability between samples. It may be that 20% wt/wt AMP is not enough peptide to see a substantial change in the spectral shape, at least for these bacteria. Because the production of large AMP quantities was an obstacle at the time this work was done, it was decided to use the AMP available for future experiments.

Unlike the case for *E. coli* LA8, treatment of *E. coli* JM109 with 17% wt/wt MSI-78 (Figure 4.2) induced changes in the Δ_2 values (Table 4.3). The increase in the mean square width of the order parameter distribution, Δ_2, presumably reflects the increase in intensity close to the methyl deuteron doublet and the reduction of the sharp edges that occurs only in the presence of the AMP. Those changes indicate a change of the order parameter profile that is reflected in Δ_2. A reduction of the quadrupolar splitting in the plateau region of the order parameter profile is commonly reported in the ^{2}H NMR studies of model lipid systems when they are treated with different AMPs [48, 83–88]. The transfer, however, of intensity from the prominent edges region to narrower splittings as a result of AMP treatment is, to the best of our knowledge, only seen in the ^{2}H NMR spectra of deuterated-rich-membrane of whole bacterial cells [6, 8]. It is interesting to consider the types of changes in lipid order and/or structure that are consistent with the changes in the shapes of the NMR spectra with AMPs. On the one hand, highly curved structures like hexagonal phases or lipid pores give rise to increases in the intensity at the narrower splittings along with smaller quadrupolar splittings than the ones observed in a lipid bilayer in a liquid-crystalline phase. In effect, the order parameter profiles of highly curved lipid structures tend to present a less pronounced plateau region and show a more linear decay of order along the

chain. The generation of toroidal pores by AMPs has been suggested in previous NMR studies, including Marcotte *et al.* in 2003 [89], Bertelsen *et al.* in 2012 [90] and, Kwon *et al.* in 2013 [91], and it is possible that perturbation of bilayers in this way might result in an order parameter profile consistent with the spectral changes seen in Figure 4.2. On the other hand, in model lipid bilayers treated with AMP, there is a decrease in the order parameter in the plateau region without the increase of intensity at narrow splittings. This has generally been interpreted as AMP-induced-disordering of the head group region.

A preferential interaction of certain AMPs with specific lipid domains [92, 93] led to the proposal of an additional mechanism of AMPs that involves the modification of lipid domains [78, 94, 95]. Lipid domains can be described as membrane areas with different lipid composition. The existence of those domains in bacterial membranes has been discussed at length [78, 96–99]. To explore the possibility that lipid domains underlie either the highly ordered components of the spectra, or relate to the AMP-induced changes observed in later chapters, it is important to consider the size of the domains and if they are likely to be observable on the timescale of these NMR experiments.

4.5.3 Can lipid domains be measured during the timescale of a ^{2}H NMR measurement?

The formation of domains has been suggested to depend on lipid charge and intrinsic curvature, and has been related to the distribution of cardiolipin and membrane proteins in the bacterial membrane [99]. Mukhopadhyay *et al.* proposed a theoretical model that suggests that lipids with a certain intrinsic curvature can aggregate and form lipid domains [100]. Because of the intrinsic curvature of those lipids side by side, the size of a lipid domain can be defined with a curvature ratio. Mukhopadhyay *et al.* predicted an optimal domain size of $\gamma = 10^{-1}$ nm which is an area of approximately 31.4×10^3 Å or $\sim$ 500 lipids with a polar head area of $\sim$ 64 Å^2 each [100]. In order to be able to observe a two-component ^{2}H NMR spectrum, the fraction of lipids exchanging between environments on the timescale of the NMR observation must be small. The minimum domain size for which distinct spectral components could be observed can be estimated by considering a single

fluid lipid bilayer, where the lipids are free to diffuse with a diffusion constant $D \sim 10\ \mu m^2/\text{s}$ [100], and an experimental timescale of $\tau \lesssim 10^{-5}$ s [62]. During the time of an NMR observation, a labeled lipid is able to sample an area of A $\sim \pi\langle r\rangle^2 = 4\pi \text{D}\tau = 125.7 \times 10^3$ Å^2. Thus, during a ^{2}H NMR measurement, a labeled lipid is able to sample an area approximately four times bigger than the predicted size of a bacterial membrane lipid domain. The resulting spectrum would be expected to reflect a two-weighted average lipid environment. This comparison also suggests that the source of the ordered phase components observed in the *E. coli* JM109 and *B. subtilis* spectra is unlikely to be ordered phase domains within the bacterial membranes. Thus, the existence of small lipid domains is possible but it is unlikely to be directly detectable during a ^{2}H NMR measurement.

Chapter 5

B. subtilis Interaction with AMPs

The main goal of this project is to determine if the peptidoglycan layer in the bacterial cell envelope impacts the interaction between the bacterial lipid membrane and two different AMPs, MSI-78 and BP100. Section 4.3 described the characterization of the ^{2}H NMR spectra of *B. subtilis*, which was the first step toward achieving the main goal. The next step was to study the changes in *B. subtilis* ^{2}H NMR spectra in the presence of MSI-78 and BP100. To do so, the ^{2}H NMR spectra of *B. subtilis* treated with each peptide at different concentrations were obtained and compared with the control spectra.

5.1 Changes in the ^{2}H NMR spectra of deuterium-enriched *B. subtilis* induced by MSI-78

Figure 5.1(a) shows the absolute intensity ^{2}H NMR spectra and Figure 5.1(b) the spectra normalized by area of *B. subtilis* in absence of MSI-78 in black, in the presence of 10% wt/wt of MSI-78 in blue and in the presence of 20% wt/wt of MSI-78 in pink. Comparison of the reference spectrum and the spectra of MSI-78-treated samples in Figure 5.1(b) shows a significant change in the spectral shape with the addition of the peptide. The changes in the spectral shape resulting from the interaction with the AMP included a reduction of the prominent edges at $\sim \pm$ 12.5 kHz and an increase of the intensity at narrower splittings. Changes in

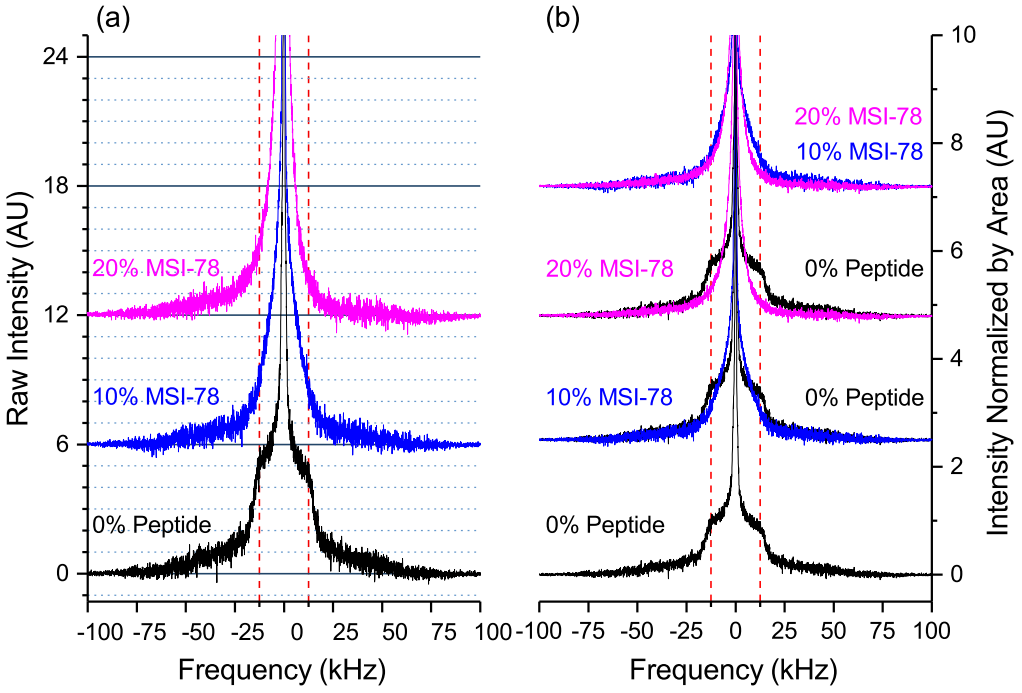

FIGURE 5.1: Change in ^{2}H NMR spectra of *B. subtilis* induced by the presence of MSI-78. Black: reference spectrum (NS53) with no peptide; Blue: with 10% MSI-78 (wt/wt); Magenta: with 20% MSI-78 (wt/wt). (a): Absolute Intensity spectra. (b): Spectra normalized by area. Samples were prepared using the protocol explained in Sections 3.2.2.3 and 3.5. Dashed lines at ±12.5 kHz are shown to facilitate comparison of the spectra. Each spectrum represents 32,000 scans recorded over eight hours at 37°C in a 9.4 T NMR spectrometer.

the spectral shape are slightly more pronounced for the sample treated with 20% wt/wt MSI-78 than for the sample treated with 10% wt/wt MSI-78. The changes in the spectral shape are consistent with a reduction in the average orientational order of the acyl chains in the membrane.

Table 5.1 shows the comparison of the M_1, M_2, and Δ_2 values for the ^2H NMR spectra of *B. subtilis* in the absence and presence of MSI-78. While the shape of the spectra with 10 and 20% MSI-78 appear substantially different from the reference spectrum and all the control spectra shown in Figure 4.3, the changes in M_1 and M_2 resulting from treatment with 10% MSI-78 are not different within the estimated uncertainty. However, Δ_2 provides a better reflection of the spectral shape changes and increases noticeably as AMP concentration increases. In fact,

TABLE 5.1: M_1, M_2 and Δ_2 values, as defined in section 2.3.2.1, for ^2H NMR spectra of *B. subtilis* in the absence of AMP (average over six samples shown in Table 4.4) and in the presence of MSI-78 shown in Figure 5.1

Peptide Concentration % (wt/wt)	M_1 $\times 10^4 (s^{-1})$	M_2 $\times 10^9 (s^{-2})$	Δ_2
0 (Average over untreated samples)	6.2 ± 1	8.4 ± 3	0.59 ± 0.08
10	6.1	9.5	0.92
20	4.4	6.5	1.45

after treatment with 20% MSI-78, Δ_2 more than doubled relative to its value for the untreated sample.

5.2 Changes on the ^{2}H NMR spectra of deuterium-enriched *B. subtilis* induced by BP100

Figure 5.2(a) shows the absolute intensity ^{2}H NMR spectra and Figure 5.2(b) the spectra normalized by area of *B. subtilis* in the absence of BP100, in black, and in the presence of 20% wt/wt BP100, in red. The comparison between the reference spectrum (black) and the BP100 treated sample (red) shows a significant change in the spectral shape. As with 20% wt/wt MSI-78, the presence of 20% wt/wt BP100 causes a reduction of the prominent edges at $\sim \pm$ 12.5 kHz and an increase of the intensity at smaller splittings. Only one concentration of BP100 was tested due the similarity of the effect of 20% wt/wt MSI-78 with the effect of 20% wt/wt BP100. The changes in the spectral shape are consistent with a decrease in the average orientational order of the acyl chains in the membrane.

Table 5.2 shows the comparison of the M_1, M_2, and Δ_2 values for the ^2H NMR spectrum of *B. subtilis* in the absence and presence of BP100. The observed decrease in M_1 value upon the addition of BP100 indicates a shift of the splittings to smaller values. There is also a decrease in the M_2 values upon the addition of 20% BP100 and a considerable increase in the Δ_2 values upon the addition of 20%

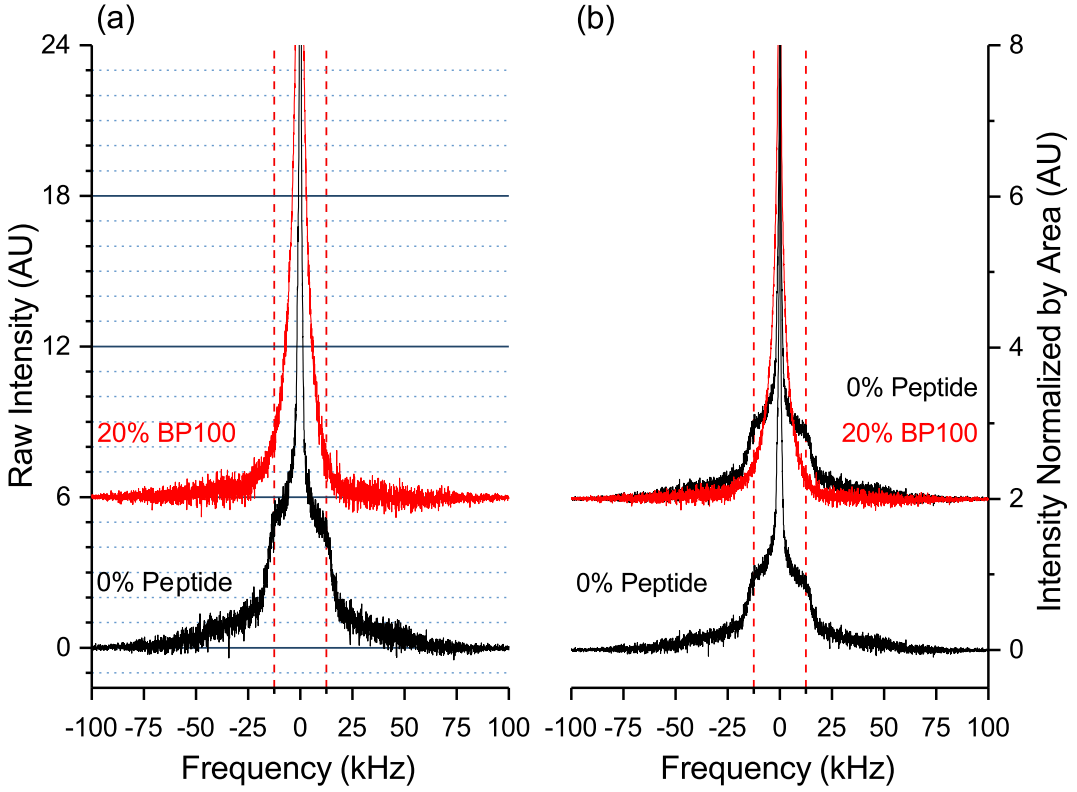

FIGURE 5.2: Change in ^{2}H NMR spectra of *B. subtilis* induced by the presence of BP100. Black: reference spectrum (NS53) with no peptide; Red: with 20% BP100 (wt/wt). (a): Absolute Intensity spectra. (b): Spectra normalized by area. Samples were prepared using the protocol explained in Sections 3.2.2.3 and 3.5. Dashed lines at ±12.5 kHz are shown to facilitate comparison of the spectra. Each spectrum represents 32,000 scans recorded over eight hours at 37°C in a 9.4 T NMR spectrometer.

BP100. This behavior indicates that the distribution of quadrupolar splittings is getting broader, despite the decrease in the average splitting.

5.3 Discussion

This chapter provided descriptions of the changes induced by the AMPs, MSI-78 (Figure 5.1) and BP100 (Figure 5.2), in the ^{2}H NMR spectra of *B. subtilis*. This is the first ^{2}H NMR observation of the whole cell lipid membrane disruption by

TABLE 5.2: M_1, M_2 and Δ_2 values, as defined in section 2.3.2.1, for ^2H NMR spectrum of *B. subtilis* in the absence of AMP (average over six samples shown in Table 4.4) and presence of BP100 shown in Figure 5.2.

Peptide Concentration % (wt/wt)	M_1 $\times 10^4 (s^{-1})$	M_2 $\times 10^9 (s^{-2})$	Δ_2
0 (Average over untreated samples)	6.2 ± 1	8.4 ± 3	0.59 ± 0.08
20	3.5	3.7	1.20

BP100. This chapter also reports the first static ^{2}H NMR observation of *B. subtilis* in the presence of any AMPs. MSI-78 and BP100 were found to cause similar changes in the membrane spectra. Those changes included a reduction of intensity in the prominent edge region and a concomitant increase at narrow splittings. While the AMP-induced disruption in the prominent edge region has been observed in model membranes, the increase in intensity at narrower splittings has been, to the best of my knowledge, observed only in the ^{2}H NMR spectra of AMP-treated whole bacterial cells, and not in model membranes. This would suggest that there is a significant difference in how AMPs interact with membranes in bacteria, as compared to their interaction with membranes in model lipid-only-systems. As shown in Figure 5.1, in the case of MSI-78, the changes were concentration dependent, i.e. more pronounced in the 20% than in the 10% MSI-78 treatment. These characteristic changes in the spectra of AMP-treated *B. subtilis* were also observed in *E. coli* JM109 in the presence of MSI-78.

The AMP-induced reduction in the prominent edges and the attendant increase in intensity at narrower splittings were also reflected in the M_1 and Δ_2 values. For both BP100 and MSI-78, there was an increase in Δ_2 and a decrease in M_1 associated with the presence of 20% wt/wt of AMP (see Table 5.1 for MSI-78 and 5.2 for BP100). The decrease in M_1 and the increase in Δ_2 indicate a lower mean order parameter and a greater relative mean squared width of the order parameter distribution. These changes are consistent with an increase in the disorder along the whole acyl chain and a disruption in the lipid bilayer of the AMP treated samples. 2.1

5.3.1 Comparison of the effect of MSI-78 and BP100 on the ^{2}H NMR spectra of deuterium-enriched *B. subtilis*.

In order to assess possible differences between the effects of MSI-78 and BP100 on the *B. subtilis* membrane, ^{2}H NMR spectra of *B. subtilis* in the presence of the same concentrations of MSI-78 and BP100 were plotted together in Figure 5.3.

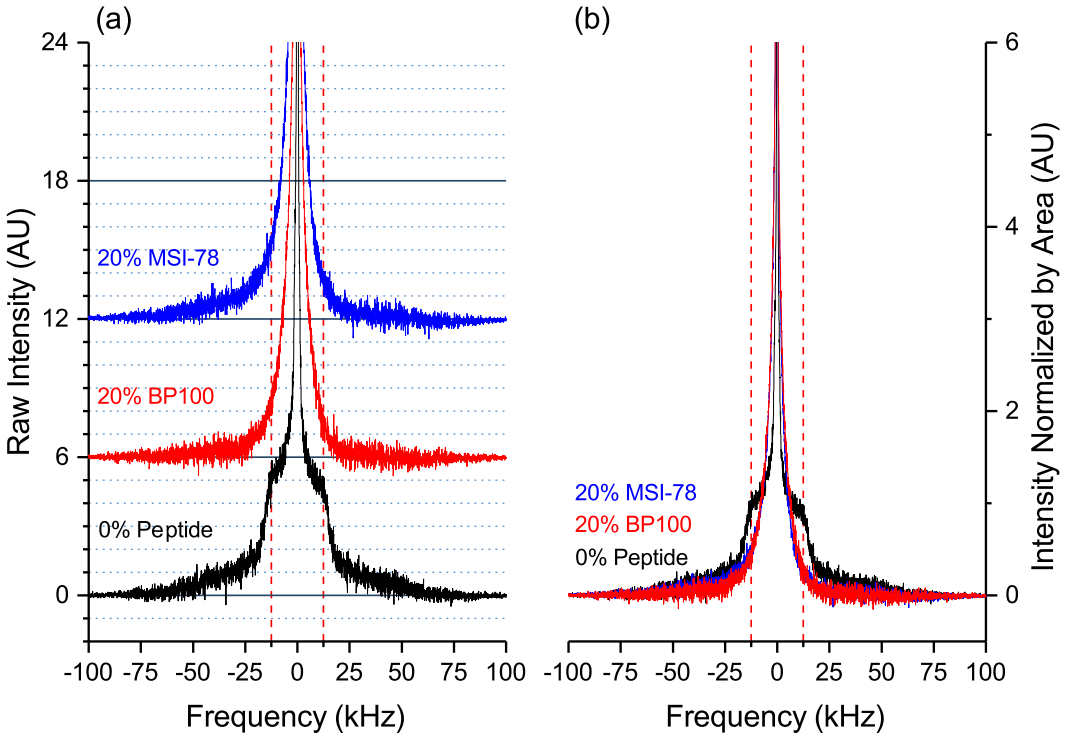

FIGURE 5.3: Comparison of the changes in ^{2}H NMR spectra of *B. subtilis* induced by the presence of BP100 and MSI-78. Black: reference spectrum (NS53) with no peptide; Red: with 20% BP100 (wt/wt): Blue: with 20% MSI-78 (wt/wt). (a): Absolute Intensity spectra. (b): Spectra normalized by area. Samples were prepared using the protocol explained in Sections 3.2.2.3 and 3.5. Dashed lines at ±12.5 kHz are shown to facilitate comparison of the spectra. Each spectrum represents 32,000 scans recorded over eight hours at 37°C in a 9.4 T NMR spectrometer.

Figure 5.3(a) shows the absolute intensity ^{2}H NMR spectra and Figure 5.3(b) the spectra normalized by area of *B. subtilis* in absence of AMP in black, in the presence of 20% wt/wt BP100 in red, and in the presence of 20% wt/wt MSI-78

in blue. Both AMPs caused similar changes in the ^{2}H NMR spectra of *B. subtilis*, i.e., a reduction of the prominent edges at $\sim \pm$ 12.5 kHz, and an increase of the intensity at smaller splittings. There appears to be no difference in the spectral shape changes induced by the two peptides, suggesting that the changes and membrane perturbations are not particular to either AMP and that analogous quantities of MSI-78 and BP100 causes similar levels of perturbation. This is particularly interesting since possible secondary targets have been suggested for MSI-78 and BP100. In the case of BP100, an interaction of this AMP with the LPS layer of Gram - bacteria and the lipoteichoic acid (LTA) of Gram - bacteria have been reported [58, 101, 102] as well as an interaction of MSI-78 with the bacterial ribosomes [31]. Notice that the LPS and LTA are extracellular components of the bacterial cell, and the ribosomes are located inside of the cell membrane. Summarizing, MSI-78 and BP100 caused similar levels of perturbation in the bacterial membrane despite one having an intracellular secondary target and the other one an extracellular secondary target. Both peptides are positively charged and have similar hydrophobicity (as judged by the GRAVY index[1] of -0.16 for MSI-78 and -0.19 for BP100). The charge difference alone may cause a difference in the binding affinity to lipid bilayers of both peptides; however, both of them cause the same lipid bilayer disruption at analog concentrations.

TABLE 5.3: M_1, M_2 and Δ_2 values, as defined in section 2.3.2.1, for ^2H NMR spectrum of *B. subtilis* in the absence (average over six samples shown in Table 4.4) and presence of 20 % MSI-78 and BP100 showed in Figure 5.3.

Peptide Concentration % (wt/wt)	M_1 $\times 10^4 (s^{-1})$	M_2 $\times 10^9 (s^{-2})$	Δ_2
0 (Average over untreated samples)	6.2 $\pm$ 1	8.4 $\pm$ 3	0.59 $\pm$ 0.08
20 MSI-78	4.4	6.5	1.45
20 BP100	3.5	3.7	1.20

Table 5.3 shows the comparison of the M_1, M_2 and Δ_2 values for the ^2H NMR spectrum of *B. subtilis* in the absence and presence of MSI-78 and BP100. Both AMPs generated a reduction in the M_1 and M_2 as well as an increase in the Δ_2

[1] GRAVY index (Grand Average of hydropathy) is a value used to measure the hydrophobicity of peptides or proteins. Positive values indicate more hydrophobic structures and negative value indicate more hydrophilic structures. Values close to 0 are typical of amphiphilic sequences.

values. Considering that Δ_2 is the relative mean square width of the distribution of orientational order parameter, an increase in Δ_2 is a result of the reduction of the plateau region of the orientational order profile.

Chapter 6

Peptidoglycan Disruption Does not Affect AMPs' effects on ^2H NMR Spectra of *B. subtilis* Lipid Bilayer

The main goal of this project is to determine if the peptidoglycan (PGN) layer in the bacterial cell envelope impacts the interaction between the bacterial lipid membrane and two different AMPs, MSI-78 and BP100. The chosen research approach included 1) assessing the changes in the ^{2}H NMR spectra of *B. subtilis* with the addition of MSI-78 and BP100 (Sections 5.1 and 5.2), 2) exploring possible changes in the *B. subtilis* spectra caused by the disruption of the PGN layer (Section 6.1.1), and 3) studying the *B. subtilis* spectra with the combination of a compromised PGN layer and treatment with BP100 and MSI-78 (Section 6.2).

6.1 Disrupting the PGN layer of *B. subtilis*

Lysozyme is a 129 amino acid enzyme known for its ability to hydrolyze the PGN layer of the bacterial cell wall. The lysozyme monomer can hydrolyze a specific structural linkage of the polysaccharide copolymers that contribute to PGN rigidity. Because the PGN is responsible for the stability of the bacterial shape under hypertonic conditions, disruption of the PGN layer can result in cell lysis, i.e.

breaking open the cell. Lysozyme is present in body fluids, secretions and tissues of humans and animals due to its antibiotic properties [103]. Given the antimicrobial effect of lysozyme, and the objectives of this work, it was necessary to optimize the lysozyme concentration and treatment time that disrupts the PGN without causing lysis of the cell. In 2011, Muchová *et al.* reported work that included the preparation of *B. subtilis* protoplasts [79]. Protoplasts include a Gram + bacteria whose cell walls have been largely but not entirely removed [104]. The protocol implemented by Muchová *et al.* uses lysozyme to remove the PGN layer in *B. subtilis* followed by the resuspension of the cells in a sucrose-rich buffer to prevent cell lysis due to osmotic pressure. While the goal of Muchová's *et al.* protocol was to remove, almost entirely, the PGN layer, my purpose was to induce only a partial disruption of the PGN layer. Thus, Muchová's *et al.* protocol was used as a starting point to optimize the lysozyme concentration needed to partially degrade the PGN layer in a fixed time of 10 minutes.

One of the easiest ways to observe the change in the PGN content in a bacterial cell is Gram staining. Gram staining is a method that is frequently used to differentiate Gram + and Gram - bacteria. Gram staining consists of a series of steps that include staining with crystal violet, decolorization using 95% ethyl alcohol and counterstaining with safranin. During the decolorization process, Gram + bacteria get dehydrated which induces the pores of the cell wall to shrink, causing the crystal violet to get trapped in the PGN layer and giving cells a purple colour. On the other hand, the thin PGN layer of Gram - bacteria allows the crystal violet to be washed away. This difference in the decolorization process causes Gram - bacteria to only retain the safranin solution and to appear pink in the microscope. The enzymatic disruption of the *B. subtilis'* PGN layer leads it to also appear pink after Gram staining.

Figures 6.1(a) and 6.1(b) shows the Gram staining of *B. subtilis* without lysozyme treatment. Gram staining was performed using the protocol in Section 3.4. Figure 6.1(a) includes an approximate scale bar. As expected, the colour of the untreated bacteria is purple and reflects an intact PGN layer. Figure 6.1(c) shows the Gram staining of *B. subtilis* after being treated with 0.1 mg/ml lysozyme for 10 minutes. The disruption of the PGN layer can be inferred from the change in the Gram staining colour from purple to pink. Figure 6.1(d) shows the Gram staining of *B.*

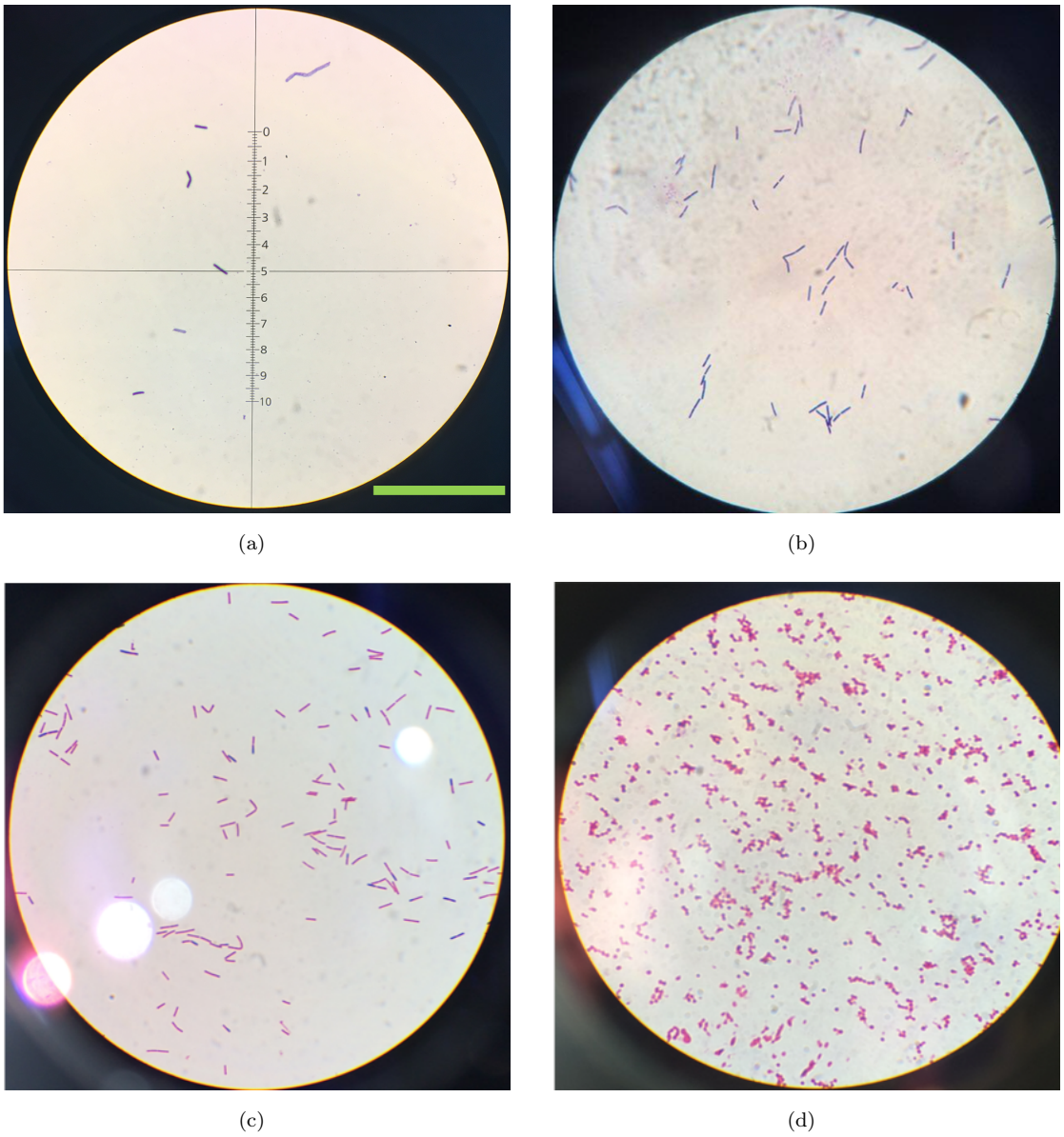

(a) (b)

(c) (d)

FIGURE 6.1: Gram staining change induced by different lysozyme treatments. Gram staining of *Bacillus subtilis* treated with (a) and (b) 0 mg/ml, (c) 0.1 mg/ml and (d) 10 mg/ml of lysozyme for 10 minutes. Bacterial samples were tested in different stages of the protocol resulting in pictures with different cell concentration. Approximate scale bar represent 5 μm (see section 3.4).

subtilis after being treated with 10 mg/ml lysozyme for 10 minutes. In addition to the change in the Gram staining colour, there are no observable rod-shape cells after treatment with 10 mg/ml lysozyme, i.e. all the cells are roughly spherical. This rounding-up indicated near-total removal of the PGN layer of *B. subtilis*, i.e. the formation of *B. subtilis* protoplasts.

6.1.1 Different lysozyme treatments do not change ^2H NMR spectra of *B. subtilis*

In order to explore the possible changes in the ^{2}H NMR *B. subtilis* spectra caused by the disruption of the PGN layer, spectra were obtained from samples treated with a lysozyme concentration from 0.01 mg/ml to 10 mg/ml of lysozyme (Figure 6.2).

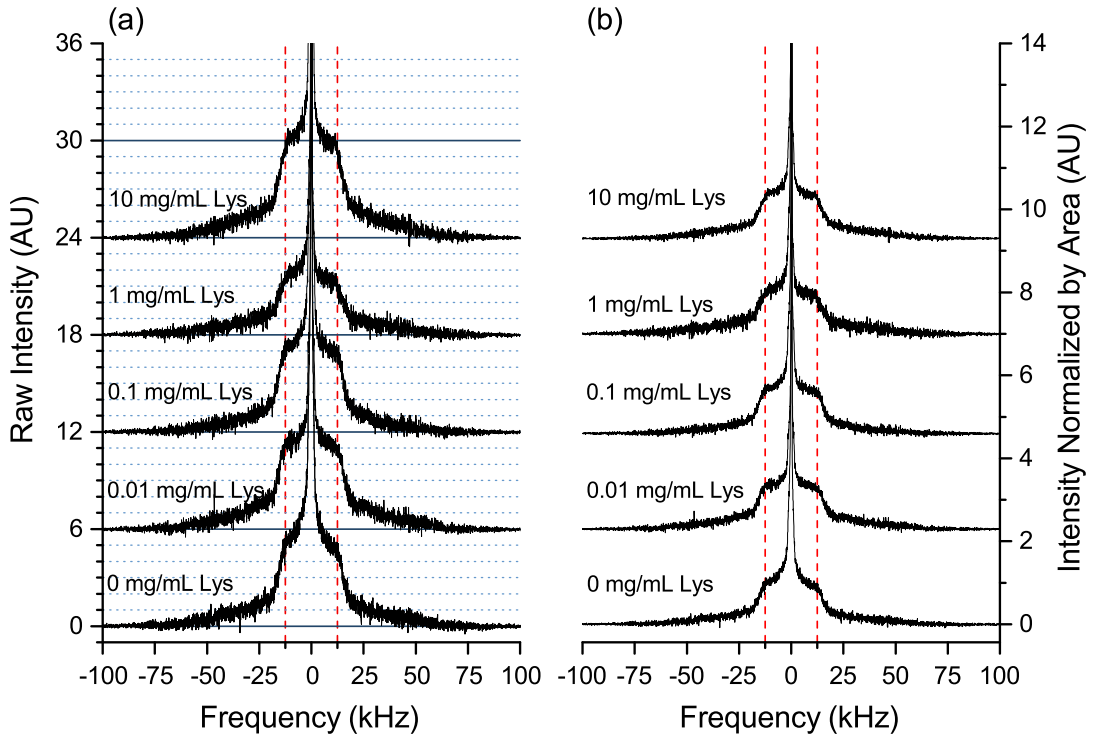

FIGURE 6.2: PGN disruption does not affect ^2H NMR spectra of *B. subtilis*. ^2H NMR spectra of *B. subtilis* enriched with deuterated acyl chains treated with up to 10 mg/ml of lysozyme. (a): Absolute intensity spectra of *B. subtilis* treated with 0 mg/ml, 0.01 mg/ml, 0.1 mg/ml, 1 mg/ml and 10 mg/ml. (b): Spectra normalized by area. Dashed lines at ±12.5 kHz are included to facilitate comparison of the spectra. Each spectrum represents 32,000 scans recorded over eight hours at 37°C in a 9.4 T NMR spectrometer.

Figure 6.2 shows spectra of *B. subtilis* treated with up to 10 mg/ml lysozyme, with the absolute intensity spectra in panel a and the normalized spectra in b. Spectra

of four different preparations treated with different concentrations of lysozyme using the protocol detailed in Section 3.3 are shown. All preparations exhibit similar signal-to-noise ratios and prominent edges at $\sim$ 12.5 kHz. These prominent edges indicate the persistence of the plateau region of the order parameter profile, which suggests little or no disruption of the acyl chains of the bacteria with lysozyme treatment alone. A low intensity spectral component between $\sim$ 12.5 and 62.5 kHz is present in all of the *B. subtilis* spectra and does not change with lysozyme treatment. There is thus no spectroscopically-observable evidence of lysozyme perturbing or disrupting the lipid bilayer of the bacterial membrane.

TABLE 6.1: M_1, M_2 and Δ_2 values, as defined in section 2.3.2.1, for ^2H NMR spectrum of *B. subtilis* (average over six samples shown in Table 4.4) and *B. subtilis* treated with different concentrations of lysozyme showed in Figure 6.2. M_1, M_2 and Δ_2 values for the untreated sample are an average over six samples, the estimated uncertainty corresponds to the standard deviation.

Lysozyme Concentration (mg/ml)	M_1 $\times 10^4 (s^{-1})$	M_2 $\times 10^9 (s^{-2})$	Δ_2
0 (Average over six untreated samples)	6.2 $\pm$ 1	8.4 $\pm$ 3	0.59 $\pm$ 0.08
0.01	8.7	15	0.49
0.1	7.6	12	0.53
1	8.8	16	0.50
10	8.6	15	0.51

Table 6.1 shows the values of the first and second moments, M_1 and M_2 along with the Δ_2 values for all the spectra shown in Figure 6.2. M_1 values for the treated samples were slightly larger than the average M_1 of untreated samples but close to the untreated sample with the highest M_1, i.e. 7.9×10^4 s^{-1}(See Table 4.4). The 1 and 10 mg/ml treated samples had a higher M_2 higher than the untreated samples, but close to the untreated sample with the highest M_2, i.e. 13×10^9 s^{-2} (See Table 4.4). The calculated Δ_2 values for the treated samples were very similar to the average of the untreated samples. The changes in the M_2 values are a result of the slightly increase in the M_1 values but, Δ_2 remains relatively unchanged.

In summary, lysozyme treatment does not appear to affect the lipid membrane structure and dynamics at all. It is quite interesting to know that while PGN is needed for cell envelope rigidity, disrupting it appears to have no effect on the membrane structure and dynamics. To follow up on this observation, I carried out experiments with lipids extracted from the bacteria to compare to intact bacteria samples.

6.1.2 Comparing spectra of deuterated lipids in intact cells, lysed cells and in lipids extracted from *B. subtilis*

A standard biochemical procedure can be used to extract the lipid component of cells with non-polar organic solvents. Bacteria were prepared with deuterated lipids as usual, and then the lipids extracted in this way. Extracted lipids were dried and then resuspended in 2×YT media, to preserve the amount of salt in the sample, as detailed in Section 3.6.

The red spectrum in Figure 6.3 shows the ^{2}H NMR spectrum of the lipids extracted from *B. subtilis*. The absolute intensity spectrum is shown in Figure 6.3(a) and the spectrum normalized by area is shown in Figure 6.3(b). In Figure 6.3(b) the lipid extract spectrum is compared with the ^{2}H NMR spectrum of intact *B. subtilis*. Both spectra display prominent edges at $\sim \pm$ 12.5 kHz and similar signal-to-noise ratios. It is only the spectrum of the whole cells, however, that exhibits intensity out to frequencies of $\sim \pm$ 62.5 kHz. Since this intensity is likely due to the bacteria retaining and storing lipids in a gel like phase state, it is not surprising that this spectral component is not present in the ^{2}H NMR spectra of the lipids extracted from *B. subtilis*.

Given how similar the spectra from the lipids alone and the lipids within the intact cells are, I was also interested in how the spectra of cell lysate would look. For this, the deuterated *B. subtilis* were broken open mechanically, via shear stress (see section 3.6 for more details about french press process), but not treated with any organic solvents.

The blue spectrum in Figure 6.3 shows the ^{2}H NMR spectrum of *B. subtilis* cell lysate. The absolute intensity spectrum is shown in Figure 6.3(a) and the spectrum

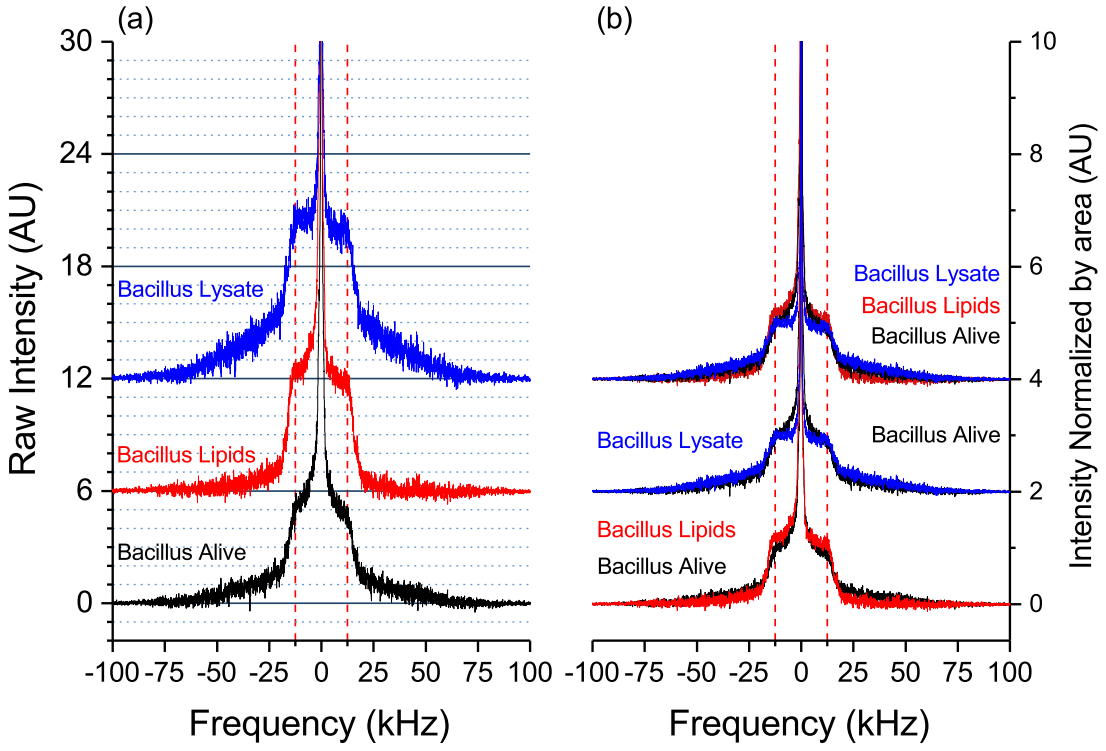

FIGURE 6.3: ^2H NMR spectra of *B. subtilis*: lipids prepared three ways. ^2H NMR spectra of Black: *B. subtilis* enriched with deuterated acyl chains. Red: Lipids extract from *B. subtilis* enriched with deuterated acyl chains and Blue: Cell lysate from *B. subtilis* enriched with deuterated acyl chains. (a): Absolute intensity spectra. (b): Spectra normalized by area. Dashed lines at ±12.5 kHz are included to facilitate comparison of the spectra. Each spectrum represents 32,000 scans recorded over eight hours at 37°C in a 9.4 T NMR spectrometer.

normalized by area is shown in Figure 6.3(b). In Figure 6.3(b) the cell lysate spectrum is compared with the ^{2}H NMR spectrum of *B. subtilis*. Both spectra display prominent edges at $\sim \pm$ 12.5 kHz and similar signal-to-noise ratios.

Table 6.2 shows the values of the first and second moments, M_1 and M_2, along with the Δ_2 values for all the spectra shown in Figure 6.3. The difference in intensity at the wide splittings out to $\sim \pm$ 62.5 kHz between the samples is reflected by the M_1 and M_2 values. The highest values of M_1 and M_2 were obtained from the cell lysate sample and the lowest values from the lipid extract sample. The calculated values of Δ_2 for the lipid extract and cell lysate from *B. subtilis* are both slightly

TABLE 6.2: M_1, M_2 and Δ_2 values, as defined in section 2.3.2.1, for ^2H NMR spectra of *B. subtilis* (average over six samples shown in Table 4.4), lipids extract from *B. subtilis* and cell lysate from *B. subtilis* showed in Figure 6.3.

Sample Description	M_1 $\times 10^4 (s^{-1})$	M_2 $\times 10^9 (s^{-2})$	Δ_2
B. subtilis (Average over six samples)	6.2 ± 1	8.4 ± 3	0.59 ± 0.08
Lipid extract from *B. subtilis*	5.1	5.3	0.47
Cell lysate from *B. subtilis*	9.9	18.3	0.39

lower than the one reported for the whole cells. However, the differences are not significant when compared with the changes caused by the AMPs.

6.2 The combined effects of PGN disruption and treatment with AMPs on *B. subtilis*

After assessing the ^{2}H NMR spectra of *B. subtilis* with a disrupted PGN layer, the final stage of this project was to evaluate the impact of the disruption of the PGN layer on the interaction between the bacterial lipid membrane and the AMPs MSI-78 and BP100. To do so, I obtained the ^{2}H NMR spectra of *B. subtilis* with a partially disrupted PGN layer in the presence of AMPs. The effects of both AMPs were observed with cells treated with two concentrations of lysozyme, 0.01 mg/ml and 0.08 mg/ml. The two concentrations of lysozyme correspond to two levels of PGN disruption. In choosing these lysozyme concentrations, the goal was to generate a PGN disruption without killing a substantial fraction of the cells. Previous studies performed in our lab showed that lysozyme concentrations above 0.09 mg/ml reduce greatly the fraction of cells alive and capable of forming colonies [105].

6.2.1 MSI-78

As discussed above, AMPs induce a concentration-dependent reduction in the intensity from the plateau region, with a concomitant increase in the intensity at narrow splittings. Concentrations higher than 20% of AMPs were not considered.

In addition to the two levels of disruption of the PGN layer, two concentrations of MSI-78 were tested, 10% and 20% wt/wt.

6.2.1.1 10% MSI-78

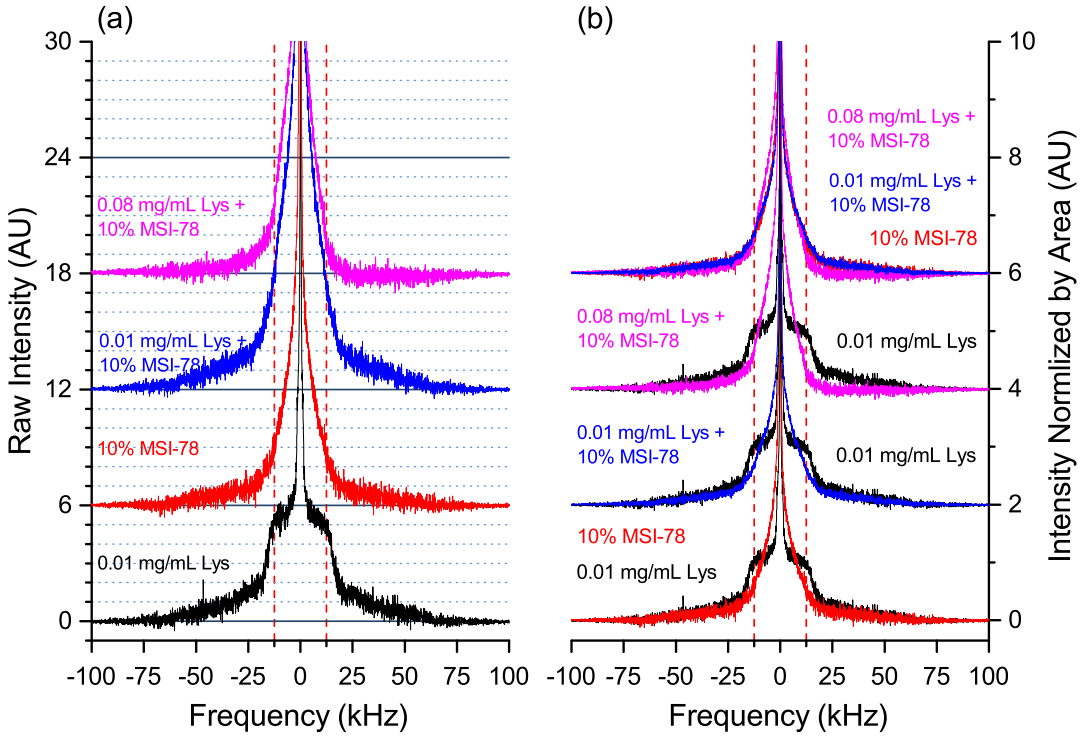

FIGURE 6.4: Disruption of the PGN layer does not change the effect of 10% MSI-78 on the ^{2}H spectra of *B. subtilis*.(a): Absolute intensity spectra of Black: cells treated with 0.01 mg/ml lysozyme for 10 min, Red: In presence of 10% MSI-78 (wt/wt), Blue: In the presence of 10% MSI-78 (wt/wt) after being treated with 0.01 mg/ml lysozyme for 10 min, Magenta: In the presence of 10% MSI-78 (wt/wt) after being treated with 0.08 mg/ml lysozyme for 10 min. (b) Spectra normalized by area. Dashed lines at ±12.5 kHz are shown to facilitate comparison of the spectra. Each spectrum represents 32,000 scans recorded in eight hours at 37°C in a 9.4 T NMR spectrometer.

Figure 6.4 shows the ^{2}H NMR spectra of *B. subtilis* treated with lysozyme only in black and with MSI-78 only in red. The spectra of the bacteria treated with the combination of the two treatments are shown in blue, for cells treated with 0.01 mg/ml lysozyme and 10% MSI-78, and in magenta for cells treated with 0.08 mg/ml lysozyme and 10% MSI-78. Figure 6.4(a) shows the absolute intensity spectra and Figure 6.4(b) the spectra normalized by area. A substantial reduction of the prominent edges at $\sim \pm$ 12.5 kHz and an increase in the intensity at the narrow splittings was observed for all the AMP treated samples. As seen from the superposition of the spectra at the top of Figure 6.4(b), the disruption of the PGN layer with 0.01 mg/mL of lysozyme does not substantially change the effect of 10% MSI-78 on the bacterial cell membrane. Nonetheless, a further disruption of the PGN layer seems to generate changes in the effect of 10% MSI-78 on the bacterial cell membrane ^{2}H NMR spectrum. Those changes included more intensity at narrow splittings ($\sim \pm$ 6 kHz) and less intensity at large splittings ($\sim \pm$ 20 kHz).

TABLE 6.3: M_1, M_2 and Δ_2 values, as defined in section 2.3.2.1, for ^2H NMR spectrum of *B. subtilis* treated with lysozyme to induce partial disruption of the PGN layer in absence (from Table 6.1) and presence of 10% MSI-78 shown in Figure 6.4.

Peptide Concentration % (wt/wt)	Lysozyme Concentration (mg/ml)	M_1 $\times 10^4 (s^{-1})$	M_2 $\times 10^9 (s^{-2})$	Δ_2
0 (Average over six samples)	0	6.2 $\pm$ 1	8.4 $\pm$ 3	0.59 $\pm$ 0.08
0	0.01	8.7	15	0.49
0	0.1	7.6	12	0.53
10	0	6.1	10	0.92
10	0.01	6.7	11	0.82
10	0.08	3.3	2.1	0.45

In addition to the direct comparison between the control spectra with the AMP + lysozyme treated spectra, M_1, M_2 and Δ_2 values were obtained. Table 6.3 shows the values of the first and second moments, M_1 and M_2, along with the Δ_2 values for all the spectra shown in Figure 6.4 and for the spectra of *B. subtilis* treated with 0.1 mg/ml lysozyme shown in Figure 6.2. The moment values (M_1 and M_2) of the PGN compromised cells treated with 10% wt/wt MSI-78 vary considerably. M_1 and M_2 for 10% MSI-78 and 0.08 mg/ml lysozyme are somewhat smaller resulting

from the increase of intensity at lower frequencies, the decrease of intensity at large splittings and the asymmetry of the spectrum. More importantly, Δ_2, which I and others have found to be most diagnostic for AMP-induced changes [1, 6, 106] is no different for this sample than for untreated cells. In this particular spectrum, there is an observable asymmetry due to a slight mistuning of the Larmor frequency before the experiment. Frequency tuning is difficult for samples containing AMP because of the sharp edges tend to disappear and the large intensity at narrow splittings gets superimposed onto the water peak. It is important to note that even though Δ_2 is sensitive to AMP-induced changes, it is also sensitive to the spectral symmetry.

6.2.1.2 20% MSI-78

Figure 6.5 shows the ^{2}H NMR spectra of *B. subtilis* treated with lysozyme only in black and with MSI-78 only in red. The spectra of the bacteria treated with the combination of the two treatments are shown in blue, for cells treated with 0.01 mg/ml lysozyme and 20% MSI-78, and in magenta for cells treated with 0.08 mg/ml lysozyme and 20% MSI-78. Figure 6.5(a) shows the absolute intensity spectra and Figure 6.5(b) the spectra normalized by area. A substantial reduction of the prominent edges at $\sim \pm$ 12.5 kHz and an increase in the intensity at the narrow splittings was observed for all the AMP-treated samples. As observed on the top spectra in Figure 6.5(b), the disruption of the PGN layer does not enhance or diminish the effect of 20% MSI-78 on the bacterial cell membrane.

Table 6.4 shows the values of the first and second moments, M_1 and M_2, along with the Δ_2 values for all the spectra shown in Figure 6.5 and the spectra of *B. subtilus* treated with 0.1 mg/ml lysozyme shown in Figure 6.2. Two of the three AMP-treated samples showed a decrease in M_1 and M_2 values. More importantly, all the AMP-treated samples demonstrated an increase in Δ_2 value, which enforces the idea that Δ_2 value is sensitive to the changes induced in the ^{2}H NMR spectra of bacterial cells treated with AMP. The combination of AMP and lysozyme resulted in an increase in the calculated Δ_2 values. However, the Δ_2 values obtained for the samples treated with lysozyme followed by 20% MSI-78 treatment were smaller than the one obtained for the only-20% MSI-78 treated sample. The experiments

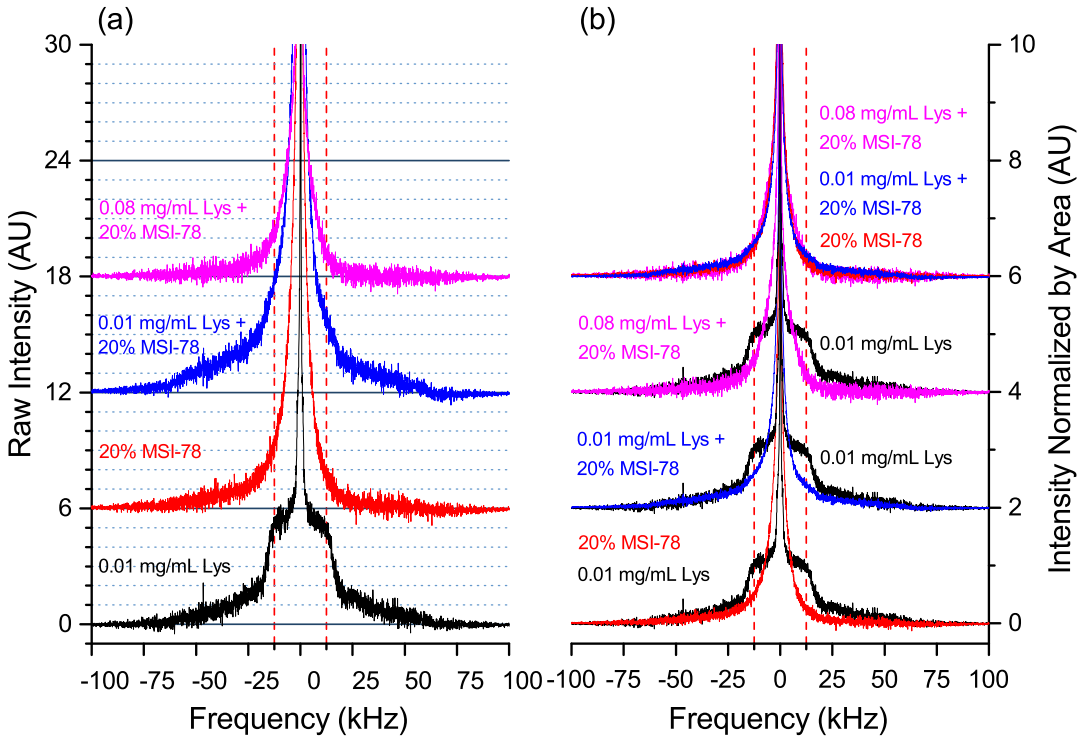

FIGURE 6.5: Disruption of the PGN layer does not change the effect of 20% MSI-78 on the ^{2}H spectra of *B. subtilis*.(a): Absolute intensity spectra of Black: cells treated with 0.01 mg/ml lysozyme for 10 min, Red: In presence of 20% MSI-78 (wt/wt), Blue: In the presence of 20% MSI-78 (wt/wt) after being treated with 0.01 mg/ml lysozyme for 10 min, Magenta: In the presence of 20% MSI-78 (wt/wt) after being treated with 0.08 mg/ml lysozyme for 10 min. (b) Spectra normalized by area. Dashed lines at ±12.5 kHz are shown to facilitate comparison of the spectra. Each spectrum represents 32,000 scans recorded in eight hours at 37°C in a 9.4 T NMR spectrometer.

would need to be repeated to determine the significance of the observed difference. In any case, if there are differences in the AMP-treated cell with and without PGN disruptions, the differences are very small compared to the effect of AMP alone.

6.2.2 BP100

Figure 6.6 shows the ^{2}H NMR spectra of *B. subtilis* treated with lysozyme only in black and with 20% BP100 only in red. The spectra of the bacteria treated with the combination of the two treatments are shown in blue, for cells treated

TABLE 6.4: M_1, M_2 and Δ_2 values, as defined in section 2.3.2.1, for ^2H NMR spectrum of *B. subtilis* treated lysozyme to induce partial disruption of the PGN layer in absence (from Table 6.1) and presence of of 20% MSI-78 shown in Figure 6.5.

Peptide Concentration % (wt/wt)	Lysozyme Concentration (mg/ml)	M_1 $\times 10^4 (s^{-1})$	M_2 $\times 10^9 (s^{-2})$	Δ_2
0 (Average over six samples)	0	6.2 ± 1	8.4 ± 3	0.59 ± 0.08
0	0.01	8.7	15	0.49
0	0.1	7.6	12	0.53
20	0	4.4	6.5	1.45
20	0.01	6.3	11	1.06
20	0.08	4.0	4.5	1.12

with 0.01 mg/ml lysozyme and 20% BP100, and in magenta for cells treated with 0.08 mg/ml lysozyme and 20% BP100. Figure 6.6(a) shows the absolute intensity spectra and Figure 6.6(b) the spectra normalized by area. A substantial reduction of the prominent edges at $\sim \pm$ 12.5 kHz and an increase in the intensity at the narrow splittings was observed for all the AMP treated samples. As observed in the top spectra in Figure 6.6(b), the disruption of the PGN layer does not enhance or diminish the effect of 20% BP100 on the bacterial cell membrane.

TABLE 6.5: M_1, M_2 and Δ_2 values, as defined in section 2.3.2.1, for ^2H NMR spectra of *B. subtilis* treated with lysozyme to induce partial disruption of the PGN layer in absence (from Table 6.1) and presence of 20% BP100 shown in Figure 6.6.

Peptide Concentration % (wt/wt)	Lysozyme Concentration (mg/ml)	M_1 $\times 10^4 (s^{-1})$	M_2 $\times 10^9 (s^{-2})$	Δ_2
0 (Average over six samples)	0	6.2 ± 1	8.4 ± 3	0.59 ± 0.08
0	0.01	8.7	15	0.49
0	0.1	7.6	12	0.53
20	0	3.5	3.7	1.20
20	0.01	3.7	4.4	1.30
20	0.08	6.1	10.5	1.08

Table 6.5 shows the values of the first and second moments, M_1 and M_2, along with the Δ_2 values for all the spectra shown in Figure 6.6 and the spectrum of *B.*

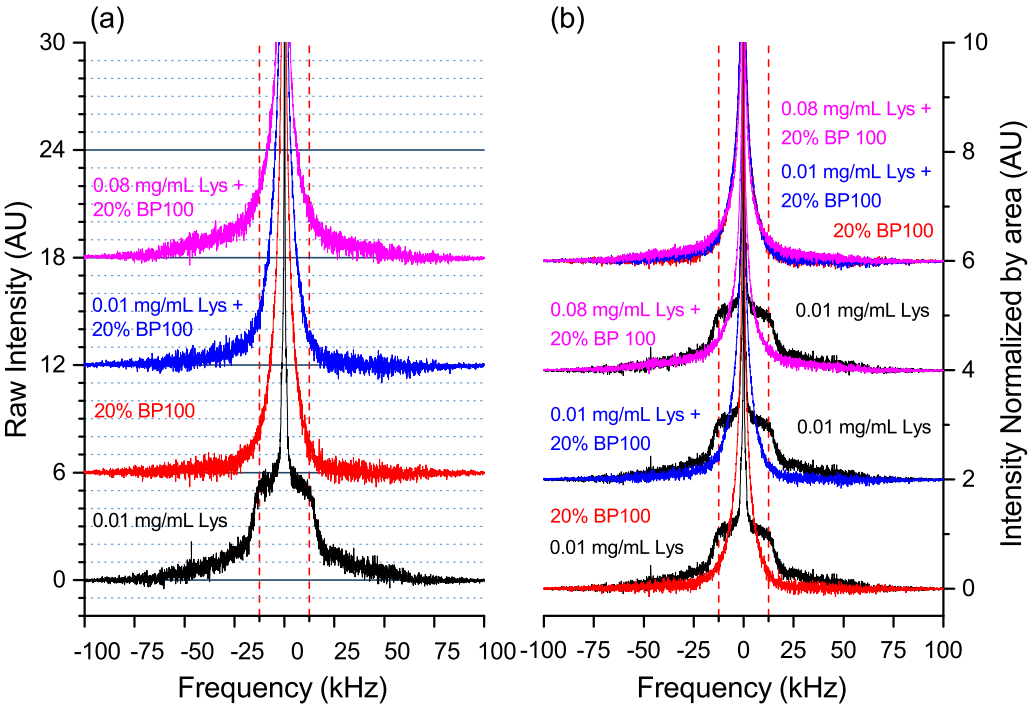

FIGURE 6.6: Disruption of the PGN layer does not change the effect of 20% BP100 on the ^{2}H spectra of *B. subtilis*.(a): Absolute intensity spectra of Black: cells treated with 0.01 mg/ml lysozyme for 10 min, Red: In presence of 20% BP100 (wt/wt), Blue: In the presence of 20% BP100 (wt/wt) after being treated with 0.01 mg/ml lysozyme for 10 min, Magenta: In the presence of 20% BP100 (wt/wt) after being treated with 0.08 mg/ml lysozyme for 10 min. (b) Spectra normalized by area. Dashed lines at ±12.5 kHz are shown to facilitate comparison of the spectra. Each spectrum represents 32,000 scans recorded in eight hours at 37°C in a 9.4 T NMR spectrometer.

subtilus treated with 0.1 mg/ml lysozyme shown in Figure 6.2. Two of the three AMP-treated samples showed a decrease in M_1 and M_2 values. All the AMP-treated samples showed an increase in the Δ_2 values demonstrating again, that Δ_2 value is sensitive to the changes induced in the ^{2}H NMR spectra of the bacteria by AMP. There were small increases in M_1 and M_2 for the combined treatment as compared to the AMP treatment alone, but the effects were small and may just reflect normal sample-to-sample variation.

6.3 Discussion

In this chapter I show that disrupting the peptidoglycan layer has no major impact on the lipid disordering effects of AMPs MSI-78 and BP100. This finding is borne out by comparison of the ^{2}H NMR spectra of *B. subtilis* treated with MSI-78 or BP100 with and without a disrupted PGN layer. Additionally, lysozyme treatment itself has no effect on lipid order, as shown by Figure 6.2 which shows ^{2}H NMR spectra *B. subtilis* of five samples treated with concentrations of lysozyme between from 0.01 mg/ml up to 10 mg/ml.

All lysozyme-treated spectra display similar characteristics including prominent edges at $\sim \pm$ 12.5 kHz. The prominent edges reflect the plateau region of the order parameter profile and indicate that the lipid bilayer is in a liquid-crystalline phase. The lack of observable differences between the spectra from the lysozyme-treated and untreated samples indicates that lysozyme does not interact directly with the lipid bilayer of the bacteria at lysozyme concentrations up to 10 mg/ml. Additionally, the ^{2}H NMR spectra suggest that disrupting the PGN layer of the *B. subtilis* cell envelope does not affect the order parameter profile, indicating no change in the structure or dynamics of the lipid bilayer. One reason this result is quite interesting is because changes in lipid domains in the membrane of Gram + bacterial cells with a disrupted PGN have been observed using fluorescence and immunofluorescence microscopy [79, 107]. However, as discussed in section 4.5.3, small lipid domains cannot be observed during the timescale of a ^{2}H NMR measurement. The absence of an effect of PGN disruption on AMP-induced changes observable directly in the spectra is also supported by the Δ_2 values calculated from the spectra (Table 6.1), which remain similar to the values of the non-treated samples.

In order to investigate the role of the PGN layer and the rest of the cell on the ^{2}H NMR spectra of *B. subtilis*, the spectra of intact cells were compared with the spectra of lipids extracted from the cells and with the spectra of mechanically lysed cells (Figure 6.3). Given the lipid extraction procedure (Section 3.6), the sample containing the lipids extracted from *B. subtilis* is expected to form giant multilamellar vesicles (GMV) filled with just media but without the PGN layer and without most of the membrane proteins. On the other hand, the sample

consisting of untreated cells contains cells with an intact PGN layer. Finally, the lysed cell sample contains cells broken open mechanically, presumably generating a heterogeneous mixture of all the cell components. This sample may contain multilamellar bilayer structures, probably with embedded proteins. The french press process is however, expected to break apart the PGN layer. In summary, the untreated *B. subtilis* sample contains an intact PGN layer, the cell lysate sample contains fragments of the PGN web and the lipids extracted from the cells contain no PGN at all.

As observed in Figure 6.3, all three samples produce spectra that indicate lipids forming bilayers in a liquid-crystalline phase. Interestingly, all samples reflect similar structure and dynamics regardless of the PGN condition or the absence of the PGN layer. The formation of lipid bilayer structures with dynamical properties similar to the intact cells even after mechanically breaking open the cells makes sense because lipid bilayers are self assembling. This lipid bilayer "reconstructing" process apparently occurs even in a protein crowded environment. Significantly, when compared with the ^{2}H NMR of lysed cells, the spectra of AMP treated cells (Figures 4.2, 5.1 and 5.2) looks very different. Thus, AMPs induce a structural modification of the bilayer structure that is dramatically different from that of even very harsh treatments such as organic extraction or mechanical lysis. It is important to mention that, given the observations from the ^{2}H NMR spectra of lysed *B. subtilis* cells and the cell viability experiment presented by Pius *et al.* [6], it seems that if the cell membranes of dead cells remains intact. ^{2}H NMR spectroscopy is unable to report differences between death or alive cells. Cell viability experiments of *B. subtilis* under conditions identical to those used in the NMR experiments would be necessary to fully interpret this observation.

The effect of the PGN disruption on the activity of MSI-78 and BP100 in *B. subtilis* was assessed by comparing the ^{2}H NMR spectra of *B. subtilis* treated with MSI-78 or BP100, with the spectra of cells treated with lysozyme followed by MSI-78 or BP100. Figure 6.4 showed no significant difference between all the spectra of *B. subtilis* treated with 10% MSI-78, regardless of the condition of the PGN layer. The three AMP-treated spectra all lack prominent edges at $\sim \pm$ 12.5 kHz and show an increase in the intensity at the narrow splittings as compared to cells without AMP. Similar behaviour was observed in the spectra of *B. subtilis*

treated with 20% MSI-78 (Figure 6.5) and 20% BP100 (Figure 6.6) regardless of whether the PGN layer was intact or disrupted.

These findings directly relate to a current open discussion in the AMP field about whether PGN promotes accumulation of AMPs on the cell membrane or, instead, entraps the AMPs thus preventing them from reaching the cell membrane [12]. This work includes one previous study that tried to address the role of the PGN on the activity and functionality of the AMPs OP-145 and LL-37 [108], the results of which will be compared with mine below after addressing the literature more specific to MSI-78 and BP100.

The results presented in Figures 6.5 and 6.6 show that disrupting the PGN does NOT affect AMPs' abilities to disrupt the lipid bilayer, at least for MSI-78 and BP100. One point to note is that, in addition to their cell lysis activities, MSI-78 has a known intra-cellular target, ribosomes, and BP100 has non-lipid extra-cellular target, LPS in Gram - and LTA in Gram + bacteria [58, 101, 102]. It is possible that membrane lysis is not the main antimicrobial mechanism for these two peptides and is just incidental to their other mechanism. However, it is not clear how possessing non-lytic activities would relate to the indifference of the AMP-induced lipid disruption to the presence of intact PGN. None-the-less, the data indicate that the PGN layer does not interact with MSI-78 and BP100 in a way that either sensitizes or protects the cells from AMP-induced bilayer disruption as previously suggested [12, 23, 108, 109].

There has been some experimental work done on the role of PGN in the effect of lysozyme on AMP treatment. Experiments monitoring the leakage of fluorescent dyes out of vesicles caused by OP-145 and LL-37 showed that the presence and absence of 0.1 wt % PGN did not affect the membrane permeability [110]. The authors suggested these findings can be explained because entrapping of AMP molecules will not occur for most AMPs, due to the porosity of the PGN to small molecules the same size as AMPs [12]. Additionally, they suggest that the PGN does not reduce the concentration of positively charged AMPs on the cell membrane since PGN is not negatively charged. The findings of Malanovic *et al.* [110] agree with my findings that MSI-78 and BP100 cause the same level of membrane disruption in cells with an intact and compromised PGN layer.

Perhaps AMPs with an affinity to the PGN layer would present a different response to the one observed here and by Malanovic *et al.* [108]. In order to obtain a better understanding, additional ^{2}H NMR studies could be done with eosinophilcin cationic protein (ECP) and oxiganan, two peptides with strong partitioning toward PGN [111–114].

In contrast to my BP100 work, other publications DID find evidence of permeabilization enhancement with a combined treatment of BP100 and lysozyme in Gram - bacteria [59]. In a 2017 study, Cabrefiga *et al.* measured MIC concentration in addition to cell membrane permeabilization with flow cytometry and fluorescence microscopy of *Erwinia amylovora* cells in the presence of SYTOX green. Cabrefiga *et al.* observed a permeabilization enhancement with the combined treatment of BP100 and lysozyme in comparison with the treatment of lysozyme or BP100 alone. This permeabilization enhancement also resulted in a reduction of the MIC concentration. Two important differences between my protocol and the Cabrefiga *et al.* protocol are that I treated with lysozyme BEFORE AMP, whereas Cabrefiga *et al.* treated with lysozyme and AMP at the same time and, I worked Gram + *B. subtilis* while Cabrefiga *et al.* used Gram -. Moreover, Gram - bacteria have an outer bacterial membrane composed of LPS among other lipids, that lysozyme cannot penetrate and thus Gram - bacteria tend to be less susceptible to lysozyme than Gram + bacteria. Given that BP100 interacts with the LPS layer on Gram - cells [58, 61, 102, 115], such as *Erwinia amylovora*, the AMP might permeabilize the outer bacterial membrane enabling the lysozyme greater access to the PGN layer. Thus, BP100 might generate a susceptibility of Gram - cells to lysozyme as a result of the BP100-LPS interaction.

Further studies reported combined treatments of lysozyme and specific AMPs as a more effective way to kill Gram + and Gram - bacteria in comparison with treating bacteria with lysozyme or AMPs alone [116–118]. Even though my protocol is different from the ones followed by Zdybicka-Barabas *et al.*, Chai *et al.* and Lee *et al.*, because I treated with lysozyme before AMPs, these studies are still relevant to understanding the interplay of AMP and lysozyme interactions with cell envelope components.

In 2012, Zdybicka-Barabas *et al.* reported an increase in the antimicrobial effectiveness of the anionic peptide 2 (GMAP2) when Gram - *E. coli* or *K. pneumoniae* cells were treated at the same time with lysozyme [116]. Zdybicka-Barabas *et al.* used β-galactosidase measurements to determine cell membrane perforation and AFM and SEM imaging to determine the cell surface alterations caused by lysozyme and anionic peptide 2 (GMAP2). That study reported an increase in the level of perforation of *E. coli* in the presence of lysozyme as well as cell envelope surface alterations caused by GMAP2 in *E. coli* and *K. pneumoniae* [116]. The authors suggested the possibility of formation of an intermolecular complex between the AMP and lysozyme that would increase the antimicrobial effectiveness of both molecules. However they also suggest that this complexation does not occur in solution without a cell membrane present.

In addition, two further studies reported synergistic action of the AMP nisin with lysozyme in Gram + bacteria [117, 118]. Both studies were performed in *Clostridium difficile* and track the antimicrobial effect of nisin, lysozyme and the combination of nisin+lysozyme. Note that even though nisin is classified as an AMP, it can only disrupt negatively charged membranes at peptide concentrations much higher than those necessary for bacterial killing or if the membranes contain lipid II [119]. The results showed that the antimicrobial effect of the mixture of lysozyme+nisin was faster than the antimicrobial effect of nisin or lysozyme alone. Since nisin belongs to the family of lantibiotics which are peptides capable of inhibiting PGN biosynthesis, the action of lysozyme+nisin on Gram + bacteria would result in a faster antimicrobial effect since both components attack the PGN layer, generating cell lysis. However, there was no indication of the cell membrane being more disrupted because of the mixture. In fact, since nisin has an extracellular target, it is probable that the mixture is not causing more membrane disruption than the AMP alone.

In sumary, Zdybicka-Barabas *et al.*, Chai *et al* and Lee *et al* reported an improvement in the bactericidal effect of GMAP2 and nisin in the presence of lysozyme [116–118]. However, these studies were intended to demonstrate lysozyme potentiation of AMP activity, NOT to address the role of PGN in AMP activity. Furthermore, only Chai *et al* and Lee *et al* used Gram + bacteria for their studies. Therefore, to the best of my knowledge, my thesis work represents one of the first

studies directed at understanding the role of the PGN layer in the AMP-disruption of lipid bilayers.

Chapter 7

Conclusions and Future Directions

As laid out in Section 2.2, it is necessary to build a bridge that connects the historical work regarding antimicrobial peptides (AMPs) interacting with model lipid bilayers to the relatively recent finding that at least some AMPs act on non-lipid targets. The main focus of this thesis was to study the importance of the peptidoglycan (PGN) layer, one of the non-lipid components of the bacterial cell envelope, in the interaction of the AMPs with lipids of the membrane. To do so, the strategy chosen was to use a technique commonly used to study model lipid systems, ^{2}H NMR, but apply it to whole bacteria.

The overall research goal, to use ^{2}H NMR of intact cells to study the importance of PGN in AMP-lipid interactions, was accomplished by way of four objectives. The first objective was the characterization of the ^{2}H NMR spectra of *B. subtilis*. The second study was to study the changes in the spectra in the presence of AMPs MSI-78 and BP100. The third objective was to look for possible changes in the *B. subtilis* spectra caused by PGN disruption alone. Finally, *B. subtilis* spectra were obtained for samples with both a compromised PGN layer and treatment with MSI-78 or BP100.

7.1 Disruption of the bacterial membrane of *B.subtilis* caused by MSI-78 and BP100

One of the most important conclusions of this work was that MSI-78 and BP100 induced changes in the ^{2}H NMR spectra of *B. subtilis* that indicate disruption of the lipid bilayer structure corresponding to an increase in lipid disorder (Figures 5.1 and 5.2). This is important since only a few ^{2}H NMR studies of whole cell have been reported since 1975 [1, 6, 8, 68, 75, 106, 120, 121] and only four of them investigated the effect of AMPs on the structure and dynamics of the lipid bilayer [6, 8, 106, 121]. While the earlier whole cell ^{2}H NMR work focussed on Gram - bacteria, this thesis provides the first characterization of the static ^{2}H NMR spectra of deuterium-rich Gram + *B. subtilis* (Figure 4.3), as well as the characterization of *E. coli* JM109 spectra (Figure 4.2) and LA8 spectra (Figure 4.1). Addition of the AMPs MSI-78 and BP100 was seen to substantially affect the ^{2}H NMR spectra of intact bacteria. Additionally, the changes to the spectral shape induced by MSI-78 are similar to the changes induced by BP100. The AMP-induced disruption in whole cells consists of the disappearance of the sharp edges at $\sim \pm$ 12.5 kHz, along with a concomitant increase in intensity at narrow splittings. The formation of toroidal pores is the most likely mechanism of membrane disruption that might explain the changes observed in this study. This type of membrane disruption has been suggested for other AMPs in previous NMR studies [89–91]. This interpretation would agree with previous studies suggesting that MSI-78 and BP100 can form toroidal pores [48, 49, 102, 122]. Additionally, while the AMP-induced reduction in the sharp edges has been observed in model lipids experiments, the increase in intensity at narrow splittings has not being observed in model lipids in the presence of AMPs [48, 83–88]. This difference of the AMP-induced changes in the ^{2}H NMR spectra of whole cells versus model systems suggests a difference in how AMPs interact with membranes in bacteria, as compared to their interaction with membranes in model-lipid-only systems. Most likely, this difference is due to the complex structure and composition of the bacterial envelope however, it is possible that this difference is due to the complex lipid composition of the cell membrane only. One strategy to test this idea would be to compare the changes

induced in the spectra by the AMPs between whole cells, lipid extract and cell lysate, as a part of the future research directions.

At 20% wt/wt concentration, MSI-78 and BP100 show the same level of cell membrane disruption (Figure 5.3). A brief review of the physicochemical properties of both peptides shows that MSI-78 and BP100 are positively charged, MSI-78's charge at pH 7 is +10 and BP100 +6. There is no apparent difference in the hydrophobicity of both peptides as judged by their GRAVY indices[1]. It is interesting that the difference in charge does not lead to a difference in membrane disruption. Perhaps hydrophobic interactions contribute to the binding energy enough so that there is no difference in AMP-bilayer binding, even with the difference in charge and consequently, electrostatic interactions. Future research directions include obtaining MIC concentrations for both AMPs in *B. subtilis* and comparing the level of cell membrane disruption of two antimicrobial peptides with an evident difference in the hydrophobicity but similar charges.

It was somewhat surprising that both MSI-78 and BP100 lead to a similar level of membrane disruption, given their difference in charge and the important role charge interactions are supposed to play in AMP mechanisms. It was thus intriguing to find in the literature that, both MSI-78 and BP100 have potential non-lipid, i.e. secondary, targets. The interaction of BP100 with the lipopolysaccharides (LPS) layer of Gram - bacteria and the lipoteichoic acid (LTA) of Gram + bacteria has been reported [101, 102] as well as the interaction of MSI-78 with the ribosomes [31]. Considering that the LPS and the LTA are components of the bacterial cell wall, i.e., located outside of the cell membrane, and the ribosomes are in the cytoplasm, i.e., located inside of the cell membrane, it is intriguing that both AMPs display the same level of lipid bilayer disruption at analogous wt/wt ratios.

Finally, since the molar bound peptide to lipid ratio (P:L) is an important reference when describing the antimicrobial activity of AMPs, an estimation of the bound P:L was performed for MSI-78. The estimated molar bound P:L ratio in my experiments at 20% MSI-78 is 0.94:1, as calculated using the same rationale

[1]GRAVY index (Grand Average of hydropathy) is a value used to measure the hydrophobicity of peptides or proteins. Positive values indicate more hydrophobic structures and negative value indicate more hydrophilic structures. Values close to 0 are typical of amphiphilic sequences.

described by Pius *et al.*[6]. It was assumed that 100 % of the AMPs are bound to the bacteria, that lipids compromise the 5.2 % of the bacterial dry weight of *B. subtilis* [123], and that lipids have an average molecular weight of 705 g/mol. A bound P:L ratio of 0.94:1 is far below the bound P:L ratios needed to inhibit bacterial growth ($\sim$ 100:1), i.e. the ratio at the MIC concentration [16]. Note that the P:L ratio necessary to generate lipid bilayer disruption and leakage in model systems is $\sim$ 1:100 (See appendix A) [16] i.e. $\sim$ 100 times less AMP than in my work. At least in terms of P:L ratio, the NMR samples are prepared with an amount of AMP expected to be sublethal. Since the level of membrane disruption was substantial even at P:L ratios of $\sim$ 1:1, it it impressive that bacteria are able to survive this much damage to their membranes.

7.2 A Weakened PGN layer did not change the ^{2}H NMR spectra of *B. subtilis*

Another main finding of this work is that the disruption of the PGN layer in *B. subtilis* did not change the ^{2}H NMR spectra. To achieve a compromised PGN layer, different concentrations of lysozyme were tested. Lysozyme is an enzyme able to hydrolyze the PGN layer of Gram + bacteria. A severe disruption of the PGN layer can cause cell lysis since this layer is, among other things, responsible for maintaining the osmotic pressure balance and cell shape. Thus, in order to keep the cells from breaking open, the lysozyme treatment of the cells was done in sucrose rich media that prevents the osmotic pressure imbalance (see section 3.3). The disruption of the PGN layer in *B. subtilis* was confirmed using a microscope, thanks to the change in the Gram staining of the lysozyme-treated cells from purple to pink (Figures 6.1(b), 6.1(c) and 6.1(d)). In addition, the severe disruption of the PGN layer induced a change in *B. subtilis* cell shape from rod to spherical shape that was observed in the microscope.

Despite the noticeable change in the *B. subtilis* cell wall and shape caused by the treatment with up to 10 mg/mL of lysozyme, it was striking that the ^{2}H NMR spectra (Figure 6.2) showed no change in the structure or lipid order of the cell membrane. Previous fluorescence and immunofluorescence microscopy studies

reported changes in the lipid domains of the cell membrane of Gram + bacteria with a disrupted PGN layer [79, 107]. However, small lipid domains can not be observed during the timescale of a ^{2}H NMR measurement (see section 4.5.3).

Previous studies reported a non-enzymatic mechanism of action for lysozyme [105, 124]. This non-enzymatic mechanism of action includes the binding and membrane disruption caused by lysozyme. This non-enzymatic mechanism has been reported by Acreman [105] using heat denatured lysozyme (DN-Lyz) and by Ibrahim et al. [124] using a D52S lysozyme mutant whose aspartic acid at position 52 was substituted with serine (D52S-Lyz). DN-Lyz and D52S-Lyz were devoid of enzymatic activity but, both were still able to kill Gram + bacteria, specifically *B. subtilis*. To help assess the relevance of the lysozyme non-enzymatic mechanism of action to my experiments, the molar lysozyme to lipid ratios (Lyz:L) of Acreman, Ibrahim *et al.*, and my *B. subtilis* experiments were estimated. The bacterial dry weight was calculated using cell concentrations reported by Acreman and Ibrahim *et al.* (2.5×10^5 [105] and 2×10^6 cells/mL [124] respectively), Acreman's relationship between the Colony Forming Unit (CFU) per mL and the absorption at 600 nm (A_{600}) ($y = (1.4211 \times 10^8)A_{600}$ [105]), and my relationship between bacterial dry weight and A_{600} from section 3.5.1. Finally, it was assumed that lipids compromise 5.2 % of the bacterial dry weight and that the lipids have an average molecular weight of 705 g/mol. The estimated Lys:L ratios were 4.3:1 for Ibrahim *et al.*, 7.8:1-13:1 for Acreman and 1:25000 - 1:2.5 for my experiments. The Lys:L ratio in my experiments was much smaller than in the other studies and thus lysozyme is unlikely to have a direct effect on the membrane. This is consistent with the lack of change in ^{2}H NMR spectra of *B. subtilis* with lysozyme treatment (Figure 6.2).

A very interesting observation in this study was how different were the ^{2}H NMR spectra of bacterial cells treated with AMPs (Figures 4.2, 4.3, 5.1 and 5.2) compared to the spectra of mechanically lysed cells (Figure 6.3). The spectra of the mechanically lysed cells show the formation of lipid bilayer structures with similar dynamical properties to the intact cell spectra. On the other hand, the spectra of bacterial cells treated with AMPs reflect a change in the order parameter profile that is consistent with a disrupted lipid bilayer with highly curved structural features. Thus, the "lytic" effect of the AMPs is the result of an active AMP-lipid

bilayer interaction that prevents the cell membrane from being restored, contrary to the mechanically lysed cells, where lipid bilayer structures rapidly self-repair. There must be something very special about what AMPs do to the membranes.

At this point it is important to remark that ^{2}H NMR spectroscopy of bacterial cells reports about the lipid bilayer state and not into the viability of the cells. For example, as shown in Figure 6.3, the ^{2}H NMR spectrum of lysed *B. subtilis* is not different from the spectra of live *B. subtilis* because the membranes from cells that were mechanically disrupted were able to reassemble with time. On the other side, the cell viability experiment presented by Pius *et al.* showed that the spectral shape obtained from *E. coli* LA8 samples remained unchanged after 12 to 18 hours of measurements despite a cell viability reduction of approximately 50% [6].

7.3 Level of cell membrane disruption caused by MSI-78 and BP100 in *B. subtilis* does not change even with a compromised PGN layer

The final part of my thesis work directly addresses an important question that, to my knowledge, has not been addressed before. There has been an ongoing discussion about whether the PGN layer of bacterial cells promotes accumulation of AMPs on the cell membrane or, instead, entraps the AMPs preventing them from reaching the lipid bilayer [12, 108]. However, only a few studies provide some insights about this specific topic. In this study I have shown that MSI-78 and BP100 cause the same level of cell membrane disruption regardless of the PGN layer state (Figures 6.5 and 6.6). This observation derives from the comparison of the ^{2}H NMR spectra of *B. subtilis* treated with MSI-78 or BP100 and the spectra of *B. subtilis* treated with lysozyme and MSI-78 or BP100. At least for these two AMPs in *B. subtilis*, PGN has no effect on their membrane-disrupting activities.

While my work focussed on intact cells, other researchers have come at PGN and AMP interaction using simple model systems. In their study, Malanovic *et al.* showed that the presence and absence of 0.1 wt % PGN did not affect the

membrane permeability induced by OP-145 and LL-37 [110]. These findings in MSI-78, BP100, OP-145 and LL-37 suggests that the PGN is not promoting the accumulation of AMPs. Perhaps this is because there is no electrostatic interaction between the AMP and the PGN and because the PGN layer is relatively permeable to particles smaller than 2 nm [12]. As part of the future research directions, it could be interesting to examine similar ^{2}H NMR studies in Gram + bacteria in the presence of peptides like eosinophicilin cationic protein (ECP) or oxiganan, two peptides whose strong affinity towards the PGN layer has been measured before [111–114]. Perhaps, those AMPs would display a different response to the one observed with MSI-78, BP100, OP-145 and LL-37.

There is a group of studies where the antimicrobial effect of lysozyme+AMP mixtures was compared with the antimicrobial effect of lysozyme or AMPs alone. These studies reported synergistic action of AMPs with lysozyme in Gram + bacteria [117, 118] and in Gram - bacteria [59, 116] as a result of a combined treatment. While Chai *et al.* [117], Lee *et al.* [118], and Cabrefiga *et al.* [59] intended to reinforce the antimicrobial effect of the AMP with a combined lysozyme+AMP treatment, Zdybicka-Barabas *et al.* [116] intended to study the antimicrobial effect of two of the hemolymph (insect blood) components at the same time. More details about these studies are part of section 6.3. There are four significant differences between these studies and mine. First, these studies are NOT intended to study the role of the PGN in the activity of the AMP. Second, only Cabrefiga *et al.* studied an AMP used in my studies [59]. Third, none of these studies were performed in *B. subtilis* and just two used Gram + bacteria. Fourth, the protocols from all of these studies differ from mine since I did not study the effect of a combined Lysozyme+AMP treatment. Rather, the AMP treatment was carried out in centrifuged samples after the lysozyme treatment. The studies performed by Cabrefiga *et al.*, Zdybicka-Barabas *et al.*, Chai *et al.* and Lee *at al* indicate that the combination of lysozyme+AMP leads to an improvement over the antimicrobial capacity of the AMP alone [59, 116–118]. However, it is not clear from these works if lysozyme action against PGN is helping the AMP disrupt the membrane, or if another mechanism is involved. Consequently, my study is the first research, performed in whole cells, about the role of the PGN in the AMP-disruption effect in the cell membrane.

In addition to the existing debate about whether the PGN layer of bacterial cells promotes accumulation of AMPs on the cell membrane or, instead, entraps the AMPs preventing them from reaching the lipid bilayer, there is similar debate about whether teichoic acids (TAs) (section 2.1.4) promote or hinder the interaction of AMPs with the cell membrane [12, 116–118]. Unlike PGN, TAs possess an overall negative charge and, thus, might have stronger interactions with AMPs [125, 126]. The interaction between positively charged AMPs and negatively charged TAs could lead to two opposite outcomes. The first possibility is that the AMPs may get trapped by the lipoteichoic acids (LTAs) and wall teichoic acids (WTAs) reducing the number of peptide molecules that actually bind to the cell membrane. This might result in just a fraction of the AMPs reaching the cell membrane and causing membrane disruption. On the other hand, the second possibility is that the AMPs may be using the TAs as a poly-anionic ladder in order to reach the cell membrane i.e., the TAs might mediate the entry of the AMPs towards the cell membrane.

Evidence of LTA possibly reducing the effective AMP concentration on the cell membrane include studies in model systems like Malanovic *et al.* and Liu *et al.* [110, 127] and in whole bacteria [127]. In 2013, Wen *et al.* showed that pre-incubating the AMP β-bungarotoxin B chain with LTA resulted in reducing the AMP's permeabilization of PG/CL vesicles, indicating that some of the AMP bound to the LTA and was sequestered from the lipid vesicles [127]. In addition, Malanovic *et al.* showed a reduction in OP-145 penetration capacity in POPG/LTA vesicles in comparison with pure POPG vesicles [110]. Both studies indicate that β-bungarotoxin B chain and OP-145 interact with LTA resulting in an attenuation of the lipid bilayer permeabilization of both peptides. Similarly, Wen *et al.* showed that β-bungarotoxin B chain demonstrated bactericidal activity against Gram + *S. aureus* only when the bacterial cells were treated with rifampin before the AMP treatment. Given that rifampin is a LTA biosynthesis inhibitor, the authors concluded that the inhibition of LTA biosynthesis in *S. aureus* made the cells prone to AMP damage [127]. Assuming that the LTA is reducing the effective AMP concentration on the cell membrane, it suggests that the absence or reduction of LTA would increase the bactericidal effect of the AMP.

On the other hand, evidence of TAs acting like a poly-anionic ladder helping

promote AMP's access to the cell membrane was presented by Koprivnjak *et al.* [128]. In their study, the authors showed how the *S. aureus tag*O mutant was selectively resistant to two AMPs, the mammalian group II phospholipase A2 (gIIA PLA_2) and the human β-defensin 3. Since the *tag*O mutant of *S. aureus* lacks WTA, Koprivnjak *et al.* suggested that the AMPs were lacking the initial rung of the poly-anionic ladder which would prevent them AMPs from reaching the cell membrane [128].

During my experiments, I partially removed the PGN layer of the *B. subtilis* cell wall during that process. In doing so it is likely that I also removed some of the WTAs linked to the PGN. It is also possible that lysozyme is also hydrolyzing the LTAs directly. In any case, if, as seems likely, the lysozyme treatment also disrupted the LTA, this did not change the level of lipid membrane disruption caused by the positively charged MSI-78 and BP100. This lack of effect could be because the disruption of the TAs is too gentle or because LTAs do not affect the ability of MSI-78 or BP100 to affect the lipids. As part of future research, it could be interesting to examine if the disruption of the electrostatic interactions between AMPs and TAs generate a change in the level of disruption caused by the AMPs.

In conclusion, I have shown that the addition of MSI-78 and BP100 leads to a decrease in the order parameter of the cell membrane acyl chains consistent with cell membrane disruption. Also, the disruption of the PGN layer of *B. subtilis* does not affect its ^{2}H NMR spectra. Finally, the disruption of the PGN does NOT affect the abilities of MSI-78 and BP100s to disrupt the lipid bilayer.

Appendix A

Numerical Calculations

A.1 Peptide to lipid ratio calculations

A.1.1 P:L ratios for 20% and 10 % MSI-78 (wt/wt) used in this work

The molar peptide to lipid ratio (P:L) is an important reference when describing the antimicrobial activity of AMPs. The difference in the P:L ratios between model system studies and sterilization experiments is one of the reasons for us to think that the non-lipid components of the bacterial cell envelope may play a role in the AMP-bacteria interaction. The molar amounts of lipid for the AMP-treated samples were calculated from the bacterial dry weight, knowing that the lipids comprise 5.2% of the bacterial dry weight [123]. For example, the sample treated with 20% MSI-78 (wt/wt) had an absorbance at 600 nm of 0.783. From the absorbance vs bacterial dry weight relationship explained in 3.5.1, a bacterial dry weight of 211 mg was obtained. Then, the approximated lipid mass was 11 mg. The average molecular weight of the lipids was 705 g/mol, from which was determined that this sample in particular had 1.6 $\times 10^{-5}$ moles of lipids.

For this sample, an MSI-78 fraction of 20% (wt/wt) required 42 mg of peptide. Since the molecular weight of MSI-78 is 2478.2 g/mol, this corresponded to 1.7 $\times 10^{-5}$ moles of peptides for this sample.

In conclusion, the molar P:L ratio for the sample treated with 20% MSI-78 (wt/wt) was 1.7:1.6 or 1:0.94. A similar calculation was performed for the 10% MSI-78 (wt/wt) sample leading to a molar P:L ratio of 1:1.8.

A.1.2 Molar P:L ratio calculations for biological studies

In order to corroborate the estimate of P:L molar ratios for biological experiments reported in the 2010 review by Wimley [16], P:L ratio were obtained from the MIC values reported from three recent biological studies [61, 129, 130]. Each of these studies was performed in different bacterial species using different AMPs. All the data from these studies used for the calculation of the molar P:L ratio are reported in Table A.1.

TABLE A.1: Reported MIC results

Strain	AMP	MIC (μM)	AMP molecular weigth (g/mol)	CFU($\times 10^6$/mL)	Ref
Staphylococcus aureus	SP1-1	6.25	1565.07	1.1	[61]
E. coli	BP100	2-4	1421.88	0.3	[129]
B. subtilis	rLH	1.9	3947.84	0.2-0.7	[130]

To estimate the amount of lipids in each sample, the number of colony forming units (CFU) per unit of volume (See Table A.1) was multiplied by the number of lipids per cell strain. The number of lipids per cell strain was calculated as the ratio between the volume of the lipid bilayer and the approximate volume of a lipid $\sim 1.4 \times 10^{-9}$ μm^3. In order to calculate the volume of the lipid bilayer of each strain multiple considerations were made. For example, *Staphylococcus aureus* cells were approximated to spheres of 0.5 μm of radio [131] with a peptidoglycan structure 24 nm width [132]. *E. coli* cells were considered as rods of 1 μm wide and 2μm long [133] with two lipid bilayers of the same thickness and a peptidoglycan structure

4.2 nm width [134]. Finally, *B. subtilis* cells were considered as rods of 0.84 μm wide and 2.8 μm long [135] with a peptidoglycan structure 50 nm width [136].

TABLE A.2: P:L molar ratios for corresponding to reported MIC

Strain	AMP	MIC (μM)	Ref	# Lipids /cell$\times 10^6$	~P:L
Staphylococcus aureus	SP1-1	6.25	[61]	8.07	400:1
E. coli	BP100	2-4	[129]	26.6	250:1
B. subtilis	1.9	rLH	[130]	17.8	150:1

Table A.2 shows the approximated P:L molar ratios for three AMPs SP1-1, BP100 and rLH calculated from MICs reported in different studies [61, 129, 130]. The calculated P:L molar ratios are within one order of magnitude of the P:L molar ratio for biological studies estimated by Wimley in 2010 [16].

A.2 Dry Weight uncertainty calculations

The bacterial dry weight of each sample was calculated from the absorbance at 600 nm and using the experimentally calculated relationship ln(Dry Weight(mg))=(1.3± 0.1)A_{600}+(4.3± 0.1) for *E.coli* JM109 or ln(Dry Weight(mg))=(1.3± 0.3)A_{600}+(4.3± 0.2) for *B. subtilis*. The dry weight, q, can thus be written in terms of the absorbance, x, as $q = e^{Ax+B}$ where A and B are the slopes and intercepts of the lines in Figures 3.1. If it is assumed that all of the uncertainty in q is associated with uncertainty in the calibration of the absorbance conversion, the uncertainty in q can be estimated by propagating the uncertainties in the fit parameters to give

$$\delta q = \sqrt{\left(\frac{\partial q}{\partial A}\delta A\right)^2 + \left(\frac{\partial q}{\partial B}\delta B\right)^2}. \tag{A.1}$$

In this case x is the absorbance at 600 nm i.e. $x = A_{600}$. Then

$$\delta q = \sqrt{(xe^{(Ax+B)}\delta A)^2 + (e^{(Ax+B)}\delta B)^2} \tag{A.2}$$

or

$$\frac{\delta q}{q} = \sqrt{(x\delta A)^2 + \delta B^2}. \tag{A.3}$$

In the case of an absorbance of $x = 0.75$ of a *B. subtilis* culture, the calculated value calculated dry weight is 200 mg, the relative uncertainty ($\delta q/q$) is 0.3 and the absolute uncertainty (δq) is 60 mg.

Bibliography

[1] C. Tardy-Laporte, A. A. Arnold, B. Genard, R. Gastineau, M. Morançais, J.-L. Mouget, R. Tremblay, and I. Marcotte, "A ^{2}H solid-state NMR study of the effect of antimicrobial agents on intact *Escherichia coli* without mutating.," *Biochimica et Biophysica Acta (BBA) - Biomembranes*, vol. 1828, no. 2, pp. 614–22, 2013.

[2] R. M. Epand and H. J. Vogel, "Diversity of antimicrobial peptides and their mechanisms of action," *Biochimica et Biophysica Acta (BBA) - Biomembranes*, vol. 1462, no. 1-2, pp. 11–28, 1999.

[3] L. M. P. Zanin, D. D. S. Alvares, M. A. Juliano, W. M. Pazin, A. S. Ito, and J. R. Neto, "Interaction of a synthetic antimicrobial peptide with model membrane by fluorescence spectroscopy," *European Biophysics Journal*, vol. 42, no. 11-12, pp. 819–831, 2013.

[4] V. Teixeira, M. J. Feio, and M. Bastos, "Role of lipids in the interaction of antimicrobial peptides with membranes," *Progress in Lipid Research*, vol. 51, no. 2, pp. 149–177, 2012.

[5] J. Davis, K. Jeffrey, M. Bloom, M. Valic, and T. Higgs, "Quadrupolar echo deuteron magnetic resonance spectroscopy in ordered hydrocarbon chains," *Chemical Physics Letters*, vol. 42, no. 2, pp. 390–394, 1976.

[6] J. Pius, M. R. Morrow, and V. Booth, "^{2}H solid-state nuclear magnetic resonance investigation of whole *Escherichia coli* interacting with antimicrobial peptide MSI-78.," *Biochemistry*, vol. 51, no. 1, pp. 118–25, 2012.

[7] J. Pius, "A novel approach to characterize the membrane-disrupting activity of antimicrobial peptides using ^{2}H Solid State NMR of whole *Escherichia coli*," Master's thesis, Memorial University of Newfoundland, 2012.

[8] N. P. Santisteban, M. R. Morrow, and V. Booth, "Protocols for studying the interaction of MSI-78 with the Membranes of Whole Gram-positive and Gram-negative Bacteria by NMR," in *Antimicrobial Peptides: Methods and Protocols*, pp. 217–230, Humana Press, New York, NY, 2017.

[9] G. Seltmann and O. Holst, *The Bacterial Cell Wall*. Springer-Verlag Berlin Heidelberg, 1 ed., 2002.

[10] C. Sohlenkamp and O. Geiger, "Bacterial membrane lipids: Diversity in structures and pathways," *FEMS Microbiology Reviews*, vol. 40, no. 1, pp. 133–159, 2015.

[11] N. T. Reichmann and A. Gründling, "Location, synthesis and function of glycolipids and polyglycerolphosphate lipoteichoic acid in Gram-positive bacteria of the phylum *Firmicutes*," *FEMS Microbiology Letters*, vol. 319, no. 2, pp. 97–105, 2011.

[12] N. Malanovic and K. Lohner, "Antimicrobial Peptides Targeting Gram-Positive Bacteria," *Pharmaceuticals*, vol. 9, no. 3, p. 59, 2016.

[13] R. Villéger, N. Saad, K. Grenier, X. Falourd, L. Foucat, M. C. Urdaci, P. Bressollier, and T.-S. Ouk, "Characterization of lipoteichoic acid structures from three probiotic *Bacillus* strains: involvement of D-alanine in their biological activity.," *Antonie van Leeuwenhoek*, vol. 106, no. 4, pp. 693–706, 2014.

[14] G. Wang, "The Antimicrobial Peptide Database," 2016. http://aps.unmc.edu/AP/about.php, (Date last accessed 2019-06-12).

[15] K. J. Williams and R. P. Bax, "Challenges in developing new antibacterial drugs.," *Current Opinion in Investigational Drugs*, vol. 10, no. 2, pp. 157–63, 2009.

[16] W. C. Wimley, "Describing the Mechanism of Antimicrobial Peptides Action with the Interfacial Activity Model," *ACS Chemical Biology*, vol. 5, no. 10, pp. 905–917, 2010.

[17] K. Matsuzaki, "Control of cell selectivity of antimicrobial peptides," *Biochimica et Biophysica Acta (BBA)- Biomembranes*, vol. 1788, no. 8, pp. 1687–1692, 2009.

[18] B. P. Mowery, S. E. Lee, D. A. Kissounko, R. F. Epand, R. M. Epand, B. Weisblum, S. S. Stahl, and S. H. Gellman, "Mimicry of Antimicrobial Host-Defense Peptides by Random Copolymers," *Journal of the American Chemical Society*, vol. 129, pp. 15474–15476, dec 2007.

[19] Y. Jin, J. Hammer, M. Pate, Y. Zhang, F. Zhu, E. Zmuda, and J. Blazyk, "Antimicrobial activities and structures of two linear cationic peptide families with various amphipathic beta-sheet and alpha-helical potentials.," *Antimicrobial agents and chemotherapy*, vol. 49, no. 12, pp. 4957–64, 2005.

[20] J.-P. S. Powers and R. E. Hancock, "The relationship between peptide structure and antibacterial activity," *Peptides*, vol. 24, no. 11, pp. 1681–1691, 2003.

[21] K. Hilpert, M. R. Elliott, R. Volkmer-Engert, P. Henklein, O. Donini, Q. Zhou, D. F. Winkler, and R. E. Hancock, "Sequence Requirements and an Optimization Strategy for Short Antimicrobial Peptides," *Chemistry & Biology*, vol. 13, no. 10, pp. 1101–1107, 2006.

[22] J. M. Rausch, J. R. Marks, R. Rathinakumar, and W. C. Wimley, "Beta-sheet pore-forming peptides selected from a rational combinatorial library: mechanism of pore formation in lipid vesicles and activity in biological membranes.," *Biochemistry*, vol. 46, no. 43, pp. 12124–39, 2007.

[23] W. C. Wimley and K. Hristova, "Antimicrobial peptides: successes, challenges and unanswered questions.," *The Journal of membrane biology*, vol. 239, no. 1-2, pp. 27–34, 2011.

[24] T. C. B. Vogt and B. Bechinger, "The Interactions of Histidine-containing Amphipathic Helical Peptide Antibiotics with Lipid Bilayers," *Journal of Biological Chemistry*, vol. 274, no. 41, pp. 29115–29121, 1999.

[25] K. B. Smith-Dupont, L. Guo, and F. Gai, "Diffusion as a Probe of the Heterogeneity of Antimicrobial Peptide-Membrane Interactions," *Biochemistry*, vol. 49, no. 22, pp. 4672–4678, 2010.

[26] M.-T. Lee, F.-Y. Chen, and H. W. Huang, "Energetics of pore formation induced by membrane active peptides.," *Biochemistry*, vol. 43, no. 12, pp. 3590–9, 2004.

[27] D.-K. Lee, J. R. Brender, M. F. M. Sciacca, J. Krishnamoorthy, C. Yu, and A. Ramamoorthy, "Lipid Composition-Dependent Membrane Fragmentation and Pore-Forming Mechanisms of Membrane Disruption by Pexiganan (MSI-78)," *Biochemistry*, vol. 52, no. 19, pp. 3254–3263, 2013.

[28] H. Jenssen, P. Hamill, and R. E. W. Hancock, "Peptide Antimicrobial Agents," *Clinical Microbiology Reviews*, vol. 19, no. 3, pp. 491–511, 2006.

[29] L. T. Nguyen, E. F. Haney, and H. J. Vogel, "The expanding scope of antimicrobial peptide structures and their modes of action," *Trends in biotechnology*, vol. 29, no. 9, pp. 464–472, 2011.

[30] D. Andreu and L. Rivas, "Animal antimicrobial peptides: An overview," *Peptide Science*, vol. 47, no. 6, pp. 415–433, 1998.

[31] A. M. Brannan, W. A. Whelan, E. Cole, and V. Booth, "Differential scanning calorimetry of whole *Escherichia coli* treated with the antimicrobial peptide MSI-78 indicate a multi-hit mechanism with ribosomes as a novel target," *PeerJ*, vol. 3, p. e1516, 2015.

[32] H. B. Tz, G. Bierbaum, K. Leopold, P. E. Reynolds, and H.-G. Sahl, "The Lantibiotic Mersacidin Inhibits Peptidoglycan Synthesis by Targeting Lipid II," *Antimicrobial Agents and Chemotherapy*, vol. 42, no. 1, pp. 154–160, 1998.

[33] K. A. Brogden, "Antimicrobial peptides: pore formers or metabolic inhibitors in bacteria?," *Nature reviews. Microbiology*, vol. 3, no. 3, pp. 238–50, 2005.

[34] J. He, A. J. Krauson, and W. C. Wimley, "Toward the de novo design of antimicrobial peptides: Lack of correlation between peptide permeabilization

of lipid vesicles and antimicrobial, cytolytic, or cytotoxic activity in living cells.," *Biopolymers*, vol. 102, no. 1, pp. 1–6, 2014.

[35] S. J. Ludtke, K. He, W. T. Heller, T. a. Harroun, L. Yang, and H. W. Huang, "Membrane pores induced by magainin," *Biochemistry*, vol. 35, no. 43, pp. 13723–13728, 1996.

[36] C.-c. Lee, Y. Sun, S. Qian, and H. W. Huang, "Transmembrane Pores Formed by Human Antimicrobial Peptide LL-37," *Biophysical Journal*, vol. 100, no. 7, pp. 1688–1696, 2011.

[37] J. Katsaras, R. Prosser, R. Stinson, and J. Davis, "Constant helical pitch of the gramicidin channel in phospholipid bilayers," *Biophysical Journal*, vol. 61, no. 3, pp. 827–830, 1992.

[38] V. Razumas, G. Niaura, Z. Talaikytė, A. Vagonis, and T. Nylander, "Interactions of cyclic AMP and its dibutyryl analogue with model membrane: X-ray diffraction and Raman spectroscopic study using cubic liquid-crystalline phases of monoolein," *Biophysical Chemistry*, vol. 90, no. 1, pp. 75–87, 2001.

[39] I. Y. Hasan and A. Mechler, "Analytical approaches to study domain formation in biomimetic membranes," *The Analyst*, vol. 142, no. 17, pp. 3062–3078, 2017.

[40] L. Guo, K. B. Smith-Dupont, and F. Gai, "Diffusion as a probe of peptide-induced membrane domain formation.," *Biochemistry*, vol. 50, no. 12, pp. 2291–7, 2011.

[41] L. Masotti, A. Spisni, and D. W. Urry, "Conformational studies on the gramicidin A transmembrane channel in lipid micelles and liposomes," *Cell Biophysics*, vol. 2, no. 3, pp. 241–251, 1980.

[42] A. Alessandrini and P. Facci, "AFM: a versatile tool in biophysics," *Measurement Science and Technology*, vol. 16, no. 6, pp. R65–R92, 2005.

[43] K. L. H. Lam, Y. Ishitsuka, Y. Cheng, K. Chien, A. J. Waring, R. I. Lehrer, and K. Y. C. Lee, "Mechanism of supported membrane disruption by antimicrobial peptide protegrin-1.," *The journal of physical chemistry. B*, vol. 110, no. 42, pp. 21282–6, 2006.

[44] S. Sinha, L. Zheng, Y. Mu, W. J. Ng, and S. Bhattacharjya, "Structure and Interactions of A Host Defense Antimicrobial Peptide Thanatin in Lipopolysaccharide Micelles Reveal Mechanism of Bacterial Cell Agglutination.," *Scientific reports*, vol. 7, no. 1, p. 17795, 2017.

[45] R. M. Epand, K. D'Souza, B. Berno, and M. Schlame, "Membrane curvature modulation of protein activity determined by NMR," *Biochimica et Biophysica Acta (BBA)- Biomembranes*, vol. 1848, no. 1, pp. 220–228, 2015.

[46] A. Lorin, M. Noël, M.-È. Provencher, V. Turcotte, S. Cardinal, P. Lagüe, N. Voyer, and M. Auger, "Determining the Mode of Action Involved in the Antimicrobial Activity of Synthetic Peptides: A Solid-State NMR and FTIR Study," *Biophysical Journal*, vol. 103, no. 7, pp. 1470–1479, 2012.

[47] M. Zasloff, "Magainins, a class of antimicrobial peptides from *Xenopus* skin: isolation, characterization of two active forms, and partial cDNA sequence of a precursor," *Proceedings of the National Academy of Sciences*, vol. 84, no. 15, pp. 5449–5453, 1987.

[48] A. Ramamoorthy, S. Thennarasu, D.-K. Lee, A. Tan, and L. Maloy, "Solid-state NMR investigation of the membrane-disrupting mechanism of antimicrobial peptides MSI-78 and MSI-594 derived from magainin 2 and melittin.," *Biophysical journal*, vol. 91, no. 1, pp. 206–16, 2006.

[49] K. J. Hallock, D. K. Lee, and A. Ramamoorthy, "MSI-78, an analogue of the magainin antimicrobial peptides, disrupts lipid bilayer structure via positive curvature strain," *Biophysical Journal*, vol. 84, no. 5, pp. 3052–3060, 2003.

[50] H. M. Lamb and L. R. Wiseman, "Pexiganan Acetate," *Drugs*, vol. 56, no. 6, pp. 1047–1052, 1998.

[51] E. Pérez-Payá, M. Orzáez, L. Mondragón, D. Wolan, J. A. Wells, A. Messeguer, and M. J. Vicent, "Molecules that modulate Apaf-1 activity.," *Medicinal research reviews*, vol. 31, no. 4, pp. 649–75, 2011.

[52] B. H. Steiner H, Hultmark D, Engström A, Bennich H, "Sequence and specificity of two antibacterial proteins involved in insect immunity.," *Nature*, vol. 292, pp. 246–8, 1981.

[53] H. Boman, D. Wade, I. Boman, B. Wåhlin, and R. Merrifield, "Antibacterial and antimalarial properties of peptides that are cecropin-melittin hybrids," *FEBS Letters*, vol. 259, no. 1, pp. 103–106, 1989.

[54] F. G. Fischer and W. P. Neumann, "The venom of the honeybee. III. On the chemical knowledge of the principle active constituent (melittin)," *Biochemische Zeitschrift*, vol. 335, pp. 51–61, 1961.

[55] E. Habermann and J. Jentsch, "Sequence analysis of melittin from tryptic and peptic degradation products," *Hoppe-Seyler's Zeitschrift fur physiologische Chemie*, vol. 348, no. 1, pp. 37–50, 1967.

[56] E. Schröder, "The synthesis for the melittin partial sequence 1-20 and 7-20.," *Justus Liebigs Annalen der Chemie*, vol. 711, pp. 227–33, 1968.

[57] D. Andreu, J. Ubach, A. Boman, B. Wåhlin, D. Wade, R. Merrifield, and H. G. Boman, "Shortened cecropin A-melittin hybrids Significant size reduction retains potent antibiotic activity," *FEBS Letters*, vol. 296, no. 2, pp. 190–194, 1992.

[58] I. M. Torcato, Y. H. Huang, H. G. Franquelim, D. Gaspar, D. J. Craik, M. A. Castanho, and S. Troeira Henriques, "Design and characterization of novel antimicrobial peptides, R-BP100 and RW-BP100, with activity against Gram-negative and Gram-positive bacteria," *Biochimica et Biophysica Acta (BBA)- Biomembranes*, vol. 1828, no. 3, pp. 944–955, 2013.

[59] J. Cabrefiga and E. Montesinos, "Lysozyme enhances the bactericidal effect of BP100 peptide against *Erwinia amylovora*, the causal agent of fire blight of rosaceous plants," *BMC Microbiology*, vol. 17, no. 1, p. 39, 2017.

[60] R. Ferre, M. N. Melo, A. D. Correia, L. Feliu, E. Bardají, M. Planas, and M. Castanho, "Synergistic Effects of the Membrane Actions of Cecropin-Melittin Antimicrobial Hybrid Peptide BP100," *Biophysical Journal*, vol. 96, no. 5, pp. 1815–1827, 2009.

[61] C. S. Alves, M. N. Melo, H. G. Franquelim, R. Ferre, M. Planas, L. Feliu, E. Bardají, W. Kowalczyk, D. Andreu, N. C. Santos, M. X. Fernandes, and M. A. R. B. Castanho, "*Escherichia coli* cell surface perturbation and

disruption induced by antimicrobial peptides BP100 and pepR," *Journal of Biological Chemistry*, vol. 285, no. 36, pp. 27536–27544, 2010.

[62] J. H. Davis, "The description of membrane lipid conformation, order and dynamics by ^{2}H-NMR," *Biochimica et Biophysica Acta (BBA) - Reviews on Biomembranes*, vol. 737, no. 1, pp. 117–171, 1983.

[63] J. Seelig, "Deuterium magnetic resonance: theory and application to lipid membranes," *Quarterly Reviews of Biophysics*, vol. 10, p. 353, aug 1977.

[64] L. J. Burnett and B. H. Muller, "Deuteron Quadrupole Coupling Constants in Three Solid Deuterated Paraffin Hydrocarbons: C2D6, C4D10, C6D14," *The Journal of Chemical Physics*, vol. 55, no. 12, pp. 5829–5831, 1971.

[65] A. Seelig and J. Seelig, "Effect of a single cis double bond on the structure of a phospholipid bilayer," *Biochemistry*, vol. 16, no. 1, pp. 45–50, 1977.

[66] M. Bloom, J. H. Davis, and A. L. Mackay, "Direct determination of the oriented sample nmr spectrum from the powder spectrum for systems with local axial symmetry," *Chemical Physics Letters*, vol. 80, pp. 198–202, may 1981.

[67] G. W. Stockton, K. G. Johnson, K. W. Butler, A. P. Tulloch, Y. Boulanger, I. C. P. Smith, J. H. Davis, and M. Bloom, "Deuterium NMR study of lipid organisation in *Acholeplasma laidlawii* membranes," *Nature*, vol. 269, no. 5625, pp. 267–268, 1977.

[68] J. H. Davis, C. P. Nichol, G. Weeks, and M. Bloom, "Study of the cytoplasmic and outer membranes of *Escherichia coli* by deuterium magnetic resonance," *Biochemistry*, vol. 18, no. 10, pp. 2103–2112, 1979.

[69] H. I. Petrache, S. W. Dodd, and M. F. Brown, "Area per Lipid and Acyl Length Distributions in Fluid Phosphatidylcholines Determined by ^{2}H NMR Spectroscopy," *Biophysical Journal*, vol. 79, no. 6, pp. 3172–3192, 2000.

[70] G. Casella and R. L. Berger, *Statistical inference*. Thomson Learning, second ed., 2002.

[71] J. Davis, "Deuterium magnetic resonance study of the gel and liquid crystalline phases of dipalmitoyl phosphatidylcholine," *Biophysical Journal*, vol. 27, no. 3, pp. 339–358, 1979.

[72] L. T. DeCarlo, "On the meaning and use of kurtosis," *Psychological Methods*, vol. 2, no. 3, pp. 292–307, 1997.

[73] T. Okuno and T. Yokomizo, "Basic Techniques for Lipid Extraction from Tissues and Cells," in *Bioactive Lipid Mediators* (T. Yokomizo and M. Murakami, eds.), pp. 331–336, Tokyo: Springer Japan, 2015.

[74] R. S. Prosser, J. H. Davis, F. W. Dahlquist, and M. A. Lindorfer, "Deuterium nuclear magnetic resonance of the gramicidin A backbone in a phospholipid bilayer," *Biochemistry*, vol. 30, no. 19, pp. 4687–4696, 1991.

[75] G. W. Stockton, K. Johnson, K. W. Butler, C. F. Polnaszek, R. Cyr, and I. C. Smith, "Molecular order in *acholeplasma laidlawii* membranes as determined by deuterium magnetic resonance of biosynthetically-incorporated specifically-labelled lipids," *Biochimica et Biophysica Acta (BBA) - Biomembranes*, vol. 401, no. 3, pp. 535–539, 1975.

[76] J. F. Wilkinson, "Carbon and Energy Storage in Bacteria," *Journal of General Microbiology*, vol. 32, pp. 171–176, aug 1963.

[77] A. J. García-Sáez, S. Chiantia, J. Salgado, and P. Schwille, "Pore formation by a Bax-derived peptide: effect on the line tension of the membrane probed by AFM.," *Biophysical journal*, vol. 93, no. 1, pp. 103–12, 2007.

[78] R. M. Epand and R. F. Epand, "Lipid domains in bacterial membranes and the action of antimicrobial agents," *Biochimica et Biophysica Acta (BBA) - Biomembranes*, vol. 1788, no. 1, pp. 289–294, 2009.

[79] K. Muchová, A. J. Wilkinson, and I. Barák, "Changes of lipid domains in *Bacillus subtilis* cells with disrupted cell wall peptidoglycan," *FEMS Microbiology Letters*, vol. 325, no. 1, pp. 92–98, 2011.

[80] D. Marsh, *Handbook of Lipid Bilayers*. CRC Press, feb 2013.

[81] J. Gidden, J. Denson, R. Liyanage, D. M. Ivey, and J. O. Lay, "Lipid compositions in *Escherichia coli* and *Bacillus subtilis* during growth as determined by MALDI-TOF and TOF/TOF mass spectrometry," *International Journal of Mass Spectrometry*, vol. 283, pp. 178–184, jun 2009.

[82] B. K. Tan, M. Bogdanov, J. Zhao, W. Dowhan, C. R. H. Raetz, and Z. Guan, "Discovery of a cardiolipin synthase utilizing phosphatidylethanolamine and phosphatidylglycerol as substrates," *Proceedings of the National Academy of Sciences*, vol. 109, pp. 16504–16509, oct 2012.

[83] E. S. Salnikov, A. J. Mason, and B. Bechinger, "Membrane order perturbation in the presence of antimicrobial peptides by ^{2}H solid-state NMR spectroscopy," *Biochimie*, vol. 91, pp. 734–743, jun 2009.

[84] P. J. Sherman, R. J. Jackway, J. D. Gehman, S. Praporski, G. A. McCubbin, A. Mechler, L. L. Martin, F. Separovic, and J. H. Bowie, "Solution structure and membrane interactions of the antimicrobial peptide fallaxidin 4.1a: An NMR and QCM study," *Biochemistry*, vol. 48, no. 50, pp. 11892–11901, 2009.

[85] G. Orädd, A. Schmidtchen, and M. Malmsten, "Effects of peptide hydrophobicity on its incorporation in phospholipid membranes - An NMR and ellipsometry study," *Biochimica et Biophysica Acta (BBA)- Biomembranes*, vol. 1808, no. 1, pp. 244–252, 2011.

[86] B. Bechinger and E. S. Salnikov, "The membrane interactions of antimicrobial peptides revealed by solid-state NMR spectroscopy," *Chemistry and Physics of Lipids*, vol. 165, pp. 282–301, 2012.

[87] S. L. Grage, S. Afonin, S. Kara, G. Buth, and A. S. Ulrich, "Membrane Thinning and Thickening Induced by Membrane-Active Amphipathic Peptides," *Frontiers in Cell and Developmental Biology*, vol. 4, p. 65, jun 2016.

[88] J. Wolf, C. Aisenbrey, N. Harmouche, J. Raya, P. Bertani, N. Voievoda, R. Süss, and B. Bechinger, "pH-Dependent Membrane Interactions of the Histidine-Rich Cell-Penetrating Peptide LAH4-L1," *Biophysical Journal*, vol. 113, no. 6, pp. 1290–1300, 2017.

[89] I. Marcotte, K. L. Wegener, Y. H. Lam, B. C. Chia, M. R. De Planque, J. H. Bowie, M. Auger, and F. Separovic, "Interaction of antimicrobial peptides from Australian amphibians with lipid membranes," *Chemistry and Physics of Lipids*, vol. 122, pp. 107–120, jan 2003.

[90] K. Bertelsen, J. Dorosz, S. K. Hansen, N. C. Nielsen, and T. Vosegaard, "Mechanisms of Peptide-Induced Pore Formation in Lipid Bilayers Investigated by Oriented 31 P Solid-State NMR Spectroscopy," *PLoS ONE*, vol. 7, p. e47745, oct 2012.

[91] B. Kwon, A. J. Waring, and M. Hong, "A 2 H Solid-State NMR Study of Lipid Clustering by Cationic Antimicrobial and Cell-Penetrating Peptides in Model Bacterial Membranes," *BPJ*, vol. 105, pp. 2333–2342, 2013.

[92] K. Lohner, A. Latal, R. I. Lehrer, and T. Ganz, "Differential scanning microcalorimetry indicates that human defensin, HNP-2, interacts specifically with biomembrane mimetic systems," *Biochemistry*, vol. 36, no. 6, pp. 1525–1531, 1997.

[93] F. Jean-François, S. Castano, B. Desbat, B. Odaert, M. Roux, M. H. Metz-Boutigue, and E. J. Dufourc, "Aggregation of cateslytin β-sheets on negatively charged lipids promotes rigid membrane domains. A new mode of action for antimicrobial peptides?," *Biochemistry*, vol. 47, no. 24, pp. 6394–6402, 2008.

[94] R. F. Epand, M. A. Schmitt, S. H. Gellman, and R. M. Epand, "Role of membrane lipids in the mechanism of bacterial species selective toxicity by two α/β-antimicrobial peptides," *Biochimica et Biophysica Acta (BBA) - Biomembranes*, vol. 1758, no. 9, pp. 1343–1350, 2006.

[95] M. Wenzel, M. Rautenbach, J. A. Vosloo, T. Siersma, C. H. Aisenbrey, E. Zaitseva, W. E. Laubscher, W. van Rensburg, J. C. Behrends, B. Bechinger, and L. W. Hamoen, "The multifaceted antibacterial mechanisms of the pioneering peptide antibiotics tyrocidine and gramicidin S," *mBio*, vol. 9, no. 5, pp. 1–20, 2018.

[96] I. Fishov and C. L. Woldringh, "Visualization of membrane domains in *Escherichia coli*," *Molecular Microbiology*, vol. 32, no. 6, pp. 1166–1172, 1999.

[97] F. Kawai, M. Shoda, R. Harashima, Y. Sadaie, H. Hara, and K. Matsumoto, "Cardiolipin Domains in *Bacillus subtilis* Marburg Membranes," *Journal of Bacteriology*, vol. 186, no. 5, pp. 1475–1483, 2004.

[98] K. Matsumoto, J. Kusaka, A. Nishibori, and H. Hara, "Lipid domains in bacterial membranes," *Molecular Microbiology*, vol. 61, no. 5, pp. 1110–1117, 2006.

[99] R. M. Epand and R. F. Epand, "Domains in bacterial membranes and the action of antimicrobial agents," *Molecular BioSystems*, vol. 5, no. 6, p. 580, 2009.

[100] R. Mukhopadhyay, K. C. Huang, and N. S. Wingreen, "Lipid Localization in Bacterial Cells through Curvature-Mediated Microphase Separation," *Biophysical Journal*, vol. 95, no. 3, pp. 1034–1049, 2008.

[101] K. L. Piers and R. E. W. Hancock, "The interaction of a recombinant cecropin/melittin hybrid peptide with the outer membrane of *Pseudomonas aeruginosa*," *Molecular Microbiology*, vol. 12, no. 6, pp. 951–958, 1994.

[102] G. P. Carretero, G. K. Saraiva, A. C. Cauz, M. A. Rodrigues, S. Kiyota, K. A. Riske, A. A. dos Santos, M. F. Pinatto-Botelho, M. P. Bemquerer, F. J. Gueiros-Filho, H. Chaimovich, S. Schreier, and I. M. Cuccovia, "Synthesis, biophysical and functional studies of two BP100 analogues modified by a hydrophobic chain and a cyclic peptide," *Biochimica et Biophysica Acta (BBA)- Biomembranes*, vol. 1860, no. 8, pp. 1502–1516, 2018.

[103] G. Lesnierowski and J. Kijowski, "Lysozyme," in *Bioactive Egg Compounds*, ch. 6, pp. 33–42, Berlin, Heidelberg: Springer Berlin Heidelberg, 2007.

[104] J. M. Ghuysen, "Use of bacteriolytic enzymes in determination of wall structure and their role in cell metabolism.," *Bacteriological reviews*, vol. 32, no. 4, pp. 425–464, 1968.

[105] M. Acreman, "Does Peptidoglycan Sensitize or Protect Gram-Positive *Bacillus subtilis* from the Bactericidal Activity of Antimicrobial Peptides GAD-1 and GAD-2," Bachelor's thesis, Memorial University of Newfoundland, 2016.

[106] M. Laadhari, A. A. Arnold, A. E. Gravel, F. Separovic, and I. Marcotte, "Interaction of the antimicrobial peptides caerin 1.1 and aurein 1.2 with intact bacteria by 2 H solid-state NMR," *Biochimica et Biophysica Acta (BBA) - Biomembranes*, vol. 1858, no. 12, pp. 2959–2964, 2016.

[107] L. A. Vega, G. C. Port, and M. G. Caparon, "An Association Between Peptidoglycan Synthesis and Organization of the *Streptococcus pyogenes* ExPortal," *mBio*, vol. 4, no. 5, 2013.

[108] N. Malanovic and K. Lohner, "Gram-positive bacterial cell envelopes: The impact on the activity of antimicrobial peptides," *Biochimica et Biophysica Acta (BBA) - Biomembranes*, vol. 1858, no. 5, pp. 936–946, 2016.

[109] M. N. Melo, R. Ferre, and M. a. R. B. Castanho, "Antimicrobial peptides: linking partition, activity and high membrane-bound concentrations.," *Nature reviews. Microbiology*, vol. 7, no. 3, pp. 245–50, 2009.

[110] N. Malanovic, R. Leber, M. Schmuck, M. Kriechbaum, R. A. Cordfunke, J. W. Drijfhout, A. De Breij, P. H. Nibbering, D. Kolb, and K. Lohner, "Phospholipid-driven differences determine the action of the synthetic antimicrobial peptide OP-145 on Gram-positive bacterial and mammalian membrane model systems," *Biochimica et Biophysica Acta (BBA)- Biomembranes*, vol. 1848, no. 10, pp. 2437–2447, 2015.

[111] M. Torrent, S. Navarro, M. Moussaoui, M. V. Nogués, and E. Boix, "Eosinophil cationic protein high-affinity binding to bacteria-wall lipopolysaccharides and peptidoglycans," *Biochemistry*, vol. 47, no. 11, pp. 3544–3555, 2008.

[112] M. Melo, D. Dugourd, and M. Castanho, "Omiganan Pentahydrochloride in the Front Line of Clinical Applications of Antimicrobial Peptides," *Recent Patents on Anti-Infective Drug Discovery*, vol. 1, no. 2, pp. 201–207, 2006.

[113] M. N. Melo and M. A. R. B. Castanho, "Omiganan interaction with bacterial membranes and cell wall models. Assigning a biological role to saturation," *Biochimica et Biophysica Acta (BBA)- Biomembranes*, vol. 1768, no. 5, pp. 1277–1290, 2007.

[114] O. P. Neelay, C. A. Peterson, M. E. Snavely, T. C. Brown, A. F. TecleMariam, J. A. Campbell, A. M. Blake, S. C. Schneider, and M. E. Cremeens, "Antimicrobial peptides interact with peptidoglycan," *Journal of Molecular Structure*, vol. 1146, pp. 329–336, 2017.

[115] M. C. Manzini, K. R. Perez, K. A. Riske, J. C. Bozelli, T. L. Santos, M. A. Da Silva, G. K. Saraiva, M. J. Politi, A. P. Valente, F. C. Almeida, H. Chaimovich, M. A. Rodrigues, M. P. Bemquerer, S. Schreier, and I. M. Cuccovia, "Peptide:Lipid ratio and membrane surface charge determine the mechanism of action of the antimicrobial peptide BP100. Conformational and functional studies," *Biochimica et Biophysica Acta (BBA)- Biomembranes*, vol. 1838, no. 7, pp. 1985–1999, 2014.

[116] A. Zdybicka-Barabas, P. Mak, A. Klys, K. Skrzypiec, E. Mendyk, M. J. Fiołka, and M. Cytryńska, "Synergistic action of *Galleria mellonella* anionic peptide 2 and lysozyme against Gram-negative bacteria," *Biochimica et Biophysica Acta (BBA)- Biomembranes*, vol. 1818, no. 11, pp. 2623–2635, 2012.

[117] C. Chai, K. S. Lee, and S. W. Oh, "Synergistic inhibition of *Clostridium difficile* with nisin-lysozyme combination treatment," *Anaerobe*, vol. 34, pp. 24–26, 2015.

[118] K.-S. Lee, C. Chai, G.-S. Imm, S.-W. Oh, and Y. S. Kim, "Inactivation of *Clostridium difficile* spore outgrowth by synergistic effects of nisin and lysozyme," *Canadian Journal of Microbiology*, vol. 63, no. 7, pp. 638–643, 2017.

[119] H. Brötz, M. Josten, I. Wiedemann, U. Schneider, F. Götz, G. Bierbaum, and H. G. Sahl, "Role of lipid-bound peptidoglycan precursors in the formation of pores by nisin, epidermin and other lantibiotics," *Molecular Microbiology*, vol. 30, pp. 317–327, oct 1998.

[120] X. L. Warnet, M. Laadhari, A. A. Arnold, I. Marcotte, and D. E. Warschawski, "A ^{2}H magic-angle spinning solid-state NMR characterisation of lipid membranes in intact bacteria," *Biochimica et Biophysica Acta (BBA) - Biomembranes*, vol. 1858, no. 1, pp. 146–152, 2015.

[121] V. Booth, D. E. Warschawski, N. P. Santisteban, M. Laadhari, and I. Marcotte, "Recent progress on the application of ^{2}H solid-state NMR to probe the interaction of antimicrobial peptides with intact bacteria," *Biochimica et Biophysica Acta (BBA) - Proteins and Proteomics*, 2017.

[122] J. Misiewicz, S. Afonin, S. L. Grage, J. Van Den Berg, E. Strandberg, P. Wadhwani, and A. S. Ulrich, "Action of the multifunctional peptide BP100 on native biomembranes examined by solid-state NMR," *Journal of Biomolecular NMR*, vol. 61, pp. 287–298, apr 2015.

[123] D. G. Bishop, L. Rutberg, and B. Samuelsson, "The Chemical Composition of the Cytoplasmic Membrane of *Bacillus subtilis*," *European Journal of Biochemistry*, vol. 2, no. 4, pp. 448–453, 1967.

[124] H. Ibrahim, T. Matsuzaki, and T. Aoki, "Genetic evidence that antibacterial activity of lysozyme is independent of its catalytic function," *FEBS Letters*, vol. 506, pp. 27–32, 2001.

[125] A. Peschel, "How do bacteria resist human antimicrobial peptides?," *Trends in Microbiology*, vol. 10, no. 4, pp. 179–186, 2002.

[126] D. Münch and H.-G. Sahl, "Structural variations of the cell wall precursor lipid II in Gram-positive bacteria - Impact on binding and efficacy of antimicrobial peptides," *Biochimica et Biophysica Acta (BBA) - Biomembranes*, vol. 1848, no. 11, pp. 3062–3071, 2015.

[127] Y. L. Wen, B. J. Wu, P. H. Kao, Y. S. Fu, and L. S. Chang, "Antibacterial and membrane-damaging activities of β-bungarotoxin B chain," *Journal of Peptide Science*, vol. 19, no. 1, pp. 1–8, 2013.

[128] T. Koprivnjak, C. Weidenmaier, A. Peschel, and J. P. Weiss, "Wall Teichoic Acid Deficiency in *Staphylococcus aureus* Confers Selective Resistance to Mammalian Group IIA Phospholipase A_2 and Human β-Defensin 3," *Infection and Immunity*, vol. 76, no. 5, pp. 2169–2176, 2008.

[129] A. Dangel, N. Ackermann, O. Abdel-Hadi, R. Maier, K. Önder, P. Francois, C. W. Müller, J. Pané-Farré, S. Engelmann, J. Schrenzel, J. Heesemann,

and C. Lindermayr, "A de novo-designed antimicrobial peptide with activity against multiresistant *Staphylococcus aureus* acting on RsbW kinase," *FASEB Journal*, vol. 27, no. 11, pp. 4476–4488, 2013.

[130] Z. G. Tian, T. T. Dong, Y. L. Yang, D. Teng, and J. H. Wang, "Expression of antimicrobial peptide LH multimers in *Escherichia coli* C43(DE3)," *Applied Microbiology and Biotechnology*, vol. 83, pp. 143–149, 2009.

[131] J. M. Monteiro, P. B. Fernandes, F. Vaz, A. R. Pereira, A. C. Tavares, M. T. Ferreira, P. M. Pereira, H. Veiga, E. Kuru, M. S. Vannieuwenhze, Y. V. Brun, S. R. Filipe, and M. G. Pinho, "Cell shape dynamics during the staphylococcal cell cycle," *Nature Communications*, vol. 6, p. 8055, nov 2015.

[132] S. J. Seligman and M. R. Pincus, "A model for the three-dimensional structure of peptidoglycan in staphylococci," *Journal of Theoretical Biology*, vol. 124, pp. 275–292, feb 1987.

[133] A. O. Henriques, P. Glaser, P. J. Piggot, and C. P. Moran Jr, "Control of cell shape and elongation by the rodA gene in *Bacillus subtilis*," *Molecular Microbiology*, vol. 28, no. 2, pp. 235–247, 1998.

[134] J. C. Gumbart, M. Beeby, G. J. Jensen, and B. Roux, "*Escherichia coli* Peptidoglycan Structure and Mechanics as Predicted by Atomic-Scale Simulations," *PLoS Computational Biology*, vol. 10, p. e1003475, feb 2014.

[135] B. Volkmer and M. Heinemann, "Condition-Dependent Cell Volume and Concentration of *Escherichia coli* to Facilitate Data Conversion for Systems Biology Modeling," *PLoS ONE*, vol. 6, no. 7, p. e23126, 2011.

[136] E. J. Hayhurst, L. Kailas, J. K. Hobbs, and S. J. Foster, "Cell wall peptidoglycan architecture in *Bacillus subtilis*," *Proceedings of the National Academy of Sciences of the United States of America*, vol. 105, no. 38, pp. 14603–14608, 2008.